Title

Mechanisms of activation and modulation of homomeric and heteromeric metabotropic glutamate receptors

Author

Habrian, Chris

Publication Date

2021

Peer reviewed|Thesis/dissertation

Mechanism of activation and modulation of homomeric and heteromeric metabotropic glutamate receptors

By

Chris H. Habrian

A dissertation submitted in partial satisfaction of the

requirements for the degree of

Doctor of Philosophy

in

Biophysics

in the

Graduate Division of the

University of California, Berkeley

Committee in charge:

Professor Ehud Y. Isacoff, Chair
Professor Andreas Martin
Professor John Kuriyan
Professor Diana Bautista

Spring 2021

Abstract

Mechanisms of activation and modulation of homomeric and heteromeric metabotropic glutamate receptors

Chris H. Habrian

Doctor of Philosophy in Biophysics

University of California, Berkeley

Professor Ehud Y. Isacoff, Chair

Synaptic plasticity underlies all learning and memory and is a cornerstone of neurological function. The adaptive and flexible nature of these processes makes them complex and challenging to define with the precision needed to develop quantitative models or effective therapeutics. The main excitatory neurotransmitter in the mammalian nervous system is glutamate which is also critical in setting synaptic strength and plasticity. Glutamate induces synaptic changes through two classes of receptors, ionotropic glutamate receptors and metabotropic glutamate receptors. Ionotropic glutamate receptors are glutamate gated calcium channels which can alter synaptic strength in the time scale of tens of milliseconds to 1 second. Metabotropic glutamate receptors (mGluRs) are Class C G-protein coupled receptors (GPCRs) which induce synaptic changes on the time scale of tens of seconds to minutes, hours and even days. This makes mGluRs critical to understanding the molecular induction of synaptic plasticity and very attractive therapeutic targets. Despite much effort put towards developing therapeutics that target mGluRs none have been approved by the FDA. A deeper understanding of mGluR activation will aid in designing more effective therapeutics as well as provide a more precise role of glutamate on synaptic changes.

mGluRs are obligate dimers with large N-terminal domains. Each subunit contains a clamshell like glutamate binding domain (LBD), a rigid cysteine rich domain (CRD) and the canonical 7-pass transmembrane domain that defines all GPCRs. Numerous studies of GPCRs have pointed to the fact that these receptors are highly dynamic and that ligand binding changes the time a receptor spends in several distinct conformational states. The last ten years has seen an explosion in the number of high-resolution GPCRs structures. Unfortunately, these only provide a snapshot of a subset of potential receptor conformations and the amount of knowledge on the conformational dynamics of GPCRs has lagged behind.

One very promising technique to address the questions surrounding GPCR conformational dynamics is single molecule fluorescence resonance energy transfer (smFRET). smFRET allows for very precise measurement of receptor motions and compliments the wealth of structural information to create a much more complete understanding of GPCRs.

To this end I used smFRET to measure and study the conformational motions associated with activation of mGluR homodimers and heterodimers. First I examined the effects of different regions on mGluR2 homodimer activation and mGluR2/3 heterodimer activation which

demonstrated a functional role of a LBD interface and the cysteine loop. Next I examined mGluR7, which has an incredibly low glutamate affinity, and found that while mGluR7 homodimers are virtually insensitive to glutamate, mGluR2/7 heterodimers are present in native tissue and are super sensitive to glutamate due to an apo state rotation demonstrating a potential biologic and modulatory role of heterodimerization. Lastly, I examined regions of mGluR7 and find that the lower dimer interface is responsible for very low glutamate sensitivity and that the cysteine bridge flexibility is responsible for the mGluR2/7 super sensitivity to glutamate.

This work is dedicated to my mother and father who provided me with the opportunity and freedom to pursue research and my entire family who act as a constant source of support and balance.

Table of Contents

Acknowledgements:

The opportunity to pursue the work presented here was created and maintained by several extraordinary individuals who not only created the environment that produced this work, but also provided me with daily input and advice which contributed greatly to my overall training. Firstly, I would like to thank my thesis advisor Ehud Isacoff for his support and the example he set for how an individual pursues scientific questions along with his curation of an environment that enables enjoyable interdisciplinary research. His input has ranged from instilling positivity about individual experiments to how an individual can construct a successful career, and every point in between.

Although this work represents my time as a graduate student there are individuals who were critically responsible in the time before I came to Berkeley. Dr. Kirk Kawagoe is responsible for initiating my path into research when I was a student in community college. If it were not for his advice it is very possible that I would have never contemplated research as a potential career option or met Dr. Danielle Mandikian. Dr. Danielle Mandikian not only acted as my first counselor to navigating scientific research, but also provided my first example of the intensity a person should have when doing scientific research. Dr. Enoch Baldwin provided me with my first opportunity to perform research and a level of detailed mentoring I have yet to see again. This was all done with no guarantee that he would be benefit from my training. Fortunately, I was able to spend two years working and learning in his lab which undoubtably was key to the pursuit of the work presented here. It is important to note that all three of the individuals above provided their critical guidance at a time when they were complete strangers to me, which speaks to their personal character.

There are several people in the Isacoff lab who greatly aided in my training. Most importantly Joshua Levitz and Reza Vafabakhsh. Joshua Levitz trained and guided me through understanding metabotropic glutamate receptors and acted as daily example that a scientist's first responsibility is to be scholar before anything else. Reza Vafabakhsh trained me in single molecule microscopy with an incredible level of enthusiasm and was a constant reminder that a scientist should treat their work with a level artistry and emotion as to not forget our purpose. Without both Josh and Reza I would not have been capable in pursing any of the projects presented here.

My counterpart and a critical collaborator within the Isacoff lab was Adam Hoagland, who joined as a graduate student the same year as . Adam not only provided critical analytic insights into the work in this thesis but, also provided an excellent laboratory companion with an endless list of existential questions providing a needed departure from the tunnel vision that inevitably develops when working on project. Zhu Fu has also been crucial to the work in this thesis. Without Zhu most of the microscopic observations made would prove incomplete without her biochemical and animal work. Zhu's kindness and carefulness has made her an incredible collaborator which I will miss in the future.

I have been lucky to have several post doc researchers who joined the lab around the same time as me and have also provided daily examples of how a professional research should conduct themselves. Prashant Donthamsetti not only provided a constant source of insight and direction into my ongoing projects, but also showed me how powerful a single question can be if it addresses the subtle assumptions within a biological question. Autoosa Salari has been a positive professional example of how a scientist should not be shy about the questions they find most interesting and to always embrace curiosity. Victoria Chou's constant excitement about

research has certainly made the immense amount of time spent in lab more enjoyable as well as her patience with me when I am attempting to develop an explanation for a new observation. Amy Winans has also provided a valuable professional insight and a very useful reminder that as my training continues I will have to responsible for creating my opportunities to ask questions I am interested in. Finally, I would like thank Shashank Bharill and Cherise Stanley who were both in the lab when I joined and played a large role in making me feel welcomed and creating an enjoyable environment which eases the difficulty of pursing scientific projects.

Chapter I: Introduction

Synaptic Plasticity and the role of Glutamate

A fundamental feature of the central nervous system is the ability to change over time which underlies all learning and memory[1,2]. Neuronal activity generated by an experience modifies neural circuit function and in turn modifies thoughts, emotions and behavior[3]. These higher order changes are manifested at specialized structures for neuronal communication called synapses which use neurotransmitters as a medium for communication[4]. Synaptic plasticity refers to activity dependent modification that alters the strength or efficacy of synaptic transmission[1,2]. These changes in synaptic strength determine if and where action potentials propagate and or terminate ultimately controlling information flow throughout the nervous system. This has led to understanding the mechanism of synaptic plasticity becoming a key topic in the field of neuroscience with implications impacting our understanding of normal and pathological function.

Glutamate is the main excitatory neurotransmitter and a critical neuromodulator in the mammalian central nervous system and plays a critical role in synaptic plasticity[5]. Glutamate exerts these synaptic changes through two different receptor types, ionotropic glutamate receptors and metabotropic glutamate receptors[6]. Ionotropic glutamate receptors are ligand gated calcium channels that act on the fast time scale[7]. Metabotropic glutamate receptors are class C G-protein coupled receptors that enact changes through multiple cell signaling pathways and last from tens of seconds to hours and even days[8]. This longer time scale and the modulatory nature of mGluRs makes them very attractive drug targets for several neurological disorders. Unfortunately, several decades of intense effort has yet to yield any approved drugs. This shortcoming is most likely dependent on a lack of molecular and kinetic characterization of these receptors.

G protein-coupled receptors

G-protein coupled receptors are the largest family of transmembrane proteins in the human genome with over 800 different receptors divided into 6 classes (A through F). These receptors play critical roles in virtually every cellular process and are by far the most successful drug targets acting as targets to roughly 34% of all FDA approved drugs[9]. A defining structural feature of GPCRs is a 7 pass transmembrane helix fold and canonically GPCRs activate heterotrimeric G-proteins by catalyzing the release of GDP for GTP which dissociates the trimer into Gα and Gβγ. Upon dissociation Gα and Gβγ can activate downstream signaling molecules which can alter phosphorylation state, gene expression and metabolic state of a cell[10]. GTPase activity of Gα terminates signaling along with regulatory molecules G-protein receptor kinases which phosphorylate the C-term tail of receptors which recruits β-arrestins and other desensitization and trafficking machinery[11]. There are four species of G-proteins (G_s, G_q, $G_{i/o}$ and $G_{12/13}$) that receptors can signal through[11]. An overwhelming amount of data in the last decade has demonstrated that GPCRs can not only signal through G-proteins but, can also induce cellular changes through β-arrestins, giving rise to a phenomenon called biased signaling and direct interactions with kinases[12]. This diversity of signaling pathways is also complimented by the discovering of GPCR modulating proteins called receptor activity modifying proteins(RAMPs) which are single pass transmembrane proteins that can not only alter the rate of target activation by the receptor, but can also alter the Gα

preference of the receptor[13]. The elucidation of these receptor paradigms is complemented by the atomic structure findings that receptors can have multiple inactive and active conformations and as a result do not behave as bimodal on or off switch, but instead samples an ensemble of conformations[14-17].

The recent insights into these more subtle receptor behaviors began fifteen years ago with the first crystallographic structures of β2-adrenergic receptor[18,19]. These crystallographic structures started a rapid rise of GPCR structures being published, which aided by the developments of single particle reconstruction cryo-electron microscopy, has resulted in an explosion of structures in the last 10 years. These structures have simultaneously greatly advanced the possibility of de novo drug design and in turn painted a more complex picture of receptor activation. Instead of ligands stabilizing a strictly active or strictly inactive conformation ligands change the rate at which distinct conformations are explored[14-17]. This behavior allows the receptors acute temporal responses and in turn makes understanding the dynamics of these specific conformations critical to understanding how these molecules control and interact with their effector molecules. While the wealth of structural information provides atomic level understanding of molecular interactions they only provide static snapshots of the receptors. Unfortunately the amount of insight on the conformational dynamics of these receptors has greatly lagged behind the amount of structural information.

GPCRs are divided into 6 classes, A through F. Class A and B are structurally the most simple with A only containing the 7pass transmembrane domain (TMD) and B containing the TMD and a short N-terminal domain[9]. These two classes make up the majority of studied examples. On the other hand, Class C GPCRs are characterized by large N-terminal domains and act as obligate dimers which is[20]. mGluRs make up an 8 member family within Class C GPCRs and are expressed throughout the central nervous system in and around sites of synaptic transmission[21].

Metabotropic Glutamate Receptors

The mGluR family contains 8 subtypes which are subsequently divided into three groups based on homology, pharmacology and signaling profile[8]. Group I includes mGluR1 and mGluR5 which signal thought $G\alpha_q$ and are located on the post-synaptic side of synapses, where they facilitate or induce long term depression or long term potentiation. Group II is made up of mGluR2 and mGluR3 which couple to $G\alpha_i$ and can be found pre-, post- and peri-synaptically where they typically suppress synaptic transmission. Group III contains mGluR4, mGluR6, mGluR7 and mGluR8 which are all found pre-synaptically and couple to Gαi and suppress synaptic transmission.

At the molecular level, each mGluR subunit contains a clamshell shaped glutamate binding domain followed by a rigid linker region containing several cysteine bridges called the cysteine rich domain and finally the conical 7-pass transmembrane domain[20]. mGluRs are obligate dimers with only a dimeric pair able to respond to glutamate and signal while a monomer is incapable of activating a heterotrimeric G-protein[22]. Traditionally mGluRs were considered to only assemble into homodimeric complexes, but more recently it has been shown that mGluRs can assemble into specific heteromeric combinatinations in-vitro and in-vivo[22-27].

Although all mGluRs signal through one of two G-protein pathways studies have shown that each subtype has a specific expression pattern within the brain which often overlaps with at least one other subtype[21]. In-vitro studies have also demonstrated that most receptors have glutamate affinities around 1 μM[21]. This raises the question as to why two receptors subtypes with similar glutamate affinities and signaling pathways would be required in the same location?

Another feature of synaptic transmission that plays a role in mGluR function is that the synaptic cleft is exposed to wide concentrations of neurotransmitters with specific spatio-temporal concentration profiles in small extracellular volumes[28,29]. The requirement of responding appropriately to this environment requires tuning of the receptor responses. There is a wealth of information characterizing individual mGluR subtypes but, far fewer studies have investigated modulation of mGluRs.

Analysis of LBD interface mutants and mGluR2/3 heterodimers

Biochemical studies and multiple structures of mGluR LBDs have shown that LBDs interact through multiple dimer interfaces and a cysteine bridge. In the second chapter we sought to test the effects these interactions have activation of mGluR2 homodimers using single molecule fluorescence resonance energy transfer(smFRET). We found that the hydrophobic interface in mGluR2 stabilizes the active state and that the cysteine loop of mGluR2 promotes activation through stabilizing the closed-closed LBD conformation. We then sought to use smFRET to characterize mGluR2/3 heterodimers. mGluR2 and mGluR3 homodimers differ in that mGluR3 undergoes basal activation. We find that S152 is responsible for mGluR3 basal activation and that mGluR2/3 heterodimers basal activation is half the magnitude seen in mGluR3 homodimers.

Heterodimerization gives rise to emergent properties in mGluR2/7

In the third chapter we turn our attention to mGluR7. This Group III member is unique amongst all other mGluRs in that it has a very low glutamate affinity, roughly 1mM as opposed to the low micromolar affinity seen in all other subtypes. Yet, mGluR7 is one of the most widely expressed subtypes and mGluR7 knock out mice show deficits in learning, memory consolidation and develop absence epilepsy. Using smFRET we find that glutamate affinity was in fact even lower than previously reported, ~38mM, and that maximal efficacy reached with glutamate is only 10%. We subsequently find that mGluR2 and mGluR7 share overlapping expression patterns in the hippocampus and using immunohistochemistry we see that mGluR2 and mGluR7 assemble into mGluR2/7 heterodimers in native tissues. SmFRET of mGluR2/7 reveals a higher glutamate affinity than the mGluR2/2 homodimer. Each subunit acts as a positive allosteric modulator to its partner subunit and these enhancements to activation are caused by an apo state rotation mGluR2/7 undergoes.

Allosteric mechanisms controlling affinity and efficacy of mGluR homodimers and heterodimers

In the fourth chapter I continue to examine the molecular determinants of mGluR7's unusual glutamate insensitivity. mGluR4 serves as an ideal comparative model due to its much higher glutamate affinity and high sequence similarity to mGluR7. I find that the ligand binding residues of mGluR7 has very little effect on mGluR7 affinity and efficacy and instead the lower LBD interface is responsible for mGluR7s insensitivity to glutamate. I then elucidate the mechanism responsible for the unique properties mGluR2/7. Using mGluR2/4 as a comparison, which does not see positive allostery upon heterodimerization. We see that mutating three glycine residues within the mGluR4 cysteine loop enables positive allostery of mGluR2/4 and in turn very closely resembles the emergent properties seen in mGluR2/7. This leads us to conclude that the

cysteine loop is a critical path of allosteric communication between heterodimers and that the flexibility of the loop is the determinant in positive allostery.

References:

1. Zucker, R. S., & Regehr, W. G. (2002). Short-Term Synaptic Plasticity. Annual Review of Physiology, 64(1), 355–405. doi:10.1146/annurev.physiol.64.092501.114547
2. Citri A, Malenka RC. Synaptic plasticity: multiple forms, functions, and mechanisms. Neuropsychopharmacology. 2008 Jan;33(1):18-41. doi: 10.1038/sj.npp.1301559. Epub 2007 Aug 29. PMID: 17728696.
3. Neves, G., Cooke, S. F., & Bliss, T. V. P. (2008). Synaptic plasticity, memory and the hippocampus: a neural network approach to causality. Nature Reviews Neuroscience, 9(1), 65–75. doi:10.1038/nrn2303
4. Magee, J. C., & Grienberger, C. (2020). Synaptic Plasticity Forms and Functions. Annual Review of Neuroscience, 43(1), 95–117. doi:10.1146/annurev-neuro-090919-022842
5. Zhou, Y., & Danbolt, N. C. (2014). Glutamate as a neurotransmitter in the healthy brain. Journal of Neural Transmission, 121(8), 799–817. doi:10.1007/s00702-014-1180-8
6. Reiner, A., & Levitz, J. (2018). Glutamatergic Signaling in the Central Nervous System: Ionotropic and Metabotropic Receptors in Concert. Neuron, 98(6), 1080–1098. doi:10.1016/j.neuron.2018.05.018
7. Twomey, E. C., & Sobolevsky, A. I. (2017). Structural Mechanisms of Gating in Ionotropic Glutamate Receptors. Biochemistry, 57(3), 267–276. doi:10.1021/acs.biochem.7b00891
8. Niswender, C. M. & Conn, P. J. Metabotropic glutamate receptors: physiology, pharmacology, and disease. *Annu. Rev. Pharmacol. Toxicol.* 50, 295–322 (2010).
9. Weis, W. I. & Kobilka, B. K. The molecular basis of G protein-coupled receptors activation. *Annu. Rev. Biochem.* 87, 897–919 (2018).
10. Hilger, D., Masureel, M., & Kobilka, B. K. (2018). Structure and dynamics of GPCR signaling complexes. Nature Structural & Molecular Biology, 25(1), 4–12. doi:10.1038/s41594-017-0011-7
11. Syrovatkina, V., Alegre, K. O., Dey, R., & Huang, X.-Y. (2016). Regulation, Signaling, and Physiological Functions of G-Proteins. Journal of Molecular Biology, 428(19), 3850–3868. doi:10.1016/j.jmb.2016.08.002
12. Wootten, D., Christopoulos, A., Marti-Solano, M., Babu, M. M., & Sexton, P. M. (2018). Mechanisms of signalling and biased agonism in G protein-coupled receptors. Nature Reviews Molecular Cell Biology, 19(10), 638–653. doi:10.1038/s41580-018-0049-3
13. Hay, D. L., & Pioszak, A. A. (2016). Receptor Activity-Modifying Proteins (RAMPs): New Insights and Roles. Annual Review of Pharmacology and Toxicology, 56(1), 469–487. doi:10.1146/annurev-pharmtox-010715-103120
14. Isogai, S. et al. Backbone NMR reveals allosteric signal transduction networks in the β1-adrenergic receptor. *Nature* 530, 237–241 (2016).
15. Liu, W. et al. Structural basis for allosteric regulation of GPCRs by sodium ions. *Science* 337, 232–236 (2012).
16. Manglik, A. & Kobilka, B. The role of protein dynamics in GPCR function: insights from the β2AR and rhodopsin. *Curr. Opin. Cell Biol.* 27, 136–143 (2014).
17. Nygaard, R. et al. The dynamic process of β2-adrenergic receptor activation. *Cell* 152, 532-542 (2013).
18. Rasmussen, S. G. et al. Crystal structure of the human b2 adrenergic G-protein coupled receptor. Nature 450, 383–387 (2007).
19. Rosenbaum, D. M. et al. GPCR engineering yields high-resolution structural insights into b2-adrenergic receptor function. Science 318, 1266–1273 (2007)
20. Koehl, A. et al. Structural insights into the activation of metabotropic glutamate receptors. *Nature* 566, 79–84 (2019).
21. Ferraguti, F., & Shigemoto, R. (2006). Metabotropic glutamate receptors. Cell and Tissue Research, 326(2), 483–504. doi:10.1007/s00441-006-0266-5
22. El Moustaine, D., Granier, S., Doumazane, E., Scholler, P., Rahmeh, R., Bron, P., … Pin, J.-P. (2012). Distinct roles of metabotropic glutamate receptor dimerization in agonist activation and G-protein coupling. Proceedings of the National Academy of Sciences, 109(40), 16342–16347. doi:10.1073/pnas.1205838109
23. Doumazane, E. et al. A new approach to analyze cell surface protein complexes reveals specific heterodimeric metabotropic glutamate receptors. *FASEB J.* 25, 66–77 (2011).
24. Levitz, J. et al. Mechanism of assembly and cooperativity of homomeric and heteromeric metabotropic glutamate receptors. *Neuron* 92, 143–159 (2016).
25. El Moustaine, D. et al. Distinct roles of metabotropic glutamate receptor dimerization in agonist activation and G-protein coupling. Proc. Natl Acad. Sci. USA 109, 16342–16347 (2012).
26. Yin, S. et al. Selective actions of novel allosteric modulators reveal functional heteromers of metabotropic glutamate receptors in the CNS. *J. Neurosci.* 34, 79–94 (2013).
27. Habrian, C. H., Levitz, J., Vyklicky, V., Fu, Z., Hoagland, A., McCort-Tranchepain, I., … Isacoff, E. Y. (2019). Conformational pathway provides unique sensitivity to a synaptic mGluR. Nature Communications, 10(1). doi:10.1038/s41467-019-13407-8
28. Zhou, Y., & Danbolt, N. C. (2014). Glutamate as a neurotransmitter in the healthy brain. Journal of Neural Transmission, 121(8), 799–817. doi:10.1007/s00702-014-1180-8
29. Moussawi, K., Riegel, A., Nair, S., & Kalivas, P. W. Extracellular glutamate: functional compartments operate in different concentration ranges. *Front. Syst. Neurosci*. 5, 94 (2011).

Chapter II: Mechanism of Assembly and Cooperativity of Homomeric and Heteromeric Metabotropic Glutamate Receptors

This chapter was published as an article in Neuron volume 92, issue 1, pages 143-159 in October 2016 with me as second author.

Introduction:

In order to understand the roles played by the ligand binding domain (LBD) we embarked on an investigation of how assembly and cooperativity are differentially regulated in mGluR2 homodimers and mGluR2/3 heterodimers. A previous single molecule study demonstrated a conformational pathway for mGluR2 homodimers[1]. In this model activation occurs through a rate limiting a single ligand binding event, followed immediately by a second ligand binding event. Closure of both LBDs permits rearrangement of the LBDs relative to one another which subsequently leads to TMD rearrangement and G-protein activation. To gain a more detailed understanding of this activation pathway we performed mutations at the LBD interface and cysteine loop revealing their individual contribution contributions to the glutamate induced LBD rearrangement.

Assembly into homo- or hetero-oligomeric complexes has emerged as a potentially crucial aspect of GPCR function, which can modulate sensitivity to stimuli, basal activity, effector coupling, ligand bias, kinetics, and subcellular targeting[2-4]. Breakthrough studies have provided snapshots of GPCR structures in distinct conformations[5-7] and revealed that they are extremely dynamic[8-11]. This has led to the emerging idea that conformational dynamics are central to ligand recognition, activation and signaling by GCPRs. However, little is known about the impact of oligomerization on GPCR conformational dynamics and whether or how this confers cooperativity onto signaling.

Despite the interest in GPCR oligomerization, complexes have been difficult to observe and analyze structurally or biophysically within the class A and B families of GPCRs[12]. However, class C GPCRs, which are characterized by a large extracellular ligand binding domain (LBD), have been shown to assemble into stable dimers or higher order oligomers both in crystal structures of isolated LBDs[13,14] and biochemical or spectroscopic analyses of full length proteins[15-18].

Metabotropic glutamate receptors (mGluRs) are class C GPCRs that modulate synaptic strength and serve as drug targets for neurological disorders[19]. mGluRs consist of three domains: an N-terminal bi-lobed LBD, a 7 helix trans-membrane domain (TMD) and a cysteine rich domain (CRD) that links the LBD to the TMD. Dimerization of full length mGluRs is required for G protein activation[20] and has been shown to be partially mediated by an intersubunit disulfide bridge between the LBDs[21]. Biochemical and spectroscopic studies have shown that activation coincides with intersubunit reorientation of both the extracellular and transmembrane domains of the receptor[22-25]. However, the mechanisms of dimerization and the role of dimer interfaces in activation, intersubunit communication and mGluR function are not clear.

In this study we use quantitative subunit counting to find that mGluR homo- and hetero-dimerization depends primarily on interactions at a hydrophobic interface in the upper lobe of the LBD, with modest contributions from an intersubunit disulfide bridge and TMD interaction.

Fluorescence resonance energy transfer (FRET) enables us to quantify the contribution of interface hot spots to global conformational dynamics. An approach to targeted, single subunit activation, using photoswitchable tethered ligands in dimers of defined stoichiometry, enables us to unravel the mechanism of cooperativity in mGluR activation. We find that cooperativity in dimers gives rise to boosted activity and that heterodimerization gives rise to the emergence of unique biochemical properties. Our observations lead to a model of mGluR gating that accounts for cooperativity in basal activity in the absence of agonist as well as partial and full activation across the concentration range of agonist in both homo- and heterodimers.

.

Results:

Dimerization is primarily mediated by interactions between ligand binding domains

Previous studies of mGluR oligomerization employed classical biochemical methods to assay denatured proteins *in vitro* [21,26,27] or ensemble (macroscopic) time-resolved FRET on receptors in the plasma membrane of live cells, which relies on theoretical models and is sensitive to conformational changes[16]. To analyze mGluR stoichiometry, we used single molecule subunit imaging of individual protein complexes to count photobleaching steps in green fluorescent protein (GFP)-tagged receptors. We expressed a C-terminally GFP-tagged mGluR2 (mGluR2-GFP) in *Xenopus* oocytes at low density to ensure that individual complexes would be spatially resolved as individual fluorescent spots (Fig. 2.1A; Supplementary Fig. 2.1A). Using total internal reflection (TIRF) microscopy to confine excitation to the plasma membrane, we observed GFP photobleaching (Fig. 2.1B) and found that all spots bleached in one or two steps, with ~60% bleaching in two steps (Fig. 2.1C, Supplementary Fig. 2.1A). This is consistent with mGluR2 being a dimer, with a probability of ~0.7 that its GFP is fluorescent (Supplementary Fig. 2.1A), due to 20-30% of GFPs which either mis-fold or fail to undergo chromophore maturation[28,29].

Importantly, mGluR2-GFP proved to be functional, supporting glutamate-induced currents from co-expressed G protein activated inward rectifier potassium (GIRK) channels (Supplementary Fig. 2.1A). Similar photobleaching distributions were obtained with GFP-tagged versions of mGluR3 (group II), mGluR7(group III), and mGluR1 and mGluR5 (group I); and each of these was also functional, producing glutamate-induced GIRK current (mGluR3 and 7) or calcium-activated chloride current (mGluR1 and 5) (Supplementary Fig. 2.1B-E).

We next asked which domains mediate dimerization. We truncated mGluR2-GFP by removing only the LBD (ΔLBD-GFP) or the entire extracellular domain (ΔECD-GFP). In both cases we observed a near-complete reduction in 2-step photobleaching (Fig 2.1C; Supplementary Fig. 2.1F, G), indicating that the extracellular domain, particularly the LBD, is required for efficient dimerization.

Subunit counting in *Xenopus* oocytes requires low expression levels in order to resolve single molecules in the plasma membrane. To analyze stoichiometry under high density expression, we expressed mGluR2-GFP under the CMV promoter in HEK293T cells (Supplementary Fig. 2.1H) and isolated receptors in detergent using the SimPull technique to obtain a low density of immune-purified protein on a passivated surface (Fig. 2.1D)[23]. Consistent with results from oocytes, ~60% of mGluR2-GFP spots bleached in two steps in SimPull (Supplementary Fig. 2.1H). ΔECD-GFP expressed at lower levels and had poorer surface localization compared to mGluR2-GFP (Supplementary Fig. 2.1I). Interestingly, although deletion of the extracellular domain reduced 2-step photobleaching (Fig. 2.1F, Supplementary Fig. 2.1I), this reduction was less extreme than what was seen in *Xenopus* oocytes (Fig. 2.1C). ΔECD-GFP constructs for both mGluR3 and mGluR1 showed a similar behavior (Supplementary Fig. 2.1J). These observations suggest that, at the high expression density obtained in HEK293T cells, parts of the protein other than the ECD contribute to dimerization. This interpretation was supported by the finding that SimPull from oocytes injected with 100-fold higher levels of RNA for ΔECD-GFP leads to an increase in the percentage of 2-step photobleaching spots (~30% vs.<5%) (Supplementary Fig. 2.1K).

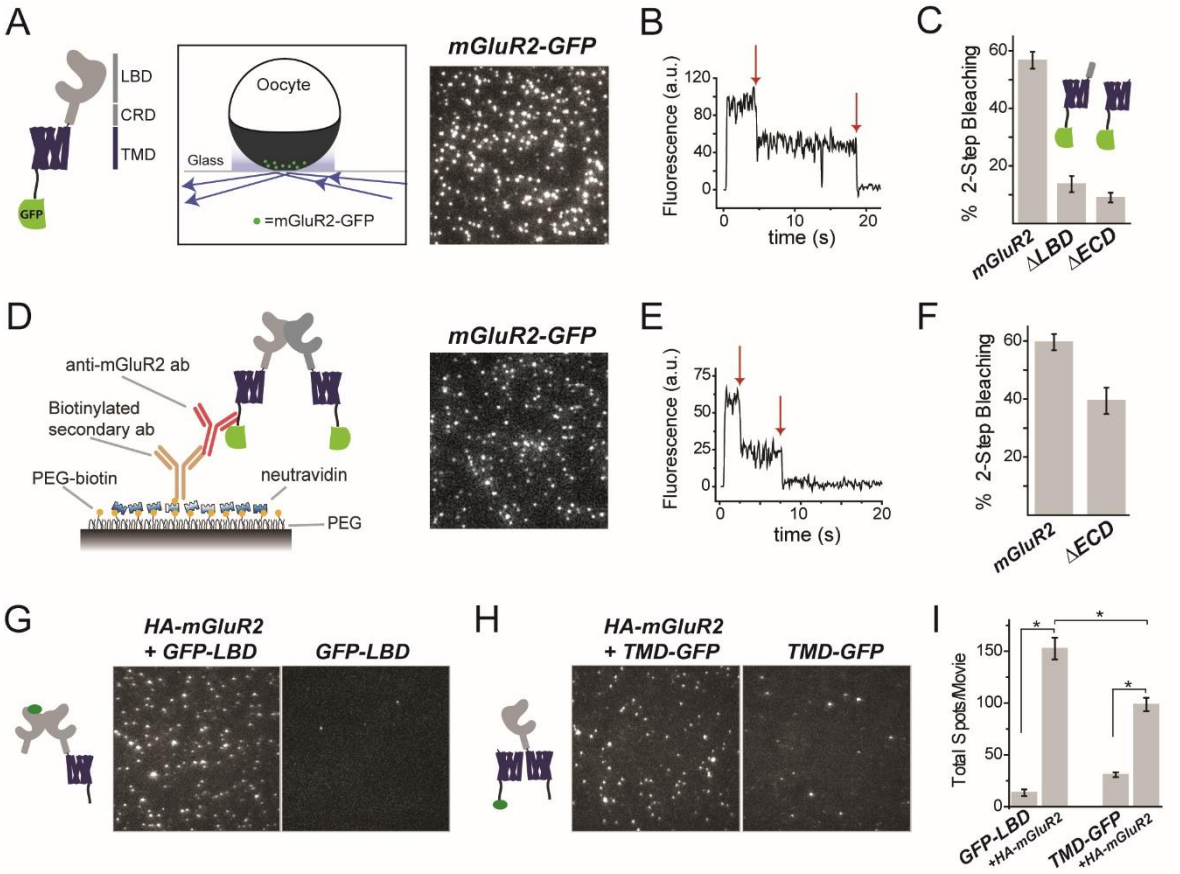

Figure 2.1, Dimerization of mGluR2 is mediated primarily by ligand binding domain. A) Left, domain structure of the mGluR2-GFP construct. LBD=Ligand Binding Domain; CRD=Cysteine Rich Domain; TMD=Transmembrane Domain. Right, schematic showing TIRF image of single mGluR2-GFP molecules in the plasma membrane of oocytes. B) Representative photobleaching trace for a single mGluR2-GFP complex. Arrows show photobleaching steps. C) Summary of photobleaching step analysis for mGluR2-GFP and truncations. ~60% 2- step photobleaching is consistent with a strict dimer with ~75% GFP maturation. D) Left, Schematic showing SimPull technique for pulldown with an anti-mGluR2 antibody. Right, representative TIRF image of single mGluR2-GFP molecules isolated from HEK293T cell lysate. E) Representative photobleaching trace for a single mGluR2-GFP complex. F) Summary of photobleaching step analysis for mGluR2-GFP and ΔECD-GFP in SimPull. G-H)TIRF images of single GFP-LBD (G) or TMD-GFP (H) subunits isolated using an anti-HA antibody in the presence or absence of full length HA-mGluR2. I) Summary of pull down efficiency for GFP-LBD and TMD-GFP in the absence or presence of HA-mGluR2. (Unpaired t-test, p=0.00003 between GFP-LBD with and without HA-SNAP; p=0.0001 between TMD-GFP with and without HA-SNAP; p=0.004 between GFP-LBD and TMD-GFP.) Error bars show S.E.M. calculated from multiple experiments (N≥3).

To further probe the roles of the LBD and the TMD in dimerization, we examined the ability of truncated domains to co-assemble with full length mGluR2. Co-expression of either "GFP-LBD" or "TMD-GFP" (ΔECD-mGluR2-GFP) with full length HA-mGluR2, followed by SimPull with anti-HA antibodies led to immobilization of GFP spots (Fig. 2.1G,H) with more efficient co-assembly of mGluR2 with the isolated LBD than with the isolated TMD (Fig. 2.1I). Most spots bleached in a single step confirming that one full length mGluR2 subunit co-assembles with a single isolated domain (92.4 ± 0.1% for GFP-LBD and 89.6± 0.8% for TMD-GFP). These

experiments confirm that the primary dimer interface is the LBD, with the TMD representing a secondary interface.

Given the primary role of the LBD in dimerization, we investigated the inter-LBD dimer interface by examining crystal structures of the isolated LBDs of mGluRs (Fig. 2.2A)[30,31]. In both the relaxed and active states, a cluster of conserved hydrophobic residues in helices B and C lie at an interface between the upper LBD lobes (LB1) (Fig. 2.2A; Supplementary Fig. 2.2A, B). In the active state, an additional interface is observed between conserved charged residues in the lower LBD lobes (LB2), where Gd3+ has been shown to bind in mGluR1[31] (Fig. 2.2A; Supplementary Fig. 2.2C). Furthermore, a conserved cysteine (C121 in mGluR2), located in the structurally unresolved loop between helices B and C, has been shown to be crucial for dimerization in denaturing gels[1]; (Fig. 2.2A; Supplementary Fig. 2.2A). We mutated residues at these potential interfaces and found a major reduction in dimerization in the plasma membrane of *Xenopus* oocytes with mutations at the LB1 interface, but only a minor reduction with a mutation of C121 to alanine (Fig. 2.2B; Supplementary Fig. 2.2D; Unpaired T-tests, p=0.003 between C121A and L103A, p=0.0003 between C121A and L154A, p=0.00006 between C121A and 3xLB1). Consistent with the weak effect of C121, application of DTT, to reduce a potential inter-subunit disulfide bond, did not alter receptor stoichiometry in wild type (WT) mGluR2-GFP

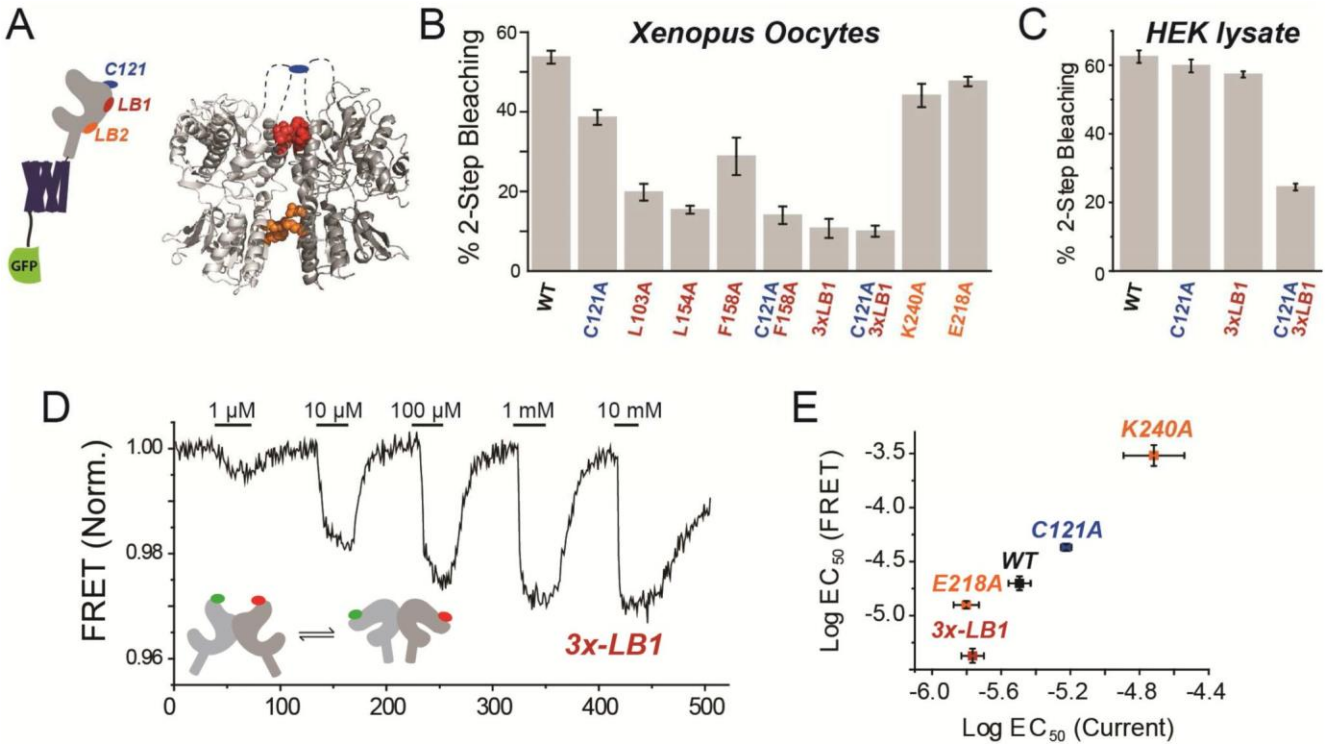

Figure 2.2, Mutational analysis of mGluR2 dimer interface: assembly and function effects. A) Schematic, left, and crystal structure of mGluR1 in the "active" state (PDB: 1EWK), right, showing 3 regions proposed to form the LBD dimer interface. B-C) Summary of stoichiometry of dimer interface mutants in oocytes and SimPull from HEK293T cell lysate "3x-LB1" is the construct containing L103A, L154A, and F158A mutations. D) Representative FRET trace showing glutamate-induced reductions in intersubunit FRET between LBDs for N-terminally SNAP and CLIP-tagged versions of mGluR2-3xLB1. E) Summary of glutamate EC50 determinations from activation of GIRK channels (current) *versus* LBD conformational change (FRET) in mGluR2WT (WT) and dimer interface mutants. Error bars show S.E.M. calculated from multiple experiments (N≥3).

(Supplementary Fig. 2.2E). However, in the background of the single mutation F158A to the

hydrophobic LB1 interface, the additional mutation of C121A further reduced dimerization (Fig. 2.2B). In contrast, LB2 mutants E218A and K240A did not significantly alter dimerization (Fig. 2.2B). Under high-density expression in HEK293T cells, followed by SimPull purification, dimerization was only reduced when all three LB1 mutations ("3xLB1") were combined with the C121A mutation (Fig. 2.2C). We also analyzed expression and surface targeting of dimer interface mutants using confocal imaging. C-terminally GFP-tagged versions of mGluR2wt, 3xLB1, C121A, and 3xLB1/C121A showed clear membrane enrichment and similar levels of fluorescence (Supplementary Fig. 2.2F). We quantified surface targeting with membrane impermeable dye conjugation to N-terminally SNAP-tagged variants and found similar levels for all variants tested (Supplementary Fig. 2.2G,H). Together these experiments show that dimerization is mediated primarily by the hydrophobic LB1 interface, along with a weak contribution from a covalent intersubunit disulfide bridge, and little contribution from the LB2 interface.

Role of mGluR2 homodimer LBD interface in conformational dynamics and activation

We next asked how the LBD dimer interfaces affect receptor function by recording glutamate-evoked currents from HEK293T cells co-expressing WT or mutant versions of mGluR2 along with the GIRK channel. Interestingly, we found that the mGluR2-C121A mutation *reduced* apparent glutamate affinity (Supplementary Fig. 2.2I), whereas weakening of the LB1 interface with the triple mutant 3xLB1 *increased* apparent glutamate affinity (Supplementary Fig. 2.2I). To directly measure the activation-associated conformational changes of the LBDs, we performed an ensemble intersubunit FRET assay in HEK293T cells using mGluRs that were fused at their N-terminus to SNAP- or CLIP-tags and conjugated to acceptor (Alexa-647) or donor (DY-547) fluorophores[22], respectively. As shown earlier, glutamate binding induces closure and reorientation of the LBD that increase distance between the fluorophores, thus reducing FRET[22]. Consistent with the GIRK assay, glutamate dose-response curves of the conformational changes associated with activation revealed that the C121A mutant reduces apparent affinity and the 3xLB1 triple mutant increases apparent affinity (Fig. 2.2D, E; Supplementary Fig. 2.2J). Neutralization of charged residues on helix F in the LB2 interface also had an effect: K240A strongly decreased the apparent glutamate affinity, as recently reported[23], while E213A, E218A, and E222A weakly increased apparent affinity (Fig. 2.2E; Supplementary Fig. 2.2K, L) (Unpaired T-test with mGluR2; p=0.0034 for E213A, p=0.0037 for E218A, and p=0.28 for E222A).

To better understand the role of the dimer interfaces in activation, we turned to single molecule FRET (smFRET), which recently revealed that group II mGluRs transition between three states with distinct FRET efficiencies: ~0.45 ("high"), ~0.35 ("medium"), and ~0.2 ("low"), with the low FRET state corresponding to the active conformation[23]. As seen before, in the absence of glutamate mGluR2WT shows few transitions out of the high FRET state, and in saturating glutamate few transitions out of the low FRET state, but at intermediate concentrations it shows rapid dynamics (Supplementary Fig. 2.3A- C). In contrast, in the absence of glutamate, mGluR2-3xLB1 showed transitions from the inactive high FRET state to the intermediate and low FRET states (Fig. 2.3A), with predominant occupancy of the activated state (Fig. 2.3B). Glutamate application further increased occupancy of the low FRET state (Fig. S3D), fully occupying it at

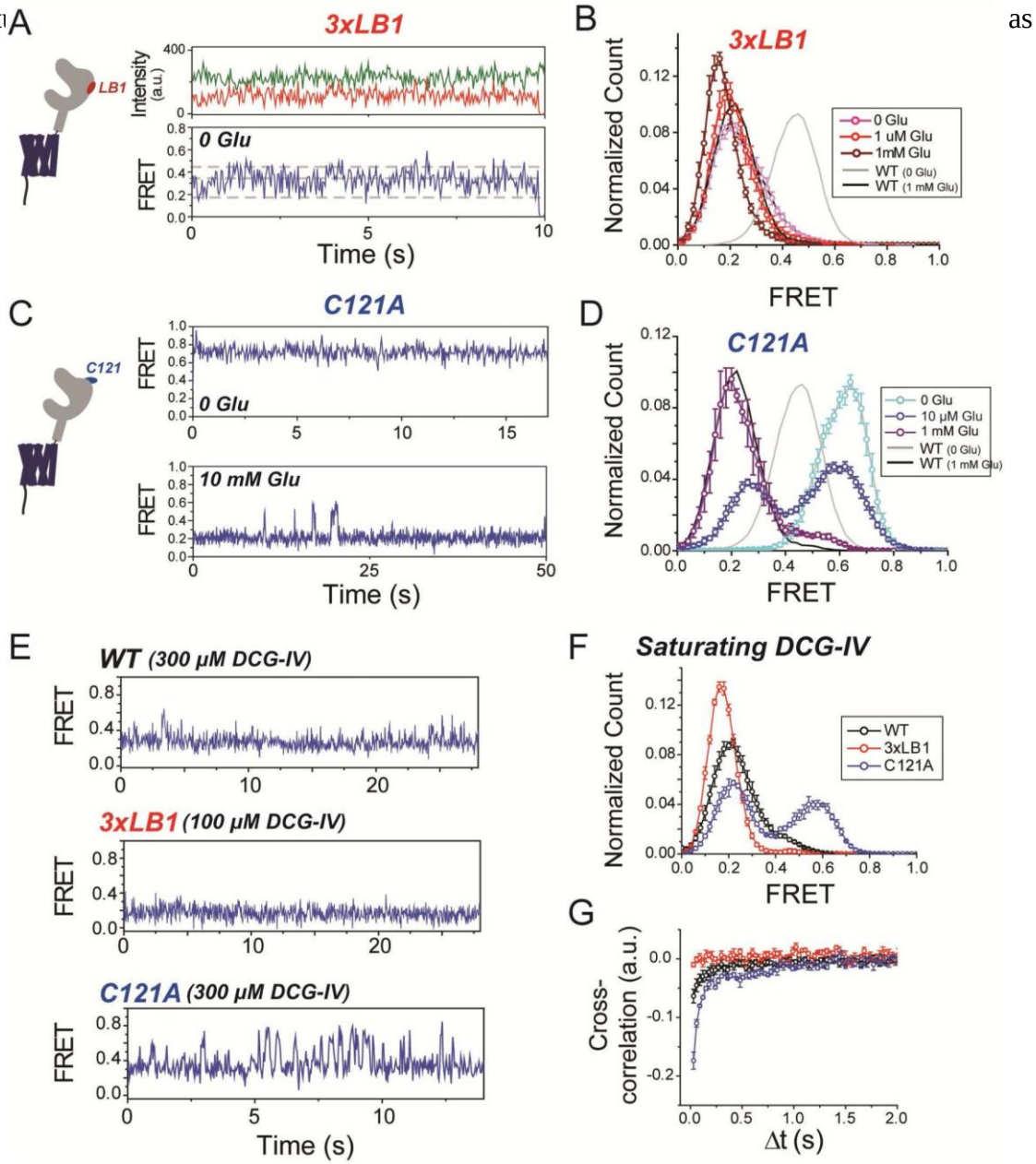

Figure 2.3, smFRET analysis of mGluR2 LBD interface mutants. A) smFRET traces of mGluR2-3xLB1 showing spontaneous dynamics in the absence of glutamate. Top, donor (green) and acceptor (red) fluorescence for a single mGluR2-3xLB1 dimer. Bottom, smFRET calculated from donor and acceptor fluorescence values in top traces. Dotted gray lines show the 3 FRET states obtained from Gaussian fits of smFRET histograms. B) Histogram showing smFRET distributions for mGluR2-3xLB1. Distributions for mGluR2WT in 0 (grey) or 1 mM glutamate (black) are shown as solid lines for comparison. C) Representative smFRET traces of mGluR2-C121A, in the absence of glutamate (top) and for mGluR2-C121A showing transitions to resting conformation in the presence of saturating 10 mM glutamate (bottom). D) Histogram showing smFRET distributions for mGluR2-C121A. Note the small increase in high FRET population for C121A in the presence of saturating glutamate compared to WT. E) Representative smFRET trace for WT, 3xLB1, and C121A showing the level of dynamics in the presence of saturating DCG-IV (100 uM for C121A; 300 uM for WT, 3xLB1). F) Histogram showing smFRET distributions for WT, 3xLB1, and C121A in the presence of saturating DCG-IV. G) Cross-correlation plots showing relative dynamics for WT, 3xLB1, and C121A in the presence of saturating DCG-IV. Error bars show S.E.M. calculated from multiple experiments (N≥3).

measured by donor and acceptor cross-correlation (Fig. S3E). Interestingly, this lowest FRET state of mGluR2(3xLB1) was lower in FRET than what was observed in mGluR2WT (Fig. 2.3B, Supplementary Fig. 2.3F), suggesting that 3xLB1 stabilizes a state with increased degrees of LBD closure and/or dimer reorientation. These observations suggest that the hydrophobic LB1 interface provides energy to prevent spontaneous LBD closure and dimer reorientation in the absence of agonist.

In contrast, in the absence of glutamate, mGluR2(C121A) displayed minimal dynamics and was shifted to a higher peak FRET of the inactive conformation (~0.6 vs. ~0.45; Fig. 2.3C, D). Application of glutamate increased the population of the low FRET conformation, but with a lower apparent affinity than seen in WT mGluR2 (Fig. 2.3D; Supplementary Fig. 2.3G, H). Even in saturating glutamate (10 mM) mGluR2(C121A) showed dynamics out of the low FRET state (Fig. 2.3C, **bottom**; Supplementary Fig. 2.3I). These observations suggest that the intersubunit disulfide bridge primes the resting conformation for the activation rearrangement and stabilizes the active state.

To further examine the differences between the hydrophobic LB1 ("3xLB1") and covalent ("C121A") interfaces, we performed smFRET experiments with the partial agonist DCG-IV which we previously showed to have partial efficacy due to partial active state occupancy at saturating concentrations[23]. Compared to mGluR2WT, at saturating DCG-IV, mGluR2(C121A) showed a much reduced occupancy of the low FRET state, while mGluR2(3xLB1) showed a greater low FRET state occupancy (Fig. 2.3E, F). Consistent with this, dynamics at saturating DCG-IV were abolished in mGluR2(3xLB1) and increased in mGluR2(C121A) (Fig. 2.3E, G). These results support the interpretation that the active state is stabilized by the 3xLB1 mutation and destabilized by the C121A mutation.

We also measured smFRET from the mGluR2(3xLB1/C121A) quadruple mutant. Similar to mGluR2(3xLB1), the quadruple mutant showed spontaneous dynamics, including visits to the active state (Supplementary Fig. 2.3J, K), indicating that an intact disulfide bond is not required for the introduction of basal conformational dynamics by the 3xLB1 mutant. However, like mGluR2(C121A), the quadruple mutant showed an increase in FRET values associated with inactive states, as well as incomplete population of the active state in saturating glutamate (Supplementary Fig. 2.3J, K). In saturating DCG-IV, mGluR2(3xLB1/C121A) populated the low FRET state at a level intermediate between that of the 3xLB1 or C121A mutant alone Supplementary Fig. 2.3M), and had a slight decrease in low FRET peak value, similar to 3xLB1 (Supplementary Fig. 2.3M). Together these observations indicate that mutations to LB1 and the disulfide interface have effects that do not occlude one another, suggesting that they act through distinct mechanisms. Having established the roles of dimer interfaces in the assembly and activation of mGluR2, we next turned to an analysis of heteromeric combinations of mGluR2.

Heterodimerization of mGluR2: preference for mGluR3 and role of the LBD

Initial biochemical studies did not find evidence for mGluR heteromerization between subtypes[15], but recent spectroscopic and biochemical studies have indicated that mGluRs can heteromerize, although there has not been complete agreement about which combinations are possible[32,33]. To assess the ability of mGluR2 to heteromerize with other subtypes, we turned again to single molecule subunit counting. We first co-expressed mGluR2-GFP with excess untagged mGluRs and measured the ability of the untagged mGluR to assemble with mGluR2-GFP to create heterodimers with only one GFP. For example, co-expression of mGluR2-GFP with untagged

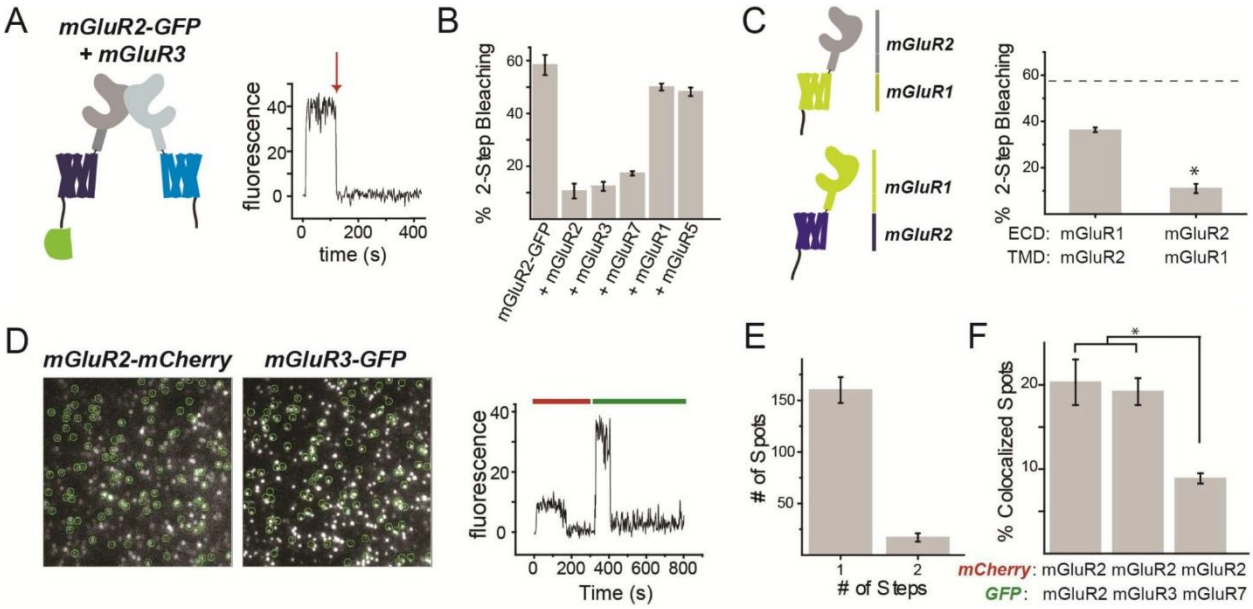

Figure 2.4, mGluR2 heterodimerizes with Group II/III mGluRs and prefers intra- over inter- group assembly. A-B) Coexpression of excess untagged group II or III mGluRs decreases 2-step photobleaching of mGluR2-GFP in *Xenopus* oocytes. C) Co-expression of chimeras between mGluR1 and mGluR2 (left) decreases 2-step photobleaching with a stronger effect when the ECD is from mGluR2 rather than mGluR1 (right). * indicates statistical significance (unpaired t-test, p=.0002). Dotted line shows the level of 2-step bleaching observed for mGluR2-GFP alone. D) Images (left) showing colocalization between mGluR2-mCherry and mGluR3-GFP and representative trace (right) showing 1-step photobleaching in red and green. E) Photobleaching step analysis showing primarily 1-step GFP photobleaching for mGluR3-GFP in complex with mGluR2-mCherry. F) Summary of colocalization analysis for mGluR2-mCherry with either mGluR2-GFP, mGluR3-GFP, or mGluR7-GFP. * indicates statistical significance (unpaired t-test, p=0.0003 between mGluR2 and mGluR7 and p=0.0007). Error bars show S.E.M. calculated from multiple experiments (N≥3).

mGluR3 (Fig. 2.4A) reduced 2-step photobleaching as drastically as did co-expression with untagged mGluR2 (Fig. 2.4B). Untagged mGluR7 was nearly as potent, but group I members mGluR1 and 5 had almost no effect (Fig. 2.4B). These observations agree with recent findings that indicated that group II/III mGluRs cannot co- assemble with group I mGluRs[16]. Consistent with this, in SimPull, mGluR2 pulled down mGluR3-GFP but not mGluR1-GFP (Supplementary Fig. 2.4A, B). Moreover, the mGluR3-GFP spots pulled down by mGluR2 showed single-step photobleaching (Supplementary Fig. 2.4C), confirming the strict heterodimerization.

To identify the domains that mediate heterodimer specificity, we made chimeras between mGluR2 and mGluR1 which contain the ECD of one and the TMD (and C-terminal) of the other (Fig. 2.4C). In oocytes and SimPull, both chimeras remained strict dimers (Supplementary Fig. 2.4D, E). When co-expressed in excess with mGluR2-GFP in *Xenopus* oocytes, both chimeras decreased the 2-step photobleaching of mGluR2-GFP, but this effect was significantly stronger for the construct containing the mGluR2 ECD (Fig. 2.4C). Consistent with this, in SimPull, mGluR2 was able to pull down both chimeras, but was significantly more efficient at pulling down the chimera with the mGluR2 ECD (Supplementary Fig. 2.4F-H).

To directly visualize heterodimers and assess their relative affinities, we performed 2-color photobleaching experiments in *Xenopus* oocytes. We co-expressed mGluR2-mCherry with either mGluR2-GFP, mGluR3-GFP, or mGluR7-GFP at similar surface densities, identified co-localized red and green spots (Fig. 2.4D) and counted photobleaching in the green channel (Fig. 2.4E). mGluR2-mCherry co-localized with all 3 variants to form strict heterodimers (Fig. 2.4E) but a

higher percentage of co-localized spots were found with mGluR2-GFP or mGluR3-GFP compared to mGluR7-GFP (Fig. 2.4F). Together, these experiments show that mGluR2 can heterodimerize with equal affinity with the other group II mGluR, mGluR3, as with itself, as well as with a group III mGluR, albeit with a lower preference.

The importance of the dimer interface in receptor activation (Fig. 2.2, 2.3), suggests that subunit interaction and cooperativity may operate in mGluR2. Furthermore, while smFRET analysis has revealed three intersubunit conformations, it remains unclear how occupancy by zero, one or two ligands in a dimer drives occupancy of those states.

Photoswitchable tethered ligands and linked dimers reveal cooperativity of mGluR2

Having seen that mGluRs dimerize *via* inter-subunit LBD interactions, and that these interactions are important for activation, we asked whether LBD-LBD interaction introduces cooperativity into the activation process. Initial work with radioligand binding and native tryptophan fluorescence suggested negative cooperativity of glutamate binding in isolated mGluR1 LBDs[34]. Ensuing work suggested that binding of glutamate to one subunit can activate mGluRs, but that binding to both subunits activates more efficiently[35], although another study suggested that activation does not occur until 2 ligands bind[36]. These studies faced the difficulty of confining ligand binding to one subunit by using mutations to lower agonist affinity in the other subunit. However, it was not possible to exclude the possibilities that low affinity mutants permit short-lived binding, that the affinity or gating of the mutant subunit is influenced by co-assembly with a wildtype subunit, or that the mutation could itself alter conformational energetics. For these reasons, we turned to the photoswitchable tethered ligand (PTL) approach in which, a cysteine residue on the outer, solvent facing surface of the LBD covalently anchors a "ligand on a string," which can be rapidly and reversibly photoisomerized to place the ligand in the orthosteric binding pocket and thereby agonize or antagonize only that subunit. This approach has been used in a variety of neurotransmitter receptors[37-39], including mGluRs[40,41].

The glutamate-presenting PTL D-MAG-0 ("MAG") (Fig. 2.5A) can be covalently attached to a cysteine substituted onto the solvent exposed surface of the LBD of mGluR2 (mGluR2(L300C)) to form "LimGluR2" (Fig. 2.5B)[40], which is activated rapidly, and with high efficacy by light, as seen by the induction of GIRK current in HEK293 cells (Fig. 2.5C). A similar MAG PTL has been shown in an ionotropic glutamate receptor to function as a high occupancy agonist with a high local concentration. To test if this is the case with mGluR2, we lowered the glutamate affinity of LimGluR2 with the mutation R57A (Supplementary Fig. 2.5A) and still observed large photocurrents with similar efficacy compared to saturating glutamate (Fig. 2.5D; Supplementary Fig. 2.5B). LimGluR2(R57A) also showed a reduced affinity for the antagonist LY341495, but retained block by a negative allosteric modulator (NAM) which binds in the TMD (Supplementary Fig. 2.5E-J). The efficient photoactivation of LimGluR2(R57A) confirms that MAG operates as a high efficacy, high occupancy agonist that makes it well-suited to study receptor cooperativity.

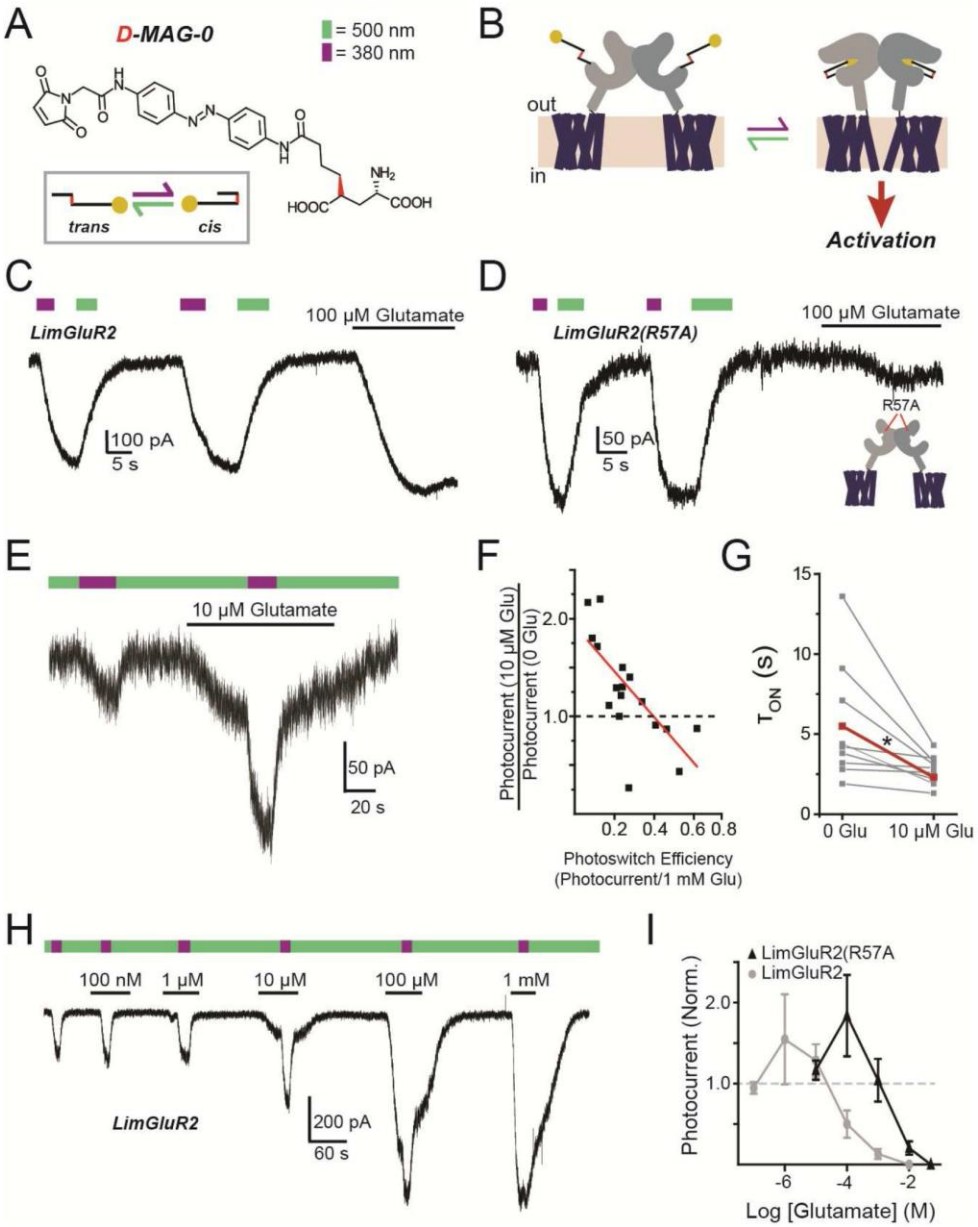

Figure 2.5, Photoactivation of tether ligands reveals cooperative activation by mGluR2. A) Chemical structure of the D-MAG-0 photoswitchable tethered ligand. Irradiation with 500 nm light (green arrow) induces the *trans*-configuration and 380 nm light (violet arrow) induces the *cis*-configuration. B) Schematic of photoactivation of mGluR2 that is conjugated to D-MAG-0 ("LimGluR2"). C) Representative HEK293T whole-cell recording where LimGluR2 is co-expressed with GIRK1(F137S) as a reporter. 380 nm light (violet bar) induces an inward current that is turned off by 500 nm light (green bar), compared to current evoked by 100uM glutamate. D) Low affinity LimGluR2(R57A) shows large photocurrents and diminished glutamate response. E) Partial D-MAG-0 labeling yields weak LimGluR2 photocurrent that is potentiated by a low concentration of glutamate. F) Summary of photocurrent potentiation (y-axis) by 10 µM glutamate as a function of degree of D-MAG-0 labeling (photoswitch efficiency; x-axis). Red line shows linear fit. G) Summary of accelerating effect of 10 µM glutamate on photocurrent kinetics. Individual cells (gray) in two conditions connected by lines, with average (red). * indicates statistical significance (paired t-test, p=0.007). H-I) Concentration-dependence of glutamate-mediated photocurrent potentiation for LimGluR2 and LimGluR2(R57A), showing representative trace from cell expressing LimGluR2 (H) and average relation (I). Error bars show S.E.M. calculated from multiple experiments (N≥3).

First, in order to generate a distribution of dimers in each cell, with either zero, one or two

attached MAGs, we under-labeled LimGluR2. Under these conditions, glutamate at or below the dissociation constant is expected to bind a fraction of the subunits, whether their LBDs are attached to MAG or not. In contrast, light will only induce liganding in MAG-labeled subunits and dimers with no labeled subunits will not respond. We found that photoswitching to the activating *cis* state evoked a small photocurrent, consistent with sparse MAG conjugation, but that the photocurrent was usually potentiated by prior application of a sub-saturating concentration of glutamate (Fig. 2.5E). The magnitude of photocurrent potentiation by glutamate depended on the extent of MAG labeling, which we determined from a measure of photoswitch efficiency, with lower MAG labeling giving greater potentiation (Fig. 2.5F). Photocurrent amplitude potentiation was accompanied by an increase in the speed of photocurrent activation (Fig. 2.5G). Since photo-agonism by MAG is equipotent to activation by glutamate[40], MAG-conjugated LBDs that bind glutamate should maintain the same occupancy when MAG is photoswitched into the binding site, displacing free glutamate, with no effect on GIRK activation. At the same time, dimers with neither LBD labeled with MAG will not respond to light. Thus, the potentiating effect of sub-saturating glutamate on the photocurrent must be due to receptors in which only one subunit is labeled with MAG, and must occur when glutamate binds to the unlabeled subunit while MAG photo-agonizes the labeled subunit. Consistent with this, photocurrent potentiation in LimGluR2 and LimGluR2(R57A) was highly concentration- dependent with the largest effects between ~EC10-EC50 and the relation was shifted to higher concentrations for the R57A mutation, (Fig. 2.5H, I; Supplementary Fig. 2.5G). Together these data suggest a supra-linear activation of mGluR2 by two agonists *versus* one.

We next aimed to determine directly if agonist binding in only one subunit can activate mGluR2 and to quantify the relationship of ligand occupancy to activation. To clearly define the stoichiometry of label-able and unlabel-able subunits we adapted a tandem dimer approach used previously for microbial opsins[43], in which a transmembrane linker connects the C-terminus of a first copy of mGluR2 to the N-terminus of a second (Fig. 2.6A, Supplementary Fig. 2.6A). The tandem dimer had the expected size on a western blot (Supplementary Fig. 2.6A), expressed reasonably well (Supplementary Fig. 2.6B), displayed normal apparent glutamate affinity (Supplementary Fig. 2.6C), and showed photobleaching patterns consistent with the predicted assembly (indicating the presence of two GFPs within each complex) (Supplementary Fig. 2.6D, E). We introduced the L300C MAG attachment site into the LBD of one subunit or both subunits within a tandem, labeled maximally with MAG and analyzed photoswitch efficiency. Tandem 300C-WT and WT-300C dimers showed weak, but clear photocurrents that were <10% in amplitude compared to the current evoked by 1 mM glutamate (Fig. 2.6B). We confirmed that these small currents were mGluR2-dependent through blockade with LY341495 (Supplementary Fig. 2.6F). These photocurrents were not dependent on ambient glutamate in our bath solution because they persisted in the low affinity 300C(R57A) mutant (Supplementary Fig. 2.6G). Consistent with the behavior described above for incomplete MAG labeling of homo-dimeric LimGluR2(L300C) (Fig. 2.5C), a low concentration (1 μM) of glutamate potentiated the photocurrent of 300C-WT (Fig. S6H). 300C-300C tandem dimers showed > 5-fold larger photoactivation than when only one subunit has a cysteine (300C-WT or WT-300C), and this level was the same as seen in homo-dimers formed by assembly of mGluR2-L300C monomers (Fig. 2.6C, D). 300C-300C tandem dimers also had faster photocurrents compared to 300C-WT tandem dimers (Supplementary Fig. 2.6I), indicating that increased occupancy increases both the amplitude and speed of activation.

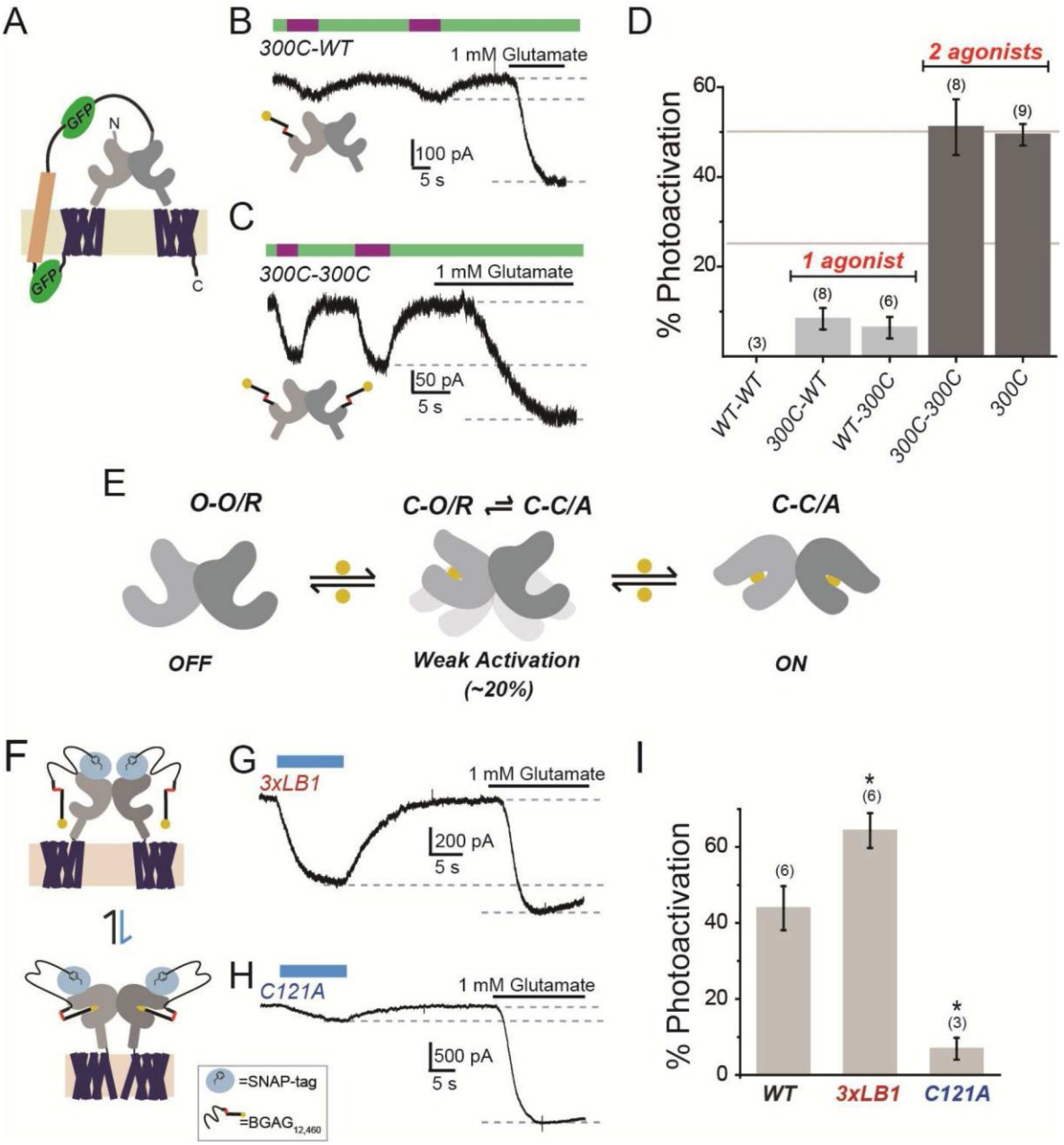

Figure 2.6, Photoactivation analysis of receptor cooperativity in tandem dimers and dimer interface mutants. A) Schematic of mGluR2 tandem dimer. Transmembrane linker contains two GFPs (green) and the transmembrane segment of the H+,K+ ATPase (beige). B-C) Representative traces showing that, compared to saturating glutamate, docking of glutamate of D-MAG-0 in a single subunit within a tandem dimer weakly activates mGluR2 B), whereas docking in both subunits strongly activates C). Tethering of D-MAG-0 to subunits is via introduced cysteine in one (300C-WT) or both (300C-300C) subunits. D) Summary of photoactivation relative to 1 mM glutamate for various conditions. Activation with 2 agonists is >5× as efficient as 1 agonist. All constructs are tandem dimers except for "300C," which is the standard non-tandem LimGluR2 construct. The numbers of cells tested for each condition are shown in parentheses. E) Model of occupancy-dependent activation of mGluR2, where LBD is either open (O) or closed (C) and the receptor is either resting (R) or activated (A). F) Schematic of SNAP-mGluR2 photoactivation by BGAG12,460. G-H) Representative traces showing photoactivation of SNAP-3xLB1 (G) or SNAP-C121A (H). I) Summary of photoactivation relative to 1 mM glutamate for dimer interface mutants. The numbers of cells tested for each condition are shown in parentheses. Error bars show S.E.M. calculated from multiple experiments (N.≥3).

Based on prior evidence that the activated state of the receptor has both LBDs closed and

reoriented (CC/A)[23], these findings suggest that one agonist weakly activates the receptor during rare spontaneous closures of the un-liganded subunit and that when two ligands are bound the receptor stably occupies this conformation and is fully activated (Fig. 2.6E).

We next sought to determine the role of the LBD interfaces in the cooperativity of mGluR2 activation by analyzing the photo-activation properties of the interface mutants with the largest effects on function, 3xLB1 and C121A. Because these mutants expressed poorly combined with the L300C substitution, we turned to an alternative approach for attachment of the photoswitchable glutamate ligand in which to an N-terminal SNAP domain is covalently labeled by benzylguanine-azobenzene-glutamate ("BGAG") to enable photo- activation in *cis* (Fig. 2.6F)[44], similar to what is observed with MAG. We used a BGAG variant, BGAG12,460, which, following maximal labeling, acts as a full agonist when bound, but provides partial activation due to incomplete photoisomerization[44] and, thus, should produce a population with a mix of receptors where 0, 1, or 2 subunits are liganded within a dimer. Thus, photoswitch efficiency relative to saturating glutamate should provide a measure of the relative activation efficiency of partially liganded dimers. Consistent with smFRET experiments, SNAP-mGluR2(3xLB1) showed enhanced photoactivation while SNAP-mGluR2(C121A) showed a major decrease in photoactivation (Fig. 2.6G-J). These results argue that weakening of the hydrophobic LB1 interface promotes intersubunit cooperativity while removal of the intersubunit disulfide (C121A) weakens the ability of subunits to communicate and produce activation of receptors liganded in only one subunit.

mGluR2/3 heterodimers: conformational dynamics, basal activity, and cooperativity

Since mGluR2 and mGluR3 readily heterodimerize in heterologous cells (Fig. 2.4, Supplementary Fig. 2.4) and have overlapping native expression patterns[45-47] that make them likely candidates for *in vivo* heterodimerization, we wondered if mGluR2/mGluR3 ("mG2/mG3") heterodimers form functional glutamate receptors. Because there are no agonists that fully distinguish mGluR2 from mGluR3, we again turned to subunit selective activation with MAG. We first asked if LimGluR2 activation can cross-activate mGluR3. To focus our analysis on the freely assembled mG2/mG3 heterodimer, without interference from mGluR2 and mGluR3 homodimers that are formed in the same cells, we targeted mGluR2 for photo-control by MAG using LimGluR2 and also introduced the mutation F756D into the same subunit, to prevent G protein coupling[48]. This photo-activatable but non- functional LimGluR2(F756D) subunit was co-expressed with a non-photo-activatable (no MAG attachment site) but functional subunit to enable GIRK photocurrent to be generated only by the heterodimeric combination of the two. First, we confirmed the expected lack of photocurrent when LimGluR2(F756D) was expressed alone (Fig. 2.7A, **left**). When mGluR2WT was co-expressed with LimGluR2(F756D), photocurrent was observed, suggesting cross-activation to the intact G protein-coupling site of the WT subunit from the MAG-liganded LimGluR2(F756D) subunit (Fig. 2.7A, **center**). When mGluR3WT was co-expressed with LimGluR2(F756D), photocurrent was also observed (Fig 2.7A, **right**), suggesting that cross-activation also occurs between mGluR2 and mGluR3, setting the stage for experiments on heteromeric cooperative interaction.

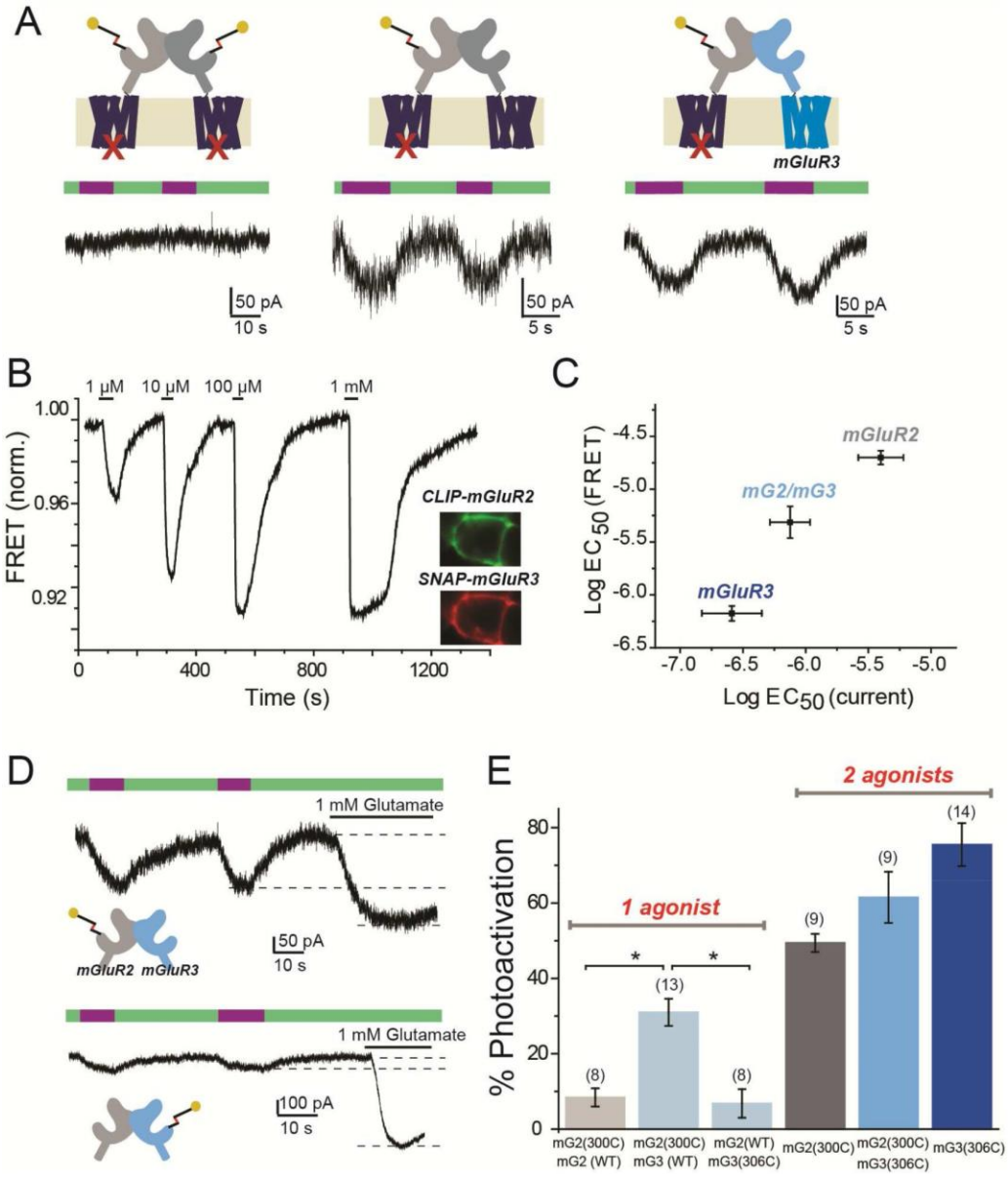

Figure 2.7, mGluR2/mGluR3 heterodimers exhibit *trans*-activation, intermediate glutamate affinity, and assymmetric cooperativity. A) LimGluR2(F756D) G protein coupling mutant has no photocurrent (left), unless co-expressed with mGluR2WT (middle) or mGluR3WT (right). B) Representative trace showing glutamate-induced decreases in ensemble FRET between co-expressed CLIP-mGluR3 (labeled with donor) and SNAP-mGluR2 (labeled with acceptor) in a HEK293T cell. Inset shows cell donor (CLIP-mGluR3) and acceptor (SNAP- mGluR2) fluorescence images. C) Summary of glutamate EC50 determinations from measurement of GIRK activation (current) versus LBD conformational change (FRET) for mGluR2, mGluR3, and mGluR2/ mGluR3 ("mG2/mG3"). FRET for mG2/mG3 obtained from co-expression, as in (B); GIRK current from tandem linked mGluR2-mGluR3 ("mG2-mG3"). D) GIRK current traces showing single-subunit photoactivation of linked mG2-mG3 heterodimers via photoactivation of only mGluR2 (top) or only mGluR3 (bottom). E) Summary of photoactivation (from left to right) with 1 subunit liganding of mGluR2 in mG2-mG2, in mG2-mG3, or 1 subunit liganding of mGluR3 in mG2-mG3, or 2 subunit labeling in unlinked mGluR2, linked mG2-mG3 or unlinked mGluR3. * indicates statistical significance (unpaired t-test, p=0.003 between mG2(300C)-mG2(WT) and mG2(300C)- mG3(WT); p=0.004 between mG2(300C)-mG3(WT) and mG2(WT)-mG3(306C). The numbers of cells tested for each condition are shown in parentheses. Error bars show S.E.M. calculated from multiple experiments (N≥3).

We first asked how the ~10-fold higher glutamate affinity of mGluR3[23,49] would influence

the behavior of mGluR2 in the mG2/mG3 heterodimer. To determine glutamate affinity, we measured ensemble inter-LBD FRET between an acceptor fluorophore on SNAP-mGluR2 and a donor fluorophore on CLIP- mGluR3 in HEK293T cells. Glutamate induced large FRET decreases, with an EC_{50} that was intermediate between that of homodimers of mGluR2 and mGluR3 (Fig. 2.7B, Supplementary Fig. 2.7A). To confirm this functionally we turned to a measure of GIRK channel activation. We obtained a pure population of mG2/mG3 heterodimers through tandem heterodimers ("mG2-mG3") which showed an intermediate apparent glutamate affinity for GIRK current activation (Fig. 2.7C, Supplementary Fig. 2.7B,C). We next asked how ligand occupancy to mGluR2 or mGluR3 subunits within a heterodimer mediates receptor activation.

To directly measure subunit interaction between mGluR2 and mGluR3, we complemented photo-agonism of mGluR2 ("LimGluR2"), with photo-agonism of mGluR3 (i.e. LimGluR3: mGluR3(Q306C) + D-MAG-0). We previously observed enhanced photoactivation of LimGluR3 relative to LimGluR2[40], which made us wonder if mGluR2 cooperativity is altered in mG2/mG3 heterodimers. Strikingly, photoactivation of only mGluR2 within a mG2(300C)-mG3(WT) heterodimer elicited robust photocurrents of ~30% amplitude relative to saturating glutamate (Fig. 2.7D, E). This photoactivation was more than 3-fold larger than what was seen when only one mGluR2 subunit was activated in an mGluR2 homodimer (Fig. 2.6B, 2.7E). In contrast, photoactivation of only the mGluR3 subunit in an mG2(WT)-mG3(306C) heterodimer showed an efficiency of ~10%, similar to single- subunit activation in the mGluR2 homodimer (Fig. 2.7D, E). Thus, unexpectedly, activation of mGluR2/3 heterodimers is asymmetric. In addition, mG2(300C)-mG3(306C) heterodimers showed intermediate photoactivation relative to LimGluR2 or LimGluR3 (Fig. 2.7E, Supplementary Fig. 2.7D). To probe the molecular mechanism of this asymmetric subunit cooperativity, we turned to inter- subunit FRET.

Whereas mGluR2 displays minimal spontaneous LBD dynamics in the absence of glutamate, mGluR3 shows rapid LBD dynamics, due primarily to partial agonism by Ca2+, which produce basal activity[23]. We asked whether the presence of mGluR3 in a mG2/mG3 heterodimer would confer basal dynamics by measuring basal FRET in the mG2/mG3 heterodimer in physiological (2 mM) Ca2+ and zero glutamate by measuring the increase in inter-subunit FRET that is induced by the competitive antagonist LY341495. Unlike in the mGluR2 homodimer, whose basal FRET was insensitive to LY341495, the basal FRET of the mG2/mG3 heterodimer was substantially reduced by LY341495 to ~60% of that seen in the mGluR3 homodimer (Fig. 2.8A,B). The mutation S152D, which targets a site implicated in Ca2+ binding[50] and reduces basal dynamics in mGluR3 homodimers[23], also reduced basal FRET in the mG2/mG3 heterodimer (Fig. 2.8B). Interestingly, introduction of S152D into just one subunit of mGluR3 reduced basal FRET to a level similar to that seen in mG2/mG3 (Fig. 2.8B). These results support a model whereby Ca2+ binds to each subunit within a dimer to produce basal activity by inducing LBD closure.

To obtain a quantitative view of mG2/mG3 conformational dynamics we performed smFRET experiments following SimPull isolation. mG2/mG3 transitioned between three distinct FRET states, with peak values similar to those observed in mGluR2 and mGluR3 homodimers. In 2 mM Ca2+ and zero glutamate, mG2/mG3 displayed rapid dynamics with frequent visits to the active, low FRET state (Fig 2.8C, **top**). The occupancy of the low FRET state was ~20%, intermediate between what was seen in mGluR2 and mGluR3 homodimers and consistent with ensemble FRET results (Fig. 2.8B). Both mG2/mG3 basal dynamics and low FRET occupancy were reduced either by application of LY341495, removal of Ca2+, or introduction of the S152D mutation (Fig. 2.8C-F; Supplementary Fig. 2.8A, B). Application of glutamate to mG2/mG3 heterodimers increased the occupancy of the low FRET state in a dose-dependent manner and decreased dynamics (Supplementary Fig. 2.8A). We also applied DCG-IV to see if this would

uncover differences in the stability of the active conformation. Compared to mGluR2, saturating DCG-IV in mG2/mG3 showed more complete occupancy of the low FRET state as well as decreased dynamics (Supplementary Fig. 2.8C, D). Together these data show that mG2/mG3 heterodimers visit the same three conformations as their parent homodimers and possess properties of mGluR3, including Ca2+-dependent basal dynamics and a stabilized active state relative to mGluR2.

We hypothesized that the enhanced single subunit activation by mGluR2 within the mG2/mG3 heterodimer is due to spontaneous closure of the mGluR3 subunit, which enhances population of the low FRET (C-C/A) state when only mGluR2 is liganded. To test this we introduced the S152D mutation into the mGluR3 subunit and measured the ability of mGluR2 to activate the mG2(WT)/mG3(S152D) receptor via D-MAG-0. As expected, photoactivation of mG2(300C)-mG3(S152D) was weaker than in mG2(300C)-mG3(WT) (Fig. 2.8G, H). Consistent with a role for receptor dynamics in determining ligand efficacy, LimGluR3(S152D) also showed reduced photocurrent efficacy compared to LimGluR3 (Fig. 2.8H; Supplementary Fig. 2.8E, FB). Together, these data support a role for basal conformational dynamics in determining ligand efficacy.

Discussion:

Dimerization has long been viewed as a defining feature of class C GPCRs. However, the molecular determinants of dimerization have been only partly defined and the function of dimerization has remained opaque. We used single molecule subunit counting in the plasma membrane of living cells and in isolated receptors to identify determinants of mGluR assembly. We confirm earlier work[22] that, unlike the formation of tetramers or higher ordered complexes in the related GABAB receptor[51,52], mGluRs from all three groups form strict homodimers, and show that this applies at both low and high expression densities. By comparing low density conditions in oocytes to high density conditions in HEK293T cell lysate, we found that dimerization is mediated by high affinity LBD interactions and lower affinity TMD interactions. In contrast to an earlier report[20], the TMD interface alone, in the absence of the entire extracellular domain, permits the formation of stable dimers at high expression densities. Analogous interactions may be relevant to Class A and B GPCRs, whose oligomerization has been the subject of ongoing debate[53,54]. Interestingly, the recent crystal structure of the TMD of mGluR1 identified an interface between TM1 helices[55], while a structure of the TMD of mGluR5 was obtained as a monomer[56]. In contrast, a recent cross-linking study suggested that activation reorients a TMD interface involving TM4, TM5 and TM6[57] and other studies have indicated that mGluR2 can interact with the 5-HT2A serotonin receptor via TM4[58-59].

The LBD interface in assembly and function

We focused our analysis on LBD interfaces, which deletion analysis showed to play a dominant role in receptor dimerization. At low expression density, mutation of the intersubunit disulfide bridge (C121 in mGluR2) compromises dimerization without eliminating it, whereas mutation of the hydrophobic LB1 interface results in complete monomerization. Thus, the conserved disulfide bond does not ensure dimerization when other interfaces are sufficiently weakened and the LB1 interface accounts for the dominant role of the LBD in dimerization. Consistent with this, the mGluR2 LBD alone efficiently dimerizes with full-length mGluR2, as previously observed with mGluR1[60].

In contrast to the requirement of trafficking to the plasma membrane on heteromerization in GABABRs[61], we find that monomerized mGluRs do traffic to the cell surface. Based on these findings, as well as the observations that mGluR2 is stationary in the plasma membrane and that application of high concentrations of DTT do not dissociate dimers, it appears that dimerization of mGluRs likely occurs in the endoplasmic reticulum, and that receptor reaches the plasma membrane as a stable dimer.

We used single molecule analysis to determine that mGluR2 readily heterodimerizes with the other group II mGluR, mGluR3, as well as with the group III mGluR, mGluR7, but not with either of the group 1 mGluRs, mGluR1 and mGluR5, consistent with earlier work[22]. When surface expression levels are matched, mGluR2 heterodimerizes with a preference for the same group (equally well with itself as with mGluR3) over group III. Chimeras between mGluR1 and mGluR2 revealed that determinants of heterodimer specificity exist in both the LBD and the TMD. Because of its dominant role in assembly, we focused on the role of LBD interactions in activation.

Strikingly, *weakening* of the LB1 dimer interface *increased* the apparent affinity of mGluR2 for both glutamate and the partial agonist DCG-IV and increased DCG-IV efficacy. These

effects were accompanied by spontaneous activation rearrangements in the absence of glutamate and by two changes to in the presence of glutamate: increased active state occupancy and a startling shift to a lower FRET level than seen in wildtype. These effects suggest that the LB1 mutations result in a larger than normal activation motion that produces a more stable activated conformation. This suggests that the normal function of the LB1 interface is to stabilize the resting conformation and, thereby, prevent basal activity in absence of glutamate, while at the same time limiting the sensitivity to glutamate.

In contrast, mutation to prevent the formation of an intersubunit disulfide bond (C121A) had the opposite effect: it *decreased* the apparent affinity for agonists and *decreased* the stability of the active state. Moreover, this mutation also increased the FRET level of the resting state suggesting that the function of the intersubunit disulfide bond is to set the resting conformation and stabilize the active state. Interestingly, LB1 interface mutations in the background of C121A still introduced basal dynamics, but did not prevent the increase in basal FRET values or the destabilization of the active state, suggesting that these interfaces work in concert via distinct mechanisms.

Subunit cooperativity in mGluR activation

The importance to activation of the dimer interface is consistent with earlier evidence that a coordinated rearrangement of the subunits within a dimer takes place upon ligand binding[14,22,24]. This raises a fundamental question about the activation mechanism: How does activation change when agonist binds to only one *versus* to both subunits in either a homodimer or heterodimer? Previous work that addressed this question in dimers composed of a wildtype subunit and a mutant subunit with a lower glutamate affinity showed that the wildtype subunit appeared to increase the affinity of the mutant subunit[24,35,36]. However, there remained a concern that mutations of the orthosteric binding pocket that lowered affinity might have also altered activation in unforeseen ways. To overcome this complication, we turned from soluble ligands to the fast and reversible light-driven liganding of a specific LBD that is enabled by a "photoswitchable glutamate on a string," D-MAG-0, that is anchored to a cysteine introduced into the LBD of a particular subunit. We showed D-MAG-0 to function as a high efficacy agonist, even in the low-affinity R57A, indicating that in its *cis* state its effective concentration is very high. Unique to a PTL, high ligand occupancy could be achieved and reversed rapidly but in only the fraction of subunits to which MAG is conjugated.

To precisely define ligand occupancy within a dimer, we developed a tandem dimer approach that allowed for the expression of heterodimeric mGluRs of defined stoichiometry. The ability to reversibly and repeatedly photoisomerize D-MAG-0, and the high signal-to- noise and reproducibility of GIRK current readout, allowed us to quantify activation even when it was weak. By targeting D-MAG-0 conjugation to one subunit within the linked dimer we found, definitively, that binding of agonist to one subunit is able to activate mGluR2. However, when two agonists were made to bind, we found that activation is ~5× larger, indicating substantial cooperativity.

Model of dimer interaction and cooperativity in mGluR activation

In order to reconcile our finding of non-linear occupancy-dependent activation with the 3 conformations observed in smFRET, we adapted earlier models of mGluR activation, in which the LBD is open (O) in absence of agonist and the receptor is in a resting intersubunit orientation (R) and the LBD is closed (C) when agonist binds, leading to a secondary reorientation rearrangement

(A) that activates the receptor[23] (Fig. 2.5E). In this updated model, spontaneous closure of the unliganded subunit is required for the receptor to enter the C-C/A state when only one ligand is bound. The ability of unliganded LBDs to close is consistent with our observation that, in the absence of glutamate, mGluR2 occasionally visits the medium FRET state. Furthermore, we hypothesize that closure of one LBD allosterically shifts the dynamic equilibrium of the unliganded subunit. This model can explain the biphasic dose response curve observed for a heterodimer between mGluR2WT and a subunit with diminished binding ("mGluR2-YADA"), when the response is effector activation[35] or smFRET measurement of occupancy of the active, low FRET state[23].

Cooperativity experiments with tandem mGluR2/mGluR3 ("mG2/mG3") heterodimers were particularly illuminating for understanding activation cooperativity. Single subunit activation of the mGluR2, but not the mGluR3, subunit displayed efficient photoactivation compared to what was observed in mGluR2 homodimers. Consistent with this, smFRET analysis of mG2/mG3 conformational dynamics revealed mGluR3-like basal dynamics that could be diminished by the introduction of mutation S152D or removal of Ca2+. Supporting the notion of a central role for receptor dynamics in the cooperative response to ligands, introduction of S152D into mG2-mG3 tandem dimers reduced the activation via the mGluR2 subunit. The observed asymmetric activation cooperativity argues that the basal dynamics of mG2/mG3 are not distributed throughout the receptor, but are confined to the mGluR3 subunit. This suggests that Ca2+ binding occurs in a subunit autonomous manner to stabilize LBD closure rather than to directly induce dimer reorientation. Furthermore, S152 is located at the hinge between the upper and lower lobes of the LBD indicating that it may provide energy for LBD closure. Finally, experiments with the partial agonist DCG-IV revealed increased low FRET occupancy for mG2/mG3, implying that the active state is more energetically favorable in the mG2/mG3 heterodimer than in the mGluR2 homodimer.

Together these experiments allow us to propose a conformational model that describes the asymmetrical activation of mG2/mG3 heterodimers where the properties of the un-liganded subunit determine efficacy (Fig. 2.8I). mG2/mG3 may provide an advantageous combination of its two parent receptors by combining the basal activity of mGluR3, which may provide a useful inhibitory tone, with the non-linear response of mGluR2 (since physiologically the mGluR3 subunit is likely to bind glutamate first due to its higher affinity), which may sharpen the response to ligand compared to mGluR3. Its unique combination of basal activity, cooperativity, and glutamate affinity, indicates that mG2/mG3 may be uniquely tuned to distinct spatiotemporal synaptic glutamate profiles. *In situ* hybridization studies have revealed a significant overlap in expression of mGluR2 and mGluR3 in a number of brain regions and cell types, including golgi cells of the cerebellum, dentate gyrus granule cells, the olfactory bulb and many parts of the thalamus and cortex[45-47], suggesting that the cooperative gating that we describe is likely to be physiologically relevant. The finding that mGluR2 and 3 readily heterodimerize also provides an important cautionary note for the interpretation of pharmacological and immunohistochemical studies, which often struggle to specifically target mGluR2 and mGluR3.

Use of smFRET to begin unraveling the molecular determinants of mGluR activation in this chapter lays the foundation of investigative work in the following chapters. mGluR2 homodimer behavior is used as a comparative model to build an understanding of mGluR7. The finding in this chapter that mGluR2/3 heterodimers exhibit an intermediate glutamate sensitivity between mGluR2 and mGluR3 homodimers respectively also serves to inform the interpretation of mGluR2/7 heterodimers examined in chapter III.

Methods:

Cloning

mGluR constructs were tagged with a C-terminal or N-terminal monomeric eGFP via a flexible 16 aa linker (TSGGSGGSRGSGGSGG). All mutations were introduced via a quick change mutagenesis kit (Stratagene). Truncated mGluR clones were produced by modifying vectors with full length mGluRs using 5' phosphorylated PCR primers to amplify the remaining sequences with the vector and re-ligate. mGluR2-ΔLBD contains aa 1-18 and 497-end, mGluR2-LBD contains aa 1-496, and mGluR2-ΔECD contains aa 1-18 and 558-end. mGluR3-ΔECD contains aa 1-23 and 566-end and mGluR1-ΔECD contains aa 1-30 and 583-end. The mGluR2-mGluR1 chimera contains aa 1-557 of mGluR2 followed by aa 583-end of mGluR1, while the mGluR1-mGluR2 chimera contains aa 1-582 mGluR1 and aa 559-end of mGluR2. N-terminal SNAP-mGluR constructs were first described by Doumazane et al, 2011. The tandem dimer constructs were produced using PCR-based methods. The first mGluR subunit (Cterminally GFP tagged) was connected to the second subunit (N-terminally GFP tagged and no signal peptide) by a 105-amino acid transmembrane domain from the H-K-ATPase as previously described (Kleinlogel et al., 2011) and a linker (same as used for GFP-tags). To characterize the molecular weight of the mGluR2 tandem construct, western blots were performed in a 6% SDS-PAGE gel. Protein was transferred to a nitrocellulose membrane and probed with an anti-mGluR2 antibody.

Single Molecule Subunit Counting and Pulldown

For subunit counting in *Xenopus* oocytes RNA for the construct of interest was injected and ~18-24 hours later cells were imaged using a 100x objective on a TIRF microscope and recorded at 20 Hz with a backilluminated EMCCD camera (Andor iXon DV-897 BV). Colocalization was performed by sequentially imaging the red and the green channels and was calculated as (# of colocalized spots/total spots). For SiMPull single molecules were imaged with a 60x objective (Olympus) using the same TIRF microscope as for subunit counting in *Xenopus* oocytes. For both *Xenopus* oocyte subunit counting and SimPull, multiple independent experiments were performed for each condition. Data analysis was performed using house-made software Representative data sets are presented to quantitatively compare conditions tested on the same days. For photobleaching experiments, error bars were calculated using counting statistics as described in (Reiner et al., 2012).

Dye labeling and ensemble FRET measurements

Cells were briefly washed with an extracellular solution containing (in mM): 135 NaCl, 5.4 KCl, 2.5 $CaCl_2$, 1 $MgCl_2$, 10 Hepes, pH 7.4 and then labeled sequentially with 2.5 uM benzylguanine Alexa-647 (Invitrogen) for 45 minutes and 5 uM benzylcytosine DY-547 (Invitrogen) for 45 minutes. The dyes were diluted in extracellular solution and were washed in between labeling with acceptor and donor. Following labeling cells were mounted on an upright, scanning confocal microscope (Zeiss LSM 780) and imaged with a 20x objective. Excitation was performed using a 561 nm laser and images were taken in the donor and acceptor channels at 1hz. Clusters of cells were analyzed together and FRET was calculated as $FRET=(I_{Acceptor})/(I_{Donor}$

$+I_{Acceptor}$) where I is intensity. FRET changes calculated for dose-response curves were normalized to saturating glutamate (1 mM or 10 mM) and dose-response curves were obtained from multiple cell clusters and averaged from multiple experiments. Fitting of dose-response curves was performed using Prism (Graphpad). All drugs were purchased from Tocris and delivered with a gravity-driven perfusion system.

Single Molecule Pulldown of mGluRs

For single molecule experiments, cells were recovered from the coverslip by incubating with Ca^{2+}-free PBS followed by gentle pipetting. Cells were then pelleted and lysed in lysis buffer consists of 10mM Tris, 150 mM NaCl, 1 mM EDTA, Protease inhibitor cocktail and 1% IGEPAL. Glass coverslips were coated with PEG and PEG-biotin at a ratio of ~100:1 as descibred in Jain et al, 2011. Prior to each experiment, coverslips were treated with neutravidin, followed by a biotinylated secondary antibody. Next, an mGluR2 or mGluR3-specific primary antibody was conjugated. Between each conjugation step, washing was performed to remove unlabeled compounds from coverslips. Lysate was then diluted in the same high potassium buffer used for functional experiments (ranging from 20x to 100x) and applied to coverslips.
Fluorescence was monitored in real time to confirm sufficient receptor attachment. Once a sufficient number of receptors had immobilized on the surface, the coverslips were washed to remove excess, unbound fluorescently-tagged receptors from solution.

smFRET measurements

Following conjugation of receptors to antibodies, single molecule imaging was performed with an inverted microscope in TIRF mode using a 60x objective. To reduce photobleaching, imaging buffer consisting of 3 mM Trolox (Sigma) and an oxygen scavenging system (of glucose oxidase (165 U/ml), catalase (2,170 U/ml) and β-D glucose (0.4% wt/wt)) was supplied in the high potassium buffer. Excitation was performed with a 532 nm laser and emission was monitored in both donor and acceptor channels using a CCD camera. Fluorescence signal was recorded in real time using home-written Visual C++software either in 8 bit or 16 bits. The movies were analyzed using either a custom-written IDL or a C++ program. In brief, an average image is created by averaging few frames from the movie (5 to 12 frames). This averaging removes the noise and increases the detection accuracy. Then the fluorescent molecules that exhibit a Gaussian intensity profile are selected in the averaged image. These molecules are then tracked over time and their fluorescent intensity is recorded to build the intensity time trace for each molecule. The traces were then analyzed in MatLab. In brief, traces that showed single step donor and acceptor photobleaching and a constant total intensity were selected and filtered as previously described [35]. Traces from many selected molecules were compiled to build FRET histograms (200-500 molecules in each case). Cross correlation was calculated using the following formula:

Whole Cell Patch Clamp and Two Electrode Voltage Clamp Electrophysiology

HEK293 cells were maintained in DMEM with 5% fetal bovine serum (vol/vol) on poly- L-lysine–coated glass coverslips. Dissociated hippocampal neurons were obtained from postnatal rats (P0–1) and plated at 75,000 cells per coverslip on poly-L-lysine–coated glass coverslips (12 mM). For autapse experiments, low density cultures of 25,000 cells per coverslip were used.

Neurons were maintained in media containing MEM supplemented with 5% FBS, B27 (Invitrogen) and GlutaMAX (Invitrogen).

HEK293 and 293T whole-cell patch-clamp electrophysiology was performed 24–48 h after transfection in high potassium solution containing 60 mM KCl, 89 mM NaCl, 1 mM MgCl2, 2 mM CaCl2 and 10 mM HEPES, pH 7.4. Glass pipettes of resistance between 3 and 6 MΩ were filled with intracellular solution containing 140 mM KCl, 10 mM HEPES, 3 mM Na2ATP, 0.2 mM Na2GTP, 5 mM EGTA and 3 mM MgCl2, pH 7.4. Cells were voltage clamped to –60 to –80 mV using an Axopatch 200A (Molecular Devices) amplifier.

Hippocampal neuron whole-cell patch-clamp electrophysiology was performed 3–6 d after transfection (12–15 d *in vitro*). For voltage-clamp recordings, a high potassium extracellular solution containing 79.5 mM NaCl, 60 mM KCl, 1.2 mM MgCl2, 2.5 mM CaCl2, 10 mM glucose and 5 mM HEPES, pH 7.4 was used. For all other experiments, extracellular solution contained 138 mM NaCl, 1.5 mM KCl, 1.2 mM MgCl2, 2.5 mM CaCl2, 10 mM glucose and 5 mM HEPES, pH 7.4. Intracellular solution contained 140 mM potassium gluconate, 10 mM NaCl, 5 mM EGTA, 2 mM MgCl2, 1 mM CaCl2, 10 mM HEPES, 2 mM MgATP and 0.3 mM Na2GTP, pH 7.2. For current-step experiments, cells were adjusted to –50 mV with current injection before current steps were initiated to normalize spike count comparisons between cells. Only cells with a resting potential ≤–45 mV were analyzed. For autapse experiments, cells were voltage clamped to –70 and stepped to 0 mV for 2 ms. Postsynaptic currents were delayed by 3 ms, which confirmed autaptic origins of transmission. Inter-stimulus intervals were ≥12 s.

EPSCs and IPSCs were identified on the basis of the kinetics of decay with EPSCs approximately ten times faster than IPSCs (~5 ms versus 50 ms), as has been described previously[55]. All pharmacological compounds were obtained from Tocris and dissolved in extracellular buffers before application using a gravity-driven perfusion system.

For most experiments, illumination was applied to the entire field of view using a Polychrome V monochromator (TILL Photonics) through a 20• objective or a Lambda DG4 high-speed wavelength switcher (Sutter Instruments) with 380-nm and 500-nm filters through a 40• objective. For bistable switching the DG-4 was coupled to the microscope through a 40• objective. Ultrafast, submillisecond photo-switching was achieved using a laser spot illumination system, for which the output of a 375/488-nm dual laser diode module (Omicron LDM) was coupled into a multi-mode fiber (10 μm, NA 0.1). The light exiting from this fiber was collimated and directed to the back aperture of the objective (Olympus 40•, NA 0.6). Intensities in the sample plane were >40 W mm–2.

pClamp software was used for both data acquisition and control of illumination. To conjugate MAG, cells were incubated in 50–100 μM MAG for 30–60 min in the dark at 23–27 °C in standard extracellular cell buffers. For RO4 experiments cells were labeled with 1 μM 11- cis retinal for 40 min and experiments were performed under dark room conditions.

Two Electrode Voltage Clamp Electrophysiology

Oocyte two-electrode voltage clamp electrophysiology was performed 48-96 hours after RNA injection with two microelectrodes (~2.5 M resistance) filled with 3 M KCl and maintained under voltage clamp at -80 mV using a Dagan TEV 200 amplifier. For Gi-coupled mGluRs (2, 3, and 7) GIRK1 and 2 RNA was injected and recordings were performed in high potassium ND96 containing (in mM): 60 KCl, 38 NaCl, 2 KCl, 1.8 CaCl2, 2 MgC12, 5 Hepes, pH 7.4. For Gq-coupled mGluRs (mGluR1 and 5) recordings were performed in standard ND96 solution

containing (in mM): 96 NaCl, 2 KCl, 1.8 CaCl2, 2 MgCl2, 5 HEPES, pH 7.4). Glutamate was applied using a gravity-driven perfusion system.

References:

1. Vafabakhsh R, Levitz J, Isacoff EY. Conformational dynamics of a class C G-protein-coupled receptor. Nature. 2015; 524:497–501
2. Gurevich VV, Gurevich EV. GPCR monomers and oligomers: it takes all kinds. Trends Neurosci. 2008; 31:74–81.
3. Lohse MJ. Dimerization in GPCR mobility and signaling. Curr Opin Pharmacol. 2010; 10:53–58. [PubMed: 19910252]
4. Ferre S, Casado V, Devi LA, Filizola M, Jockers R, Lohse MJ, Milligan G, Pin JP, Guitart X. G protein-coupled receptor oligomerization revisited: functional and pharmacological perspectives. Pharmacol Rev. 2014; 66:413–434. [PubMed: 24515647]
5. Rasmussen SG, DeVree BT, Zou Y, Kruse AC, Chung KY, Kobilka TS, Thian FS, Chae PS, Pardon E, Calinski D, et al. Crystal structure of the beta2 adrenergic receptor-Gs protein complex. Nature. 2011; 477:549–555. [PubMed: 21772288]
6. Katritch V, Cherezov V, Stevens RC. Structure-function of the G protein-coupled receptor superfamily. Annu Rev Pharmacol Toxicol. 2013; 53:531–556. [PubMed: 23140243]
7. Venkatakrishnan AJ, Deupi X, Lebon G, Tate CG, Schertler GF, Babu MM. Molecular signatures of G- protein-coupled receptors. Nature. 2013; 494:185–194. [PubMed: 23407534]
8. Nygaard R, Zou Y, Dror RO, Mildorf TJ, Arlow DH, Manglik A, Pan AC, Liu CW, Fung JJ, Bokoch MP, et al. The dynamic process of beta(2)-adrenergic receptor activation. Cell. 2013; 152:532–542. [PubMed: 23374348]
9. Manglik A, Kim TH, Masureel M, Altenbach C, Yang Z, Hilger D, Lerch MT, Kobilka TS, Thian FS, Hubbell WL, et al. Structural Insights into the Dynamic Process of beta2-Adrenergic Receptor Signaling. Cell. 2015; 161:1101–1111. [PubMed: 25981665]
10. Sounier R, Mas C, Steyaert J, Laeremans T, Manglik A, Huang W, Kobilka BK, Demene H, Granier S. Propagation of conformational changes during mu-opioid receptor activation. Nature. 2015; 524:375–378. [PubMed: 26245377]
11. Isogai S, Deupi X, Opitz C, Heydenreich FM, Tsai CJ, Brueckner F, Schertler GF, Veprintsev DB, Grzesiek S. Backbone NMR reveals allosteric signal transduction networks in the beta1-adrenergic receptor. Nature. 2016; 530:237–241. [PubMed: 26840483]
12. Vischer HF, Castro M, Pin JP. G Protein-Coupled Receptor Multimers: A Question Still Open Despite the Use of Novel Approaches. Mol Pharmacol. 2015; 88:561–571. [PubMed: 26138074]
13. Geng Y, Bush M, Mosyak L, Wang F, Fan QR. Structural mechanism of ligand activation in human GABA(B) receptor. Nature. 2013; 504:254–259. [PubMed: 24305054]
14. Kunishima N, Shimada Y, Tsuji Y, Sato T, Yamamoto M, Kumasaka T, Nakanishi S, Jingami H, Morikawa K. Structural basis of glutamate recognition by a dimeric metabotropic glutamate receptor. Nature. 2000; 407:971–977. [PubMed: 11069170]
15. Romano C, Miller JK, Hyrc K, Dikranian S, Mennerick S, Takeuchi Y, Goldberg MP, O'Malley KL. Covalent and noncovalent interactions mediate metabotropic glutamate receptor mGlu5 dimerization. Mol Pharmacol. 2001; 59:46–53. [PubMed: 11125023
16. Doumazane E, Scholler P, Zwier JM, Trinquet E, Rondard P, Pin JP. A new approach to analyze cell surface protein complexes reveals specific heterodimeric metabotropic glutamate receptors. FASEB J. 2011; 25:66–77. [PubMed: 20826542]
17. Maurel D, Comps-Agrar L, Brock C, Rives ML, Bourrier E, Ayoub MA, Bazin H, Tinel N, Durroux T, Prezeau L, et al. Cell-surface protein-protein interaction analysis with time-resolved FRET and snap-tag technologies: application to GPCR oligomerization. Nat Methods. 2008; 5:561–567. [PubMed: 18488035]
18. Comps-Agrar L, Kniazeff J, Norskov-Lauritsen L, Maurel D, Gassmann M, Gregor N, Prezeau L, Bettler B, Durroux T, Trinquet E, et al. The oligomeric state sets GABA(B) receptor signalling efficacy. EMBO J. 2011; 30:2336–2349. [PubMed: 21552208]
19. Niswender CM, Conn PJ. Metabotropic glutamate receptors: physiology, pharmacology, and disease. Annu Rev Pharmacol Toxicol. 2010; 50:295–322. [PubMed: 20055706]
20. El Moustaine D, Granier S, Doumazane E, Scholler P, Rahmeh R, Bron P, Mouillac B, Baneres JL, Rondard P,

Pin JP. Distinct roles of metabotropic glutamate receptor dimerization in agonist activation and G-protein coupling. Proc Natl Acad Sci U S A. 2012; 109:16342–16347. [PubMed: 22988116]

21. Romano C, Yang WL, O'Malley KL. Metabotropic glutamate receptor 5 is a disulfide-linked dimer. J Biol Chem. 1996; 271:28612–28616. [PubMed: 8910492]
22. Doumazane E, Scholler P, Fabre L, Zwier JM, Trinquet E, Pin JP, Rondard P. Illuminating the activation mechanisms and allosteric properties of metabotropic glutamate receptors. Proc Natl Acad Sci U S A. 2013; 110:E1416–1425. [PubMed: 23487753]
23. Vafabakhsh R, Levitz J, Isacoff EY. Conformational dynamics of a class C G-protein-coupled receptor. Nature. 2015; 524:497–501. [PubMed: 26258295]
24. Tateyama M, Kubo Y. The intra-molecular activation mechanisms of the dimeric metabotropic glutamate receptor 1 differ depending on the type of G proteins. Neuropharmacology. 2011; 61:832–841. [PubMed: 21672544]
25. Xue L, Rovira X, Scholler P, Zhao H, Liu J, Pin JP, Rondard P. Major ligand-induced rearrangement of the heptahelical domain interface in a GPCR dimer. Nat Chem Biol. 2015; 11:134–140. [PubMed: 25503927]
26. Ray K, Hauschild BC. Cys-140 is critical for metabotropic glutamate receptor-1 dimerization. J Biol Chem. 2000; 275:34245–34251. [PubMed: 10945991]
27. Tsuji Y, Shimada Y, Takeshita T, Kajimura N, Nomura S, Sekiyama N, Otomo J, Usukura J, Nakanishi S, Jingami H. Cryptic dimer interface and domain organization of the extracellular region of metabotropic glutamate receptor subtype 1. J Biol Chem. 2000; 275:28144–28151. [PubMed: 10874032]
28. Nakajo K, Ulbrich MH, Kubo Y, Isacoff EY. Stoichiometry of the KCNQ1 - KCNE1 ion channel complex. Proc Natl Acad Sci U S A. 2010; 107:18862–18867. [PubMed: 20962273]
29. Ulbrich MH, Isacoff EY. Subunit counting in membrane-bound proteins. Nat Methods. 2007; 4:319– 321. [PubMed: 17369835]
30. Muto T, Tsuchiya D, Morikawa K, Jingami H. Structures of the extracellular regions of the group II/III metabotropic glutamate receptors. Proc Natl Acad Sci U S A. 2007; 104:3759–3764. [PubMed: 17360426]
31. Tsuchiya D, Kunishima N, Kamiya N, Jingami H, Morikawa K. Structural views of the ligand-binding cores of a metabotropic glutamate receptor complexed with an antagonist and both glutamate and Gd3+ Proc Natl Acad Sci U S A. 2002; 99:2660–2665. [PubMed: 11867751]
32. Delille HK, Becker JM, Burkhardt S, Bleher B, Terstappen GC, Schmidt M, Meyer AH, Unger L, Marek GJ, Mezler M. Heterocomplex formation of 5-HT2A-mGlu2 and its relevance for cellular signaling cascades. Neuropharmacology. 2012; 62:2184–2191. [PubMed: 22300836]
33. Yin S, Noetzel MJ, Johnson KA, Zamorano R, Jalan-Sakrikar N, Gregory KJ, Conn PJ, Niswender CM. Selective actions of novel allosteric modulators reveal functional heteromers of metabotropic glutamate receptors in the CNS. J Neurosci. 2014; 34:79–94. [PubMed: 24381270]
34. Suzuki Y, Moriyoshi E, Tsuchiya D, Jingami H. Negative cooperativity of glutamate binding in the dimeric metabotropic glutamate receptor subtype 1. J Biol Chem. 2004; 279:35526–35534. [PubMed: 15199056]
35. Kniazeff J, Bessis AS, Maurel D, Ansanay H, Prezeau L, Pin JP. Closed state of both binding domains of homodimeric mGlu receptors is required for full activity. Nat Struct Mol Biol. 2004; 11:706– 713. [PubMed: 15235591]
36. Kammermeier PJ, Yun J. Activation of metabotropic glutamate receptor 1 dimers requires glutamate binding in both subunits. J Pharmacol Exp Ther. 2005; 312:502–508. [PubMed: 15466247]
37. Volgraf M, Gorostiza P, Numano R, Kramer RH, Isacoff EY, Trauner D. Allosteric control of an ionotropic glutamate receptor with an optical switch. Nat Chem Biol. 2006; 2:47–52. [PubMed: 16408092]
38. Reiner A, Levitz J, Isacoff EY. Controlling ionotropic and metabotropic glutamate receptors with light: principles and potential. Curr Opin Pharmacol. 2015; 20:135–143. [PubMed: 25573450]
39. Lin WC, Tsai MC, Davenport CM, Smith CM, Veit J, Wilson NM, Adesnik H, Kramer RH. A Comprehensive Optogenetic Pharmacology Toolkit for In Vivo Control of GABAA Receptors and Synaptic Inhibition. Neuron. 2015; 88:879–891. [PubMed: 26606997]
40. Levitz J, Pantoja C, Gaub B, Janovjak H, Reiner A, Hoagland A, Schoppik D, Kane B, Stawski P, Schier AF, et al. Optical control of metabotropic glutamate receptors. Nat Neurosci. 2013; 16:507– 516. [PubMed: 23455609]
41. Carroll EC, Berlin S, Levitz J, Kienzler MA, Yuan Z, Madsen D, Larsen DS, Isacoff EY. Two-photon brightness of azobenzene photoswitches designed for glutamate receptor optogenetics. Proc Natl Acad Sci U S A. 2015; 112:E776–785. [PubMed: 25653339]

42. Malherbe P, Knoflach F, Broger C, Ohresser S, Kratzeisen C, Adam G, Stadler H, Kemp JA, Mutel V. Identification of essential residues involved in the glutamate binding pocket of the group II metabotropic glutamate receptor. Mol Pharmacol. 2001; 60:944–954. [PubMed: 11641422]
43. Kleinlogel S, Terpitz U, Legrum B, Gokbuget D, Boyden ES, Bamann C, Wood PG, Bamberg E. A gene-fusion strategy for stoichiometric and co-localized expression of light-gated membrane proteins. Nat Methods. 2011; 8:1083–1088. [PubMed: 22056675]
44. Broichhagen J, Damijoinatas A, Levitz J, Sokol K, Leippe P, Konrad D, Isacoff EY, Trauner D. Orthogonal optical control of a class C G protein-coupled receptor using a SNAP-tethered photoswitch. ACS Central Science. 2015; 1:383–393. [PubMed: 27162996]
45. Ohishi H, Shigemoto R, Nakanishi S, Mizuno N. Distribution of the messenger RNA for a metabotropic glutamate receptor, mGluR2, in the central nervous system of the rat. Neuroscience. 1993a; 53:1009–1018. [PubMed: 8389425]
46. Ohishi H, Shigemoto R, Nakanishi S, Mizuno N. Distribution of the mRNA for a metabotropic glutamate receptor (mGluR3) in the rat brain: an in situ hybridization study. J Comp Neurol. 1993b; 335:252–266. [PubMed: 8227517]
47. Petralia RS, Wang YX, Niedzielski AS, Wenthold RJ. The metabotropic glutamate receptors, mGluR2 and mGluR3, show unique postsynaptic, presynaptic and glial localizations. Neuroscience. 1996; 71:949–976. [PubMed: 8684625]
48. Francesconi A, Duvoisin RM. Role of the second and third intracellular loops of metabotropic glutamate receptors in mediating dual signal transduction activation. J Biol Chem. 1998; 273:5615–5624. [PubMed: 9488690]
49. Conn PJ, Pin JP. Pharmacology and functions of metabotropic glutamate receptors. Annu Rev Pharmacol Toxicol. 1997; 37:205–237. [PubMed: 9131252]
50. Kubo Y, Miyashita T, Murata Y. Structural basis for a Ca2+-sensing function of the metabotropic glutamate receptors. Science. 1998; 279:1722–1725. [PubMed: 9497291]
51. Calebiro D, Rieken F, Wagner J, Sungkaworn T, Zabel U, Borzi A, Cocucci E, Zurn A, Lohse MJ. Single-molecule analysis of fluorescently labeled G-protein-coupled receptors reveals complexes with distinct dynamics and organization. Proc Natl Acad Sci U S A. 2013; 110:743–748. [PubMed: 23267088]
52. Maurel D, Comps-Agrar L, Brock C, Rives ML, Bourrier E, Ayoub MA, Bazin H, Tinel N, Durroux T, Prezeau L, et al. Cell-surface protein-protein interaction analysis with time-resolved FRET and snap-tag technologies: application to GPCR oligomerization. Nat Methods. 2008; 5:561–567. [PubMed: 18488035]
53. Lambert NA, Javitch JA. CrossTalk opposing view: Weighing the evidence for class A GPCR dimers, the jury is still out. J Physiol. 2014; 592:2443–2445. [PubMed: 24931945]
54. Bouvier M, Hebert TE. CrossTalk proposal: Weighing the evidence for Class A GPCR dimers, the evidence favours dimers. J Physiol. 2014; 592:2439–2441. [PubMed: 24931944]
55. Wu H, Wang C, Gregory KJ, Han GW, Cho HP, Xia Y, Niswender CM, Katritch V, Meiler J, Cherezov V, et al. Structure of a class C GPCR metabotropic glutamate receptor 1 bound to an allosteric modulator. Science. 2014; 344:58–64. [PubMed: 24603153]
56. Dore AS, Okrasa K, Patel JC, Serrano-Vega M, Bennett K, Cooke RM, Errey JC, Jazayeri A, Khan S, Tehan B, et al. Structure of class C GPCR metabotropic glutamate receptor 5 transmembrane domain. Nature. 2014; 511:557–562. [PubMed: 25042998]
57. Xue L, Rovira X, Scholler P, Zhao H, Liu J, Pin JP, Rondard P. Major ligand-induced rearrangement of the heptahelical domain interface in a GPCR dimer. Nat Chem Biol. 2015; 11:134–140. [PubMed: 25503927]
58. Gonzalez-Maeso J, Ang RL, Yuen T, Chan P, Weisstaub NV, Lopez-Gimenez JF, Zhou M, Okawa Y, Callado LF, Milligan G, et al. Identification of a serotonin/glutamate receptor complex implicated in psychosis. Nature. 2008; 452:93–97. [PubMed: 18297054]
59. Moreno JL, Muguruza C, Umali A, Mortillo S, Holloway T, Pilar-Cuellar F, Mocci G, Seto J, Callado LF, Neve RL, et al. Identification of three residues essential for 5-hydroxytryptamine 2A- metabotropic glutamate 2 (5-HT2A.mGlu2) receptor heteromerization and its psychoactive behavioral function. J Biol Chem. 2012; 287:44301–44319. [PubMed: 23129762]
60. Beqollari D, Kammermeier PJ. Venus fly trap domain of mGluR1 functions as a dominant negative against group I mGluR signaling. J Neurophysiol. 2010; 104:439–448. [PubMed: 20463192]
61. Margeta-Mitrovic M, Jan YN, Jan LY. A trafficking checkpoint controls GABA(B) receptor heterodimerization. Neuron. 2000; 27:97–106. [PubMed: 10939334]

Supplementary Figures:

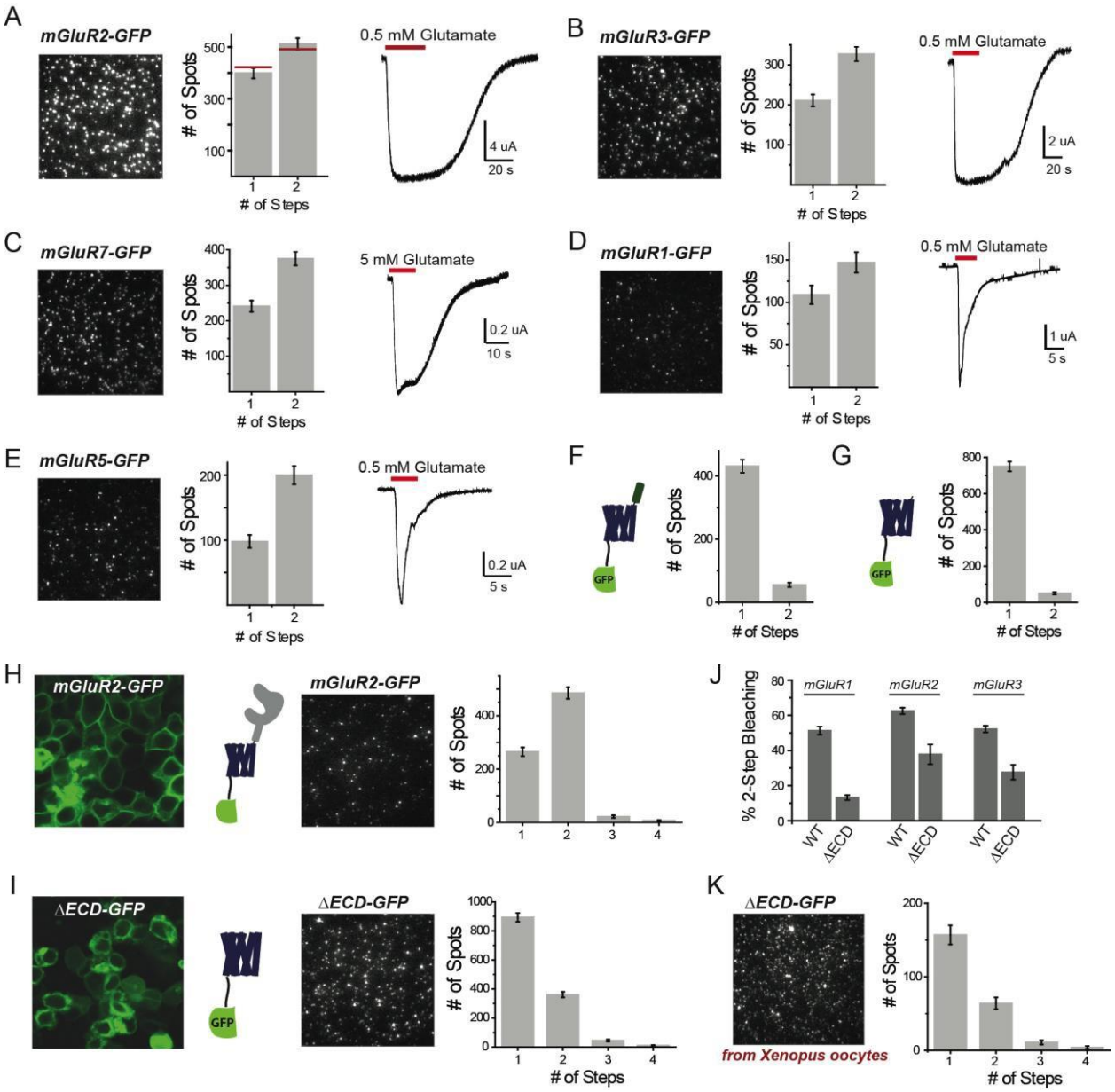

Figure S2.1, Further single molecule analysis of mGluR dimerization. A-E) mGluR2, mGluR3, mGluR7, mGluR1, and mGluR5 are each dimers. Left, representative TIRF images of each GFP-tagged receptor expressed at low density in the plasma membrane of a Xenopus oocyte. Center, photobleaching step distributions for each condition. Right, representative traces showing functionality of each GFP-tagged constructs: glutamate-evoked GIRK1/2 current (A-C); glutamate- evoked calcium-activated chloride current D-E). Error bars represent the counting uncertainty (see methods) F-G) Removal of either the LBD (ΔLBD) (F) or the entire ECD (ΔECD) (G) eliminates dimerization of mGluR2-GFP in Xenopus oocytes. Error bars show S.E.M. calculated from multiple experiments (N>5 movies). H-I) Stoichiometry analysis in SimPull from HEK293T cell lysate for mGluR2-GFP (H) and mGluR2(ΔECD)-GFP I). Left, representative confocal image showing expression of each construct in HEK 293T cells prior to lysis. Center, representative TIRF images of complexes immobilized on a passivated surface at low density. Right, photobleaching step distributions. Error bars represent the counting uncertainty. J) Summary of photobleaching step distributions from (H-I) for full-length or ΔECD versions of mGluR2-GFP, mGluR3-GFP, and mGluR1-GFP. Error bars show S.E.M. calculated from multiple experiments (N>5 movies). K) Photobleaching step distribution for mGluR2(ΔECD)-GFP in SimPull from Xenopus oocyte lysate with *high* level of expression. Error bars represent the counting uncertainty.

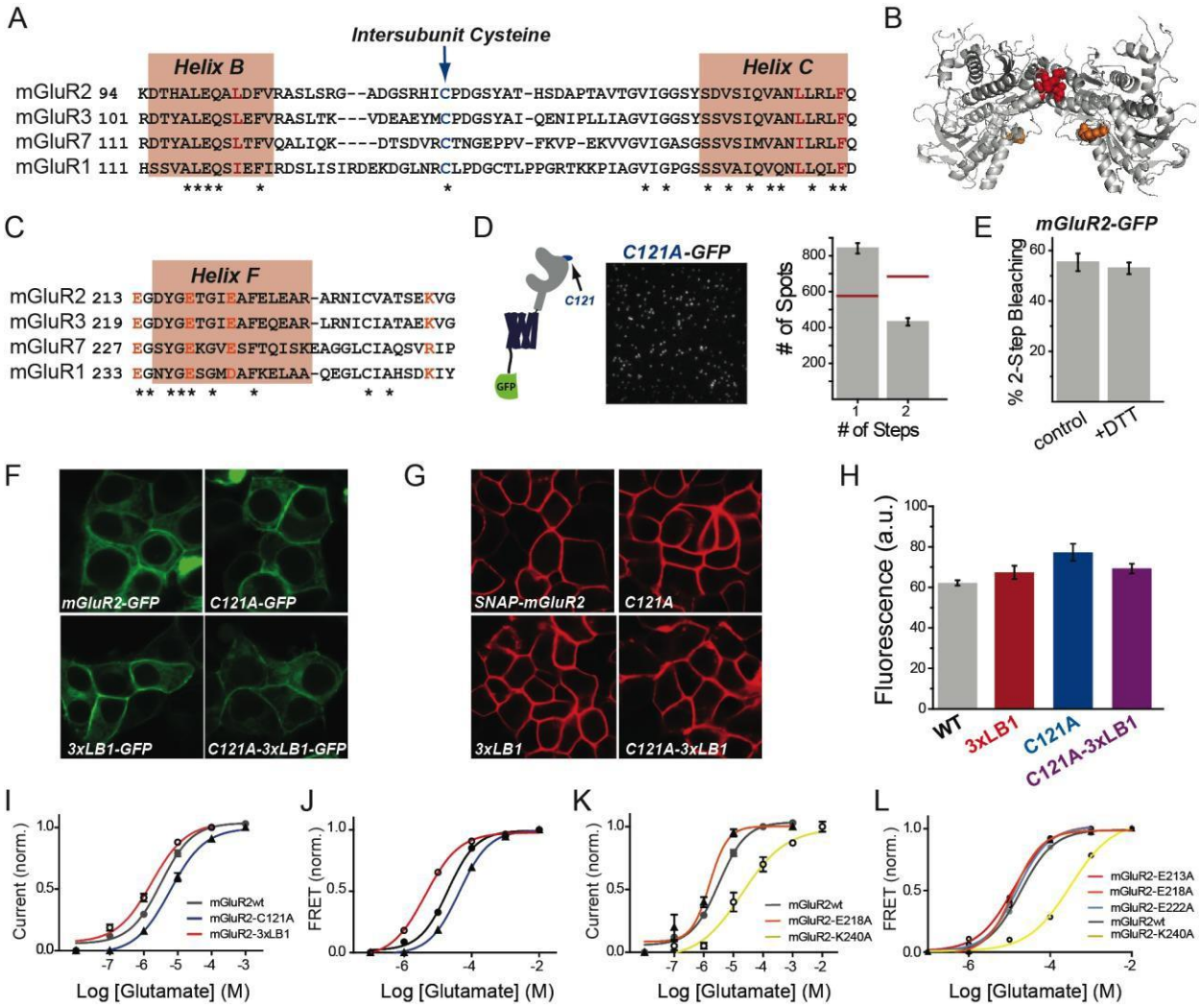

(A) **Figure S2.2, Further analysis of mGluR dimer interfaces** A) Sequence alignment for the upper lobe (LB1) LBD interfaces of mGluRs. Residues mutated to alanine for counting experiments are shown in red. * indicates sequence conservation across all mGluR subfamily members. B) Crystal structure of mGluR1 in the unliganded "relaxed" (O-O/R) state (PDB: 1EWT) showing the location of residues homologous to those mutated in mGluR2. C) Sequence alignment for the lower lobe (LB2) LBD interface of mGluRs. Residues mutated to alanine for counting experiments are shown in orange. mGluR2(C121A)-GFP partially reduces dimerization. Left, cartoon and representative TIRF image showing single mGluR2(C121A)-GFP complexes in Xenopus oocytes. Right, photobleaching step distribution. Error bars represent the counting uncertainty. E) Summary of photobleaching for mGluR2-GFP in the absence or presence of 10 mM DTT. Error bars show S.E.M. calculated from multiple experiments (N>5 movies). F-H) Analysis of expression of mGluR2 dimer interface mutants in HEK 293T cells. Confocal images show similar expression of either C-terminally GFP-tagged (F) or N-terminally SNAP-tagged and BG- Alexa-647 labeled (G) mGluR2 constructs. Quantification of Alexa-647 fluorescence is shown in (H). I-J) Glutamate dose-response curves for mGluR2(3xLB1) and mGluR2(C121A), compared to mGluR2(WT), with the response as either activation of GIRK current (A) or reduction in ensemble FRET with SNAP and CLIP-tagged receptors labeled with acceptor and donor fluorophores, respectively, (B) in HEK 293T cells. K-L) Glutamate dose-response curves for LB2 interface mutants, with the response as either activation of GIRK current (C) or reduction in ensemble FRET (D) in HEK293T cells.

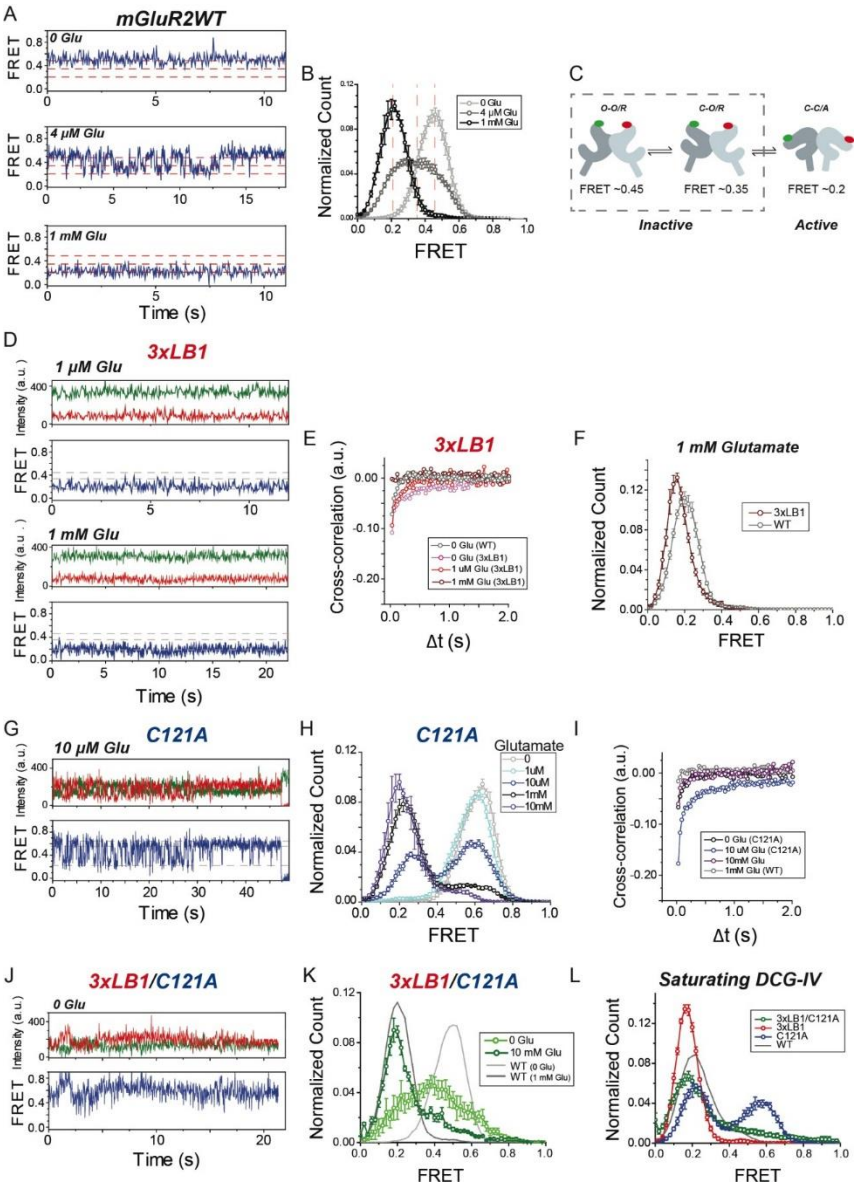

Figure S2.3, smFRET analysis of mGluR2 dimer interface mutants. A) Representative smFRET traces for wild type mGluR2 (SNAP and CLIP-tagged) in the absence (top) or presence of glutamate at a concentration near the EC_{50} (middle) or at saturation (bottom). B) Histogram showing smFRET distributions for mGluR2wt. Red dotted lines mark the three FRET peaks. C) Schematic of 3-state model of LBD activation that involves intra- (open vs. closed) and intersubunit (relaxed vs. active) conformational changes. D)Representative smFRET traces for mGluR2(3xLB1) shows primarily low FRET state occupancy in a low (top) or saturating (bottom) concentration of glutamate. E) Cross-correlation analysis for mGluR2(3xLB1) shows enhanced spontaneous dynamics in the absence of glutamate that are eliminated by saturating glutamate. F) FRET histograms in saturating glutamate show a left shift in low FRET peak location for mGluR2(3xLB1) compared to WT. G) Representative smFRET trace for mGluR2(C121A) shows rapid dynamics in intermediate glutamate. H) smFRET histograms for mGluR2(C121) in a range of glutamate concentrations. Note a substantial occupancy of the medium and high FRET states even in saturating (1 or 10 mM) glutamate. I) Cross-correlation analysis for mGluR2(C121A) shows elevated dynamics even in saturating glutamate. J-L) smFRET analysis of mGluR2(3xLB1/C121A) shows spontaneous dynamics in the absence of glutamate that are similar to 3xLBI (J), altered high and medium FRET peaks and incomplete low FRET occupancy that are similar to C121A (J, K), and intermediate low FRET occupancy in the presence of DCG-IV compared to 3xLB1 and C121A (L).

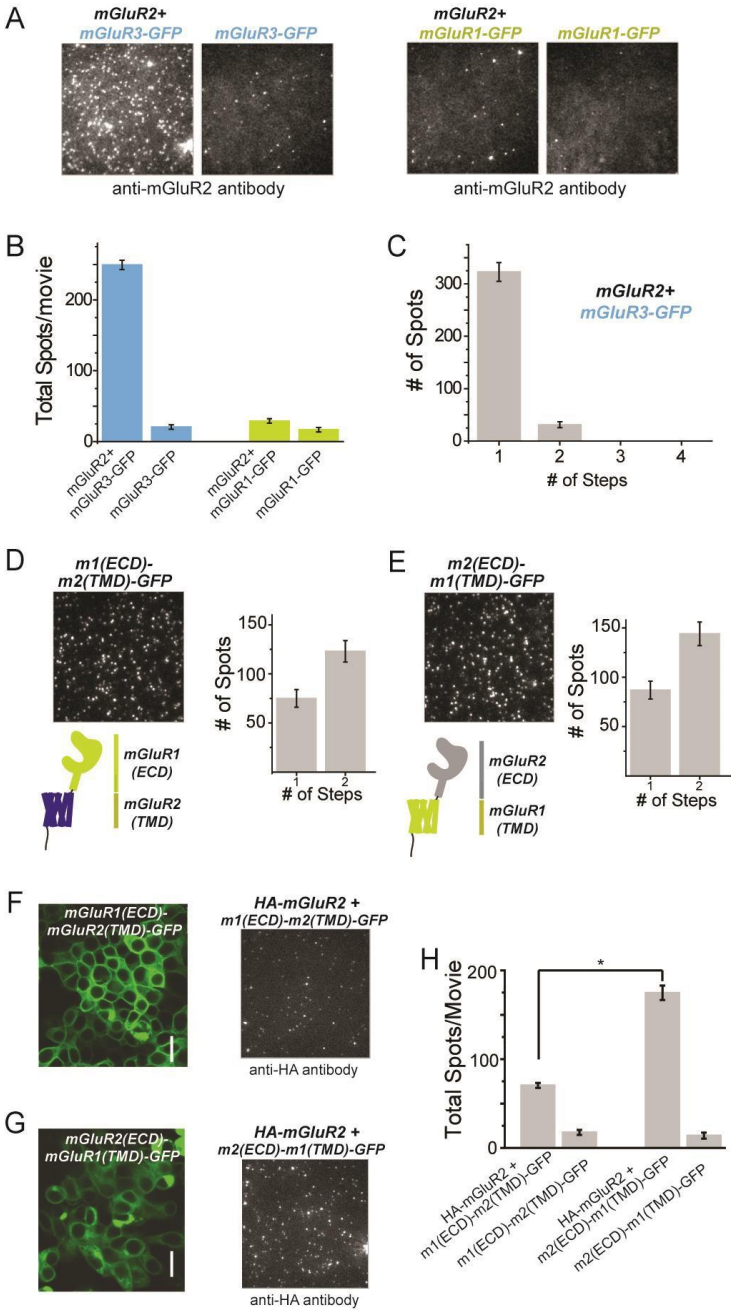

Figure S2.4, Further single molecule analysis of mGluR2 heterodimerization. A) Representative TIRF images show that pulldown of mGluR2 efficiently co-immunoprecipiates mGluR3 (left), but not mGluR1 (right), in SimPull from HEK293T cells. B) Summary of co-pulldown of mGluR3-GFP or mGluR1-GFP by mGluR2. Error bars show S.E.M. calculated from multiple experiments (N>5 movies). C) Photobleaching step distribution analysis showing that mGluR3-GFP spots immobilized via pulldown of mGluR2 primarily bleach in one step, consistent with the formation of mGluR2/mGluR3 heterodimers. D-E) mGluR1(ECD)-mGluR2(TMD) ("mG1(ECD)-mG2(TMD)-GFP") (D) and mGluR2(ECD)- mGluR1(TMD) ("mG2(ECD)-mG1(TMD)-GFP") (E) chimeras form dimers in Xenopus oocytes. Error bars represent the counting uncertainty. F-H) SimPull analysis shows that, in HEK293T cells, HA-mGluR2 co-assembles with either mG1(ECD)-mG2(TMD)-GFP or mG2(ECD)-mG1(TMD)-GFP, but does so more efficiently with mG2(ECD)-mG1(TMD)-GFP. Error bars show S.E.M. calculated from multiple experiments (N≥5 movies)

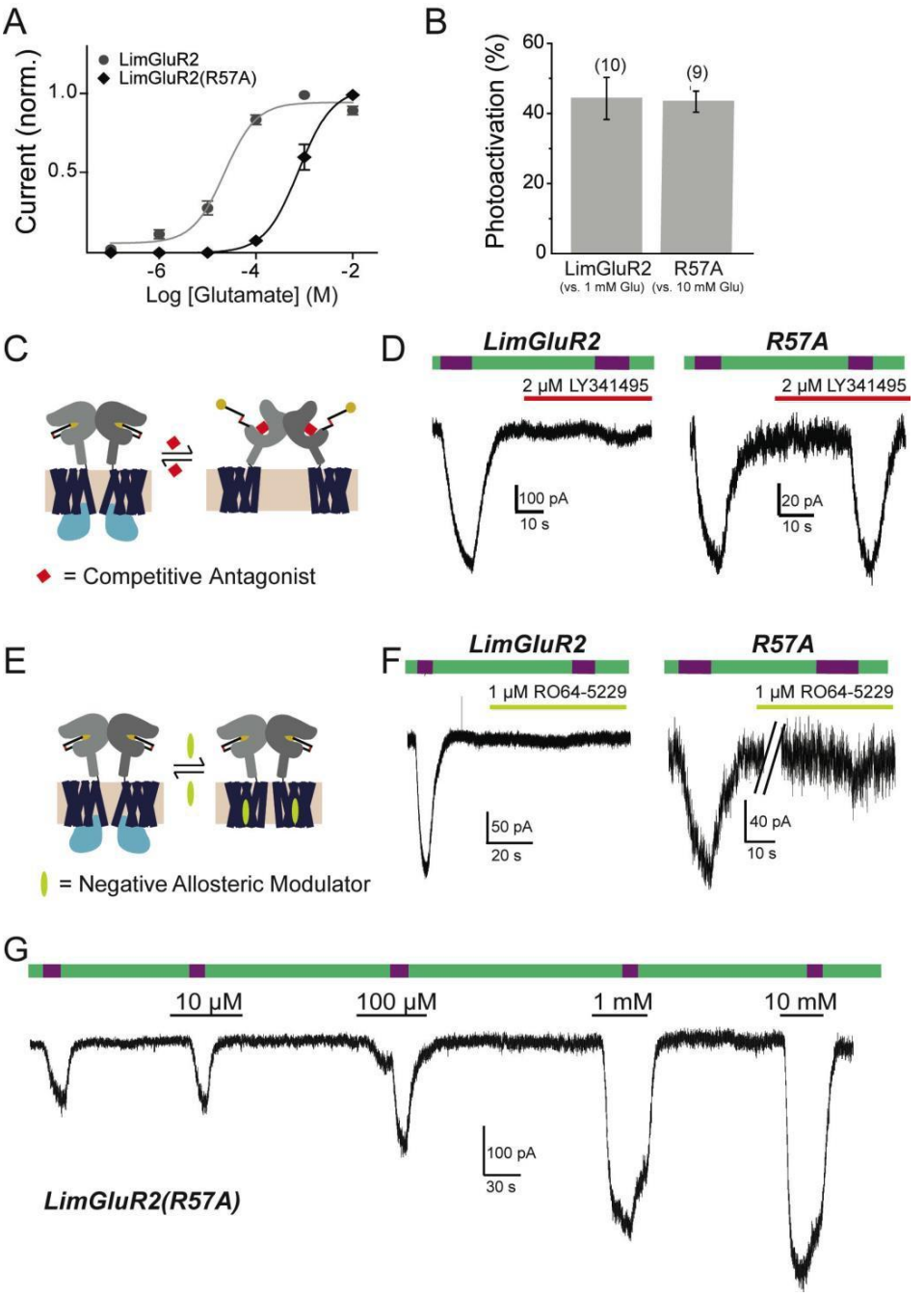

Figure S2.5, D-MAG-0 is a high-efficacy, high-affinity tethered photo-agonist of mGluR2. A) Glutamate dose-response curves for LimGluR2 (mGluR2(300C) + D-MAG-0) and low affinity mutant LimGluR2(R57A) using GIRK current in HEK293 cells as a readout. B) Summary of photoactivation (photocurrent amplitude/saturating glutamate current amplitude) for LimGluR2 and LimGluR2(R57A). The numbers of cells tested are shown in parentheses. **C-D)** 1 uM of the competitive antagonist LY341495, which binds to the orthosteric glutamate binding site (C), blocks photocurrent in LimGluR2, but not LimGluR2(R57A) (D). **E-F)** 1 uM of the negative allosteric modulator RO64-2259, which binds at an allosteric site in the TMD (E), blocks photocurrent in both LimGluR2 and LimGluR2(R57A). **G)** Photoactivation in the presence of a range of glutamate concentrations in LimGluR2(R57A) shows photocurrent potentiation at 100 uM glutamate. Error bars show S.E.M. calculated from multiple experiments (N>3 cells)

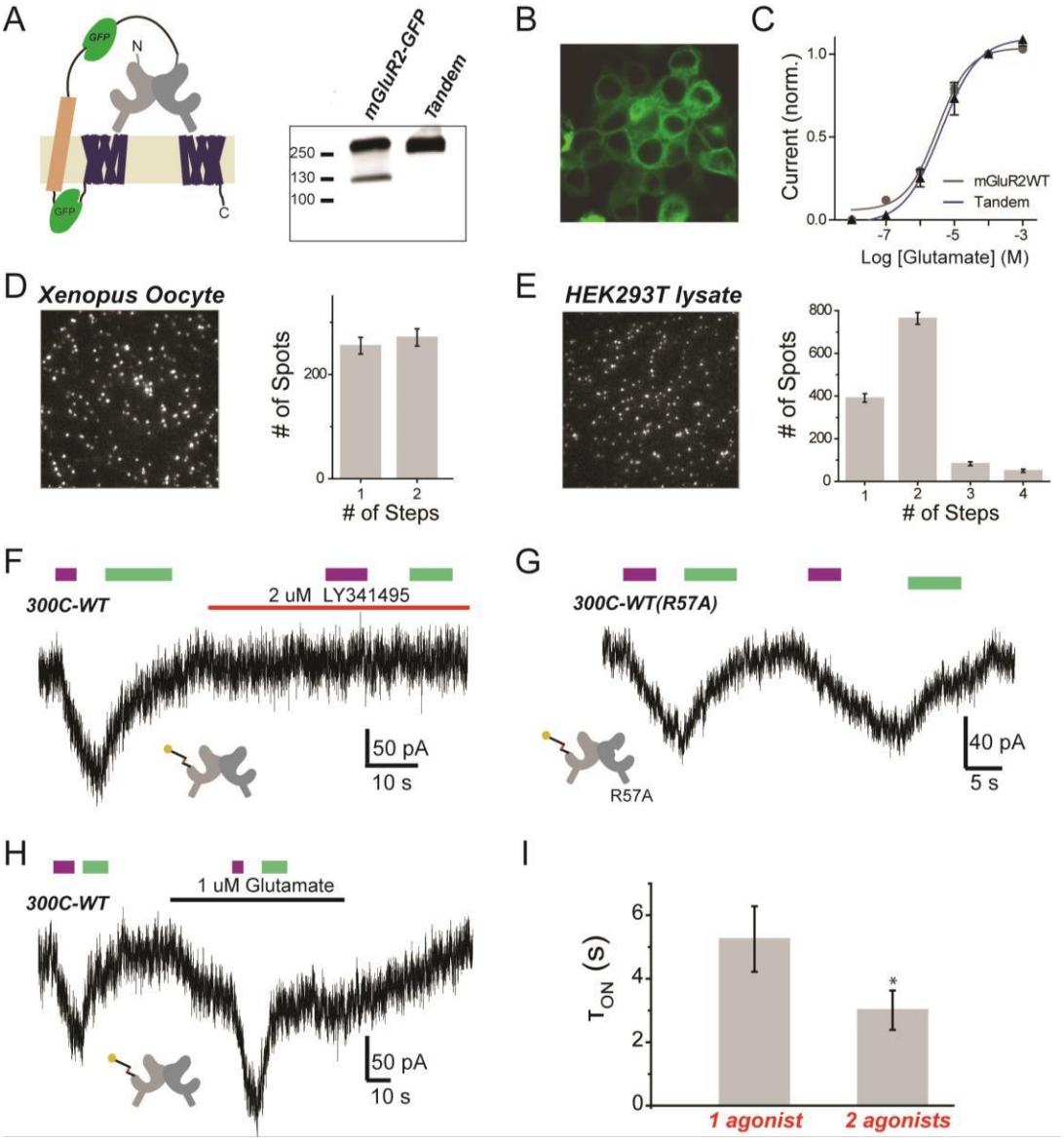

Figure S2.6, Analysis of tandem mGluR dimers and ligand occupancy-dependent cooperativity. A) Western blot analysis using an anti-mGluR2 antibody shows that the mGluR2-mGluR2 tandem dimer (tandem) has the expected molecular weight, which is similar in size to the dimer band observed for mGluR2-GFP (~270 kDa). B) Confocal image of mGluR2-mGluR2 tandem dimers in HEK 293T cells. **C)** Glutamate dose-response curves, using GIRK current readout in HEK293T cells, shows similar glutmate sensitivity for mGluR2(WT) and mGluR2-mGluR2 tandem dimers. Error bars show S.E.M. calculated from multiple experiments (N>4 cells). **D-E)** Single molecule subunit counting analysis in Xenopus oocytes (D) or SimPull from HEK293T cell lysate (E) shows the expected distribution for mGluR2-mGluR2 tandem dimers. Error bars represent the counting uncertainty. **F)** Representative GIRK current trace shows that single subunit photoactivation in mGluR2(300C)- mGluR2(wt) tandem (300C-wt) is blocked by the competitive antagonist, LY341495. **G)** Representative trace showing that single subunit activation of 300C-WT tandem dimers is maintainedwhen the WT subunit is mutated to R57A to lower glutamate affinity. This indicates that single subunit activation is not due to binding of ambient glutamate to the WT subunit. **H)** Single subunit photoactivation of 300C-WT tandem dimers is potentiated by 1 μM glutamate, a concentration below the EC_{50} (see Fig. S4A). **I)** Summary of photoactivation kinetics, as determined from single component exponential fits, for 300C-WT ("1 agonist") and 300C-300C ("2 agonists") tandem dimers. * indicates statistical significance (unpaired t-test, p=0.04). Error bars show S.E.M. calculated from multiple experiments(N>4 cells).

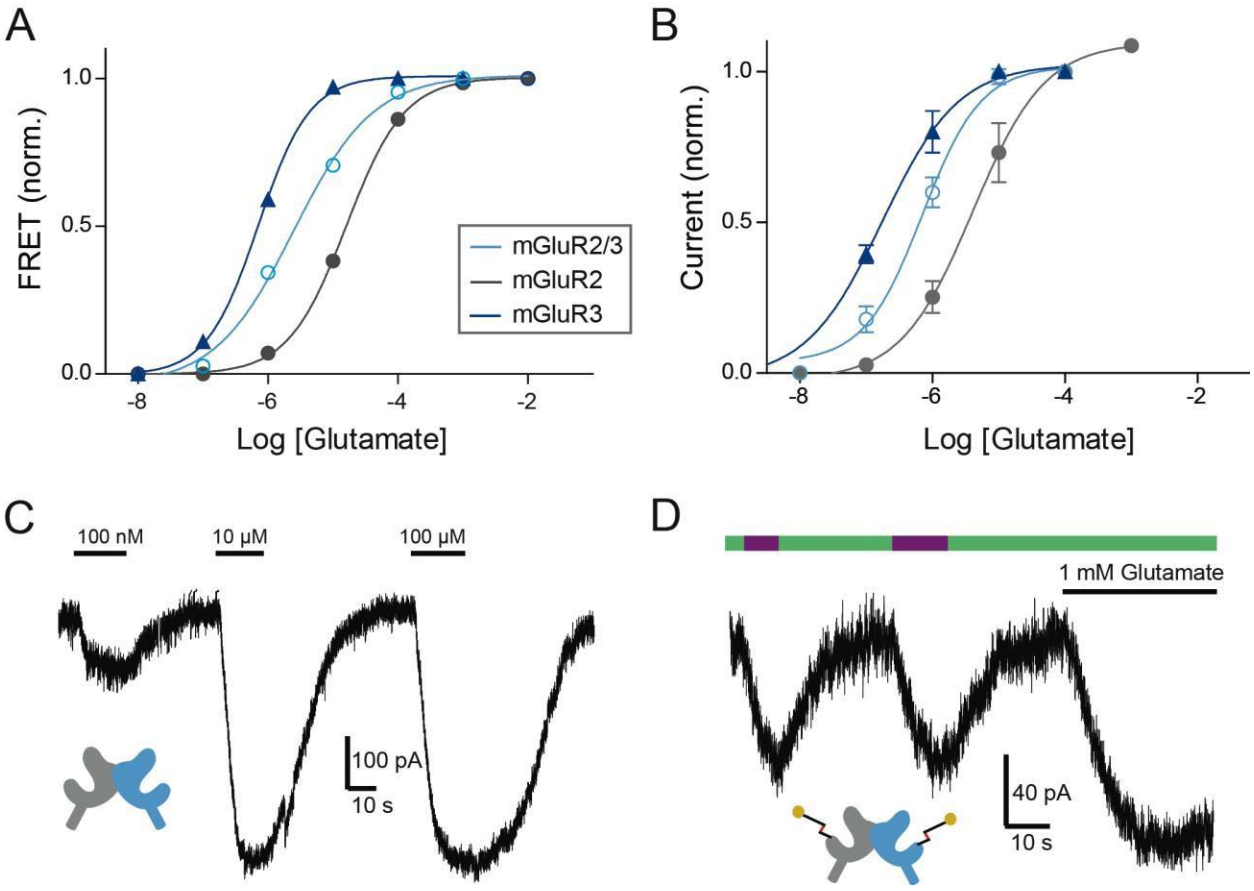

Figure S2.7, Characterization of mGluR2-mGluR3 heterodimers. A-B) Glutamate dose-response curves show an intermediate glutamate affinity for heterodimer of mGluR2 and mGluR3 compared to homodimer of mGluR2 or mGluR3. Activation measured as intersubunit LBD FRET using SNAP-mGluR3 (labeled with BG-Alexa-647 acceptor) co-expressed with CLIP-mGluR2 (labeled with BC-DY-547 donor) (A) or GIRK current using the mGluR2-mGluR3 tandem dimer (B). C) Representative GIRK current trace shows robust glutamate activation of mGluR2-mGluR3 tandem dimer. D) Representative trace shows photoactivation of mGluR2(300C)-mGluR3(306C) tandem dimer using D-MAG-0. Error bars show S.E.M. calculated from multiple experiments (N>3).

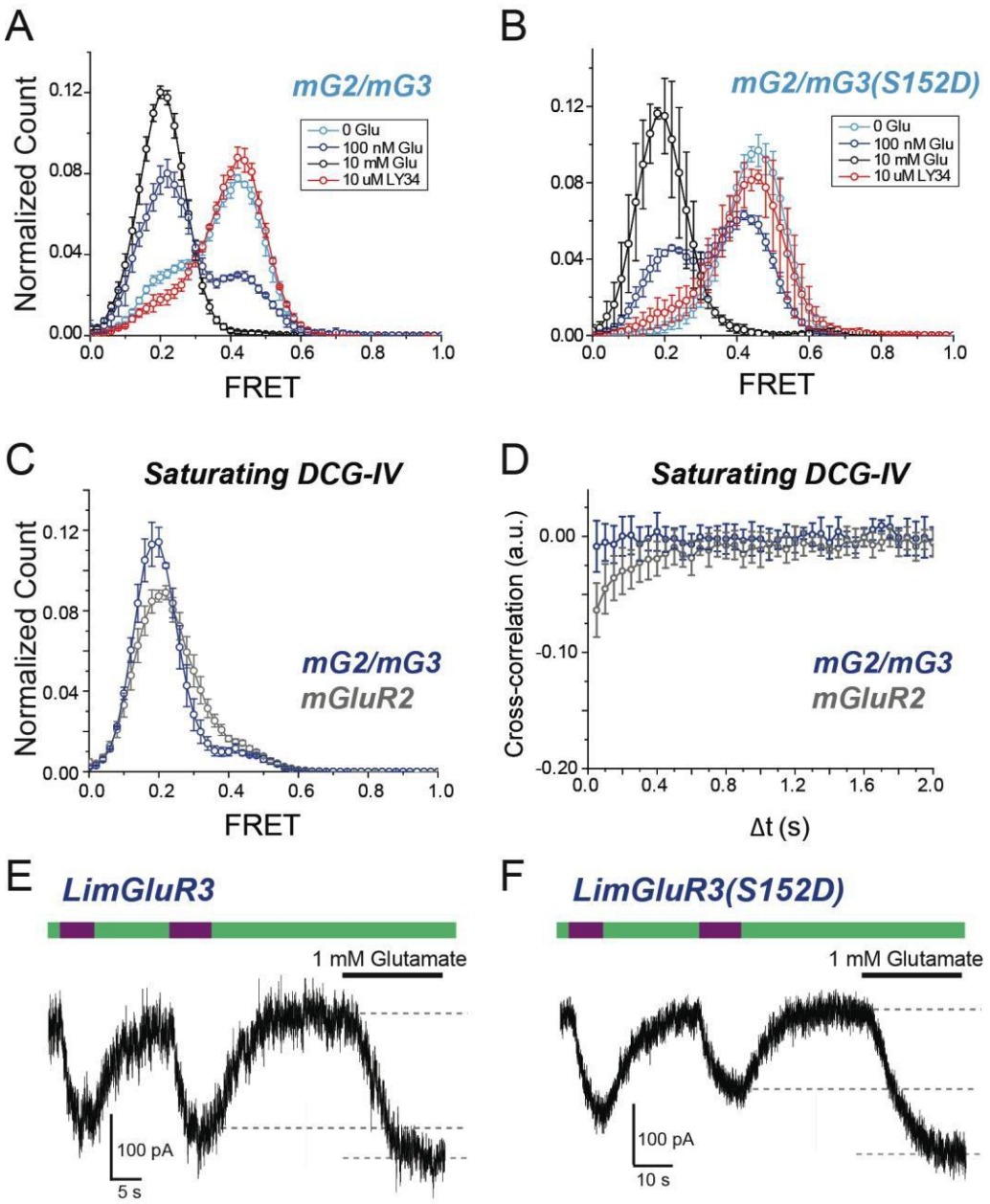

Figure S2.8, Further analysis of conformational dynamics and cooperativity in mGluR2/3 and mGluR3. A-B) smFRET histograms for mG2/mG3 (A) and mG2/mG3(S152D) (B) heterodimers. SNAP-mGluR3is labeled with BG-Alexa-647 acceptor and co-expressed CLIP-mGluR2 is labeled with BC-DY-547 donor. Application of competitive antagonist LY341495 or introduction of the S152D mutation (to eliminate the agonist effect of calcium) into the mGluR3 subunit abolishes basal dynamics in mG2/mG3. C) smFRET histogram reveals enhanced occupancy of the low FRET (activated) state in saturating DCG-IV for mG2/mG3 compared to mGluR2, consistent with stabilization of the activated state. D) Cross-correlation analysis shows decreased dynamics for mG2/mG3 compared to mGluR2 in the presence of saturating DCG-IV, consistent with stabilization of the activated state. **E-F)** Representative traces showing photoactivation of LimGluR3 (mGluR3(306C) + D-MAG-0) (E) and LimGluR3(S152D) (F). Error bars show S.E.M. calculated from multiple experiments ($N \geq 3$)

Chapter III: Conformational Pathway Provides Unique Sensitivity to a Synaptic mGluR

This chapter was published as an article in Nature Communications volume 10, article number 5572 in December 2019 with me as first author.

Introduction:

Building upon the observations made in Chapter II regarding mGluR2 homodimers we investigated a unique mGluR subtype named mGluR7 in a comparative fashion. We see that compared the mGluR2 mGluR7 displays very low glutamate affinity and efficacy. Also using findings from Chapter II involving mGluR2/3 heterodimers we have a point of reference to interpret findings of mGluR2/7 heterodimers which display much higher glutamate affinity compared to their respective homodimers.

G-protein–coupled receptors (GPCRs), the largest class of membrane signaling proteins, respond to a wide array of extracellular stimuli to initiate intracellular signaling via G proteins and arrestins[1]. Recent studies have provided snapshots of GPCR structures in distinct conformations[2-5] and revealed that they are extremely dynamic[6-13]. The conformational dynamics appear to be central to ligand recognition, activation and signaling by GCPRs[9,14,15].

Membrane receptors have evolved to respond to precise spatio-temporal concentration profiles of extracellular ligands. In the nervous system, neurotransmitter receptors encounter a wide range of neurotransmitter concentrations and spatio-temporal profiles. Key factors contributing to these dynamics are the small extracellular volume of the synaptic cleft, pumps and/or enzymes that remove neurotransmitter and diffusion. Additionally, neurotransmitter receptors can be localized within the synapse both pre- and postsynaptically as well as extrasynaptically where they can encounter different sources of neurotransmitter released either locally, which briefly reaches low millimolar levels within a synaptic cleft, and spillover from nearby synapses, which reaches lower concentrations[16]. Thus, receptor activation by transmitter needs to be tuned to suit its localization and sensitivity to transmitter. GPCRs have evolved to respond to diverse signal types at various cellular locations and produce a large variety of responses. Structural and functional diversity in receptor families can provide unique responses in ligand activation and localization, as can specialized post-translational modification or interaction with regulatory proteins[3,17,18].

Most synaptic receptors have apparent affinities (EC50s) in the low micromolar range, or lower[19-21]. One intriguing outlier is metabotropic glutamate receptor 7 (mGluR7). This receptor, one of an 8-member family of class C GPCRs[22], has been reported, based on effector activation, to have an apparent affinity that is much lower than that of the other mGluRs[23]. These properties have led to the idea that mGluR7 may only function at locations very near the site of glutamate release[24], and best at synapses with high repetitive activity and enclosed extracellular volumes[25]. Even under these conditions, it is not clear how effectively mGluR7 is activated.

mGluRs are verified targets of numerous neurological disorders and are considered to contain great potential as therapeutic targets[26-28], unfortunately many years of work have resulted in no mGluR targeting drugs approved for medical use at the present time. Recent work has, for the first time, revealed structures of the active and inactive conformations allowing for more detailed understanding and interpretation of the molecular mechanism of mGluR activation[29]. mGluRs are strict dimers[30,31] and dimerization is required for efficient G protein activation[32]. Heterodimerization can occur between group I members mGluR1 and 5 and within and between members of group II (mGluR2 and 3) and group III (mGluR4, 6, 7 and 8)[30,31]. Functional analysis of one such potential combination, mGluR2/mGluR3 (mGluR2/3), showed that heterodimerization can impart unique functional properties resulting in distinct basal activity[31]. We wondered if heterodimerization of mGluR7 would increase its activation by glutamate. While, overlapping expression suggests that mGluR7 may be co-expressed with other mGluRs and therefore might heterodimerize in the brain, only one example of heterodimer formation has been demonstrated to date in neurons, that of mGluR2/4[33,34]. But the mGluR2/4 heterodimer resembles its parents functionally, not surprisingly since they themselves have similar activation in response to glutamate[34].

To analyze the activation of the mGluR7/7 homodimer, we fluorescently labeled with donor and acceptor Foster resonance energy transfer (FRET) dyes a protein tag fused to the mGluR7 N-terminal, immediately before the ligand binding domain (LBD). We measured FRET changes between the LBDs of the dimer, which result from the conformational rearrangements of activation, in which the receptor dimer transitions from a state with both LBDs empty and open and the receptor at rest (Roo) to a state in which both LBDs are occupied by agonist and closed and the receptor is activated (Acc)[11,13,30,31,35]. Measurements in live HEK 293T cells and at the single-molecule level on immune-purified dimers[13,31] confirm very low affinity[23] and efficacy[36]. We confirm and extend these findings measuring a apparent affinity of 38 mM and a max efficacy of 10%, values too low, it would appear, to support activation by the concentrations estimated for synaptic glutamate[37,38]. However, we find that mGluR7 associates with mGluR2 in hippocampus and that the mGluR2/7 heterodimer has even higher affinity and efficacy than mGluR2/2, a wider dynamic range, showing that heterodimerization can alter the glutamate response of an mGluR. The boosted properties are associated with a special heteromeric cooperativity that boosts the affinity and efficacy of each subunit in the dimer, and which primes the receptor for activation even in absence of agonist through a unique tendency of the LBDs to enter the rotated activated conformation even when they are in the open, Apo state. Combined with unusually fast kinetics, these properties appear to make mGluR2/7 uniquely suited to activate in response to synaptic glutamate.

Results:

mGluR7 activates with very low affinity and efficacy

To understand the unusually low apparent glutamate affinity of mGluR7/7 observed earlier[23], we compared the ligand-induced conformational rearrangement of mGluR7/7 with that of mGluR2/2. As previously described[13,30], N-terminally SNAP-tagged mGluR2 expressed in HEK293T cells and labeled with Alexa-647 (acceptor) and DY-547 (donor) fluorophores (Förster radius 52Å) showed a robust glutamate-induced FRET decrease, which increased with glutamate concentration between 1 μM and 1 mM (Fig. 3.1a), with an EC50 of 18.7 $\pm$ 0.6 μM (Supplementary Fig. 3.1a). A similarly N-terminally SNAP-tagged mGluR7, expressed at comparable levels, as assessed from SNAP dye staining, showed no detectable FRET change at up to 1 mM glutamate, and a barely measurable FRET decrease at 10 mM glutamate (Fig. 3.1b), which was >30-fold smaller than that observed at 1mM glutamate in mGluR2 (Fig. 3.1c). To test whether interaction with a signaling complex affected activation, Gβγ-activated GIRK1 inward rectifier potassium channel was co-expressed with the receptor. We observed no change in the glutamate-induced FRET response of either SNAP-mGluR2 (Supplementary Fig. 3.1a) or SNAP-mGluR7 in the presence of GIRK channels (Supplementary Fig. 3.1b). Nor did a switch to another donor/acceptor dye pair, which gave robust glutamate-induced FRET responses in SNAP-mGluR2 make for detectable responses in SNAP-mGluR7 (Supplementary Fig. 3.1c). In contrast to SNAP-mGluR7, a SNAP-tagged version of another group III mGluR, mGluR4, which has been shown to have low micromolar apparent glutamate affinity (Thomsen et al., 1993), showed glutamate-induced FRET decreases that were similar in amplitude and concentration dependence to those of mGluR2 (Supplementary Fig. 3.1d), and similar to those reported earlier for several of the other mGluRs[13,30].

In HEK293T cells it was not possible to go to glutamate concentrations above 10 mM. We therefore turned to isolated receptors. Receptors expressed in HEK293T cells were labeled with a mixture of SNAP-reactive donor and acceptor fluorophores, detergent solubilized, immune-purified and tethered by biotinylated secondary antibodies at low density to coverslips that were passivated with a lawn of polyethylene glycol[13]. We used single-molecule FRET (smFRET) in order to measure the absolute FRET levels and dynamic changes associated with ligand-induced conformational changes in the LBDs. We imaged the donor and acceptor dyes using total internal reflection fluorescence (TIRF) microscopy[13,31] (Supplementary Fig. 3.1e).

Our baseline for comparison was mGluR2. As previously observed[13], in zero glutamate, the two unliganded LBDs of mGluR2 are both open and in the resting configuration (Roo) and the inter-subunit distance between donor and acceptor SNAP dyes is relatively small, giving a high FRET level of ~0.45, which can be seen in single-molecule trajectories from an individual dimer (Fig. 3.1d, left top) and in histograms that compile measurements from many dimers (Fig. 3.1e, solid grey line). At 1 mM glutamate, the LBDs of mGluR2 are maximally bound, closed and rotated into the activated conformation (Acc) to yield a low FRET level of ~0.2 (Fig. 3.1d, left bottom; Fig. 3.1e, dashed grey line). At an intermediate glutamate concentration of 10 μM, near the EC50 of the ensemble concentration-response FRET measured both in live HEK293T cells (Supplementary Fig. 3.1a) and on isolated protein in smFRET (Fig. 3.1f, red symbols), mGluR2

transitions between the high and low FRET states (Fig. 3.1d, left middle), yielding high conformational dynamics, as measured by donor-acceptor cross-correlation (Supplementary Fig. 3.1f, left).

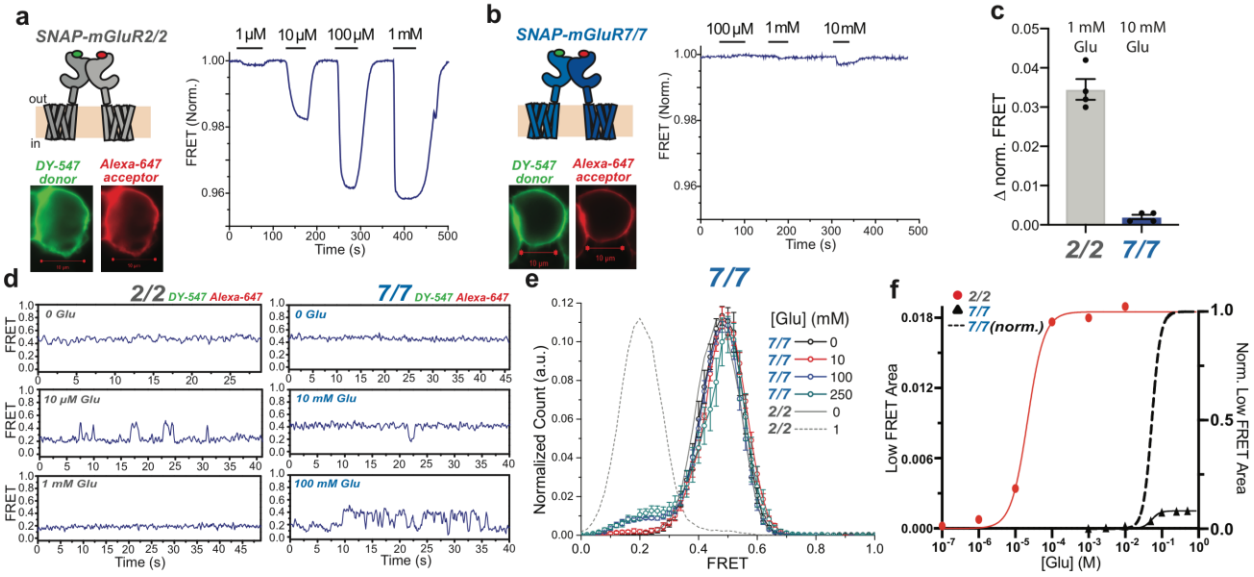

Figure 3.1, Glutamate activate mGluR7/7 with low affinity and low efficacy. a, b) Homodimers of SNAP-tagged mGluR2/2 (a) and mGluR7/7 (b). Left) Schematics (top) and images of expressing HEK293 cells labeled with a mixture of donor (green) and acceptor (red) dyes. Right) Live-cell FRET traces show responses to ascending concentrations of glutamate. Scale bars are 5 µm. c) Mean + S.E.M. fractional change in FRET of SNAP-mGluR2/SNAP- mGluR2 (1 mM glutamate, n = 3) and SNAP-mGluR7/SNAP-mGluR7 (10 mM glutamate, n = 3, *p< 0.05). Individual data points (black dots) and s.e.m. (error bars). d) Representative smFRET traces of SNAP-mGluR2/SNAP-mGluR2 (left) and SNAP-mGluR7/SNAP-mGluR7 (right) at different glutamate concentrations. e) Histogram of smFRET distributions of SNAP-mGluR7/SNAP-mGluR7 in 0 (5 movies, 288 molecules), 10 mM (6 movies, 215 molecules), 100 mM (5 movies, 261 molecules) and 250 mM (5 movies, 253 molecules) glutamate concentrations (colored symbols and interpolation lines, error bars are s.e.m.) and of SNAP-mGluR2/2 in 0 (5 movies, 230 molecules) and 1 mM (4 movies, 197 molecules) glutamate (solid and broken gray lines, respectively). f) Titration curve of low smFRET (activated state) peak in histograms of SNAP-mGluR2/SNAP-mGluR2 (red circle) and SNAP-mGluR7/ SNAP-mGluR7 (black triangle; normalized as black dashed line). Donor (BG-DY-547) and acceptor (BG-Alexa 647) dyes imaged at 10 Hz for ensemble FRET in

Similar to mGluR2, mGluR7 in zero glutamate had a stable FRET level of ~0.45 (Fig. 3.1d, right top; Fig. 3.1e, black symbols). Remarkably, at 10 mM glutamate (10-fold higher than the saturating concentration tested in mGluR2), only rare transitions were seen in mGluR7 from the high FRET state to a low FRET state of ~0.2 (Fig. 3.1d, right middle). While the low FRET level was similar to that of mGluR2, in mGluR7 these events were so short-lived and infrequent that a low FRET peak was barely observable in the pooled histogram (Fig. 3.1e, red symbols). The low FRET peak increased with increasing concentration, reaching a maximum between 100 and 250 mM (Fig. 3.1d, right bottom; Fig. 3.1e, blue and cyan symbols; Fig. 3.1f; Supplementary Fig. 3.1g,h). The EC50 of the mGluR7 low FRET peak concentration-response was 38.3 mM, an apparent glutamate affinity that is ~4,000-fold lower than that of mGluR2 (Fig. 3.1f). Single-molecule trajectories showed that, although at saturating glutamate (≥ 100 mM) transitions to the low FRET state occurred more frequently than at 10mM glutamate, the maximal occupancy of the

glutamate activated state only reached ~10% (Fig. 3.1f). The low degree of maximal activation indicates that glutamate is a low efficacy partial agonist of mGluR7.

Increasing mGluR7 efficacy

To pursue the surprising observation that glutamate is such a low efficacy agonist of mGluR7, we asked whether a point mutation in the LBD agonist binding pocket, N74K, which has been shown to increase apparent affinity of mGluR6 and mGluR7[36], would also affect efficacy. Measurements in smFRET showed that 10 mM glutamate induces more frequent activation transitions in mGluR7(N74K) (Fig. 3.2a, top) and greater occupancy of the activated low FRET (~0.2) state (Fig 3.2a, bottom) than seen in wildtype mGluR7 at $\geq$ 10X higher glutamate (Fig. 3.1e). This reflects an increase in the stabilization of glutamate binding within the LBD.

We next asked if it was possible to increase agonist binding and occupancy at the binding site of wildtype mGluR7 using a synthetic agonist. We turned to a new synthetic group III selective agonist, LSP4-2022, which is highly selective for mGluR4, activating it efficiently at nanomolar concentration[39,40]. We found that LSP4-2022 is a potent activator of mGluR7 at higher concentrations. At 20 μM LSP4-2022, smFRET traces showed frequent transitions to the low FRET activated conformation, and occupancy of the low FRET conformation reached ~65% at 3 mM LSP4-2022 (Figs. 3.2b and Supplementary Fig. 3.2a), the highest concentration we could test,

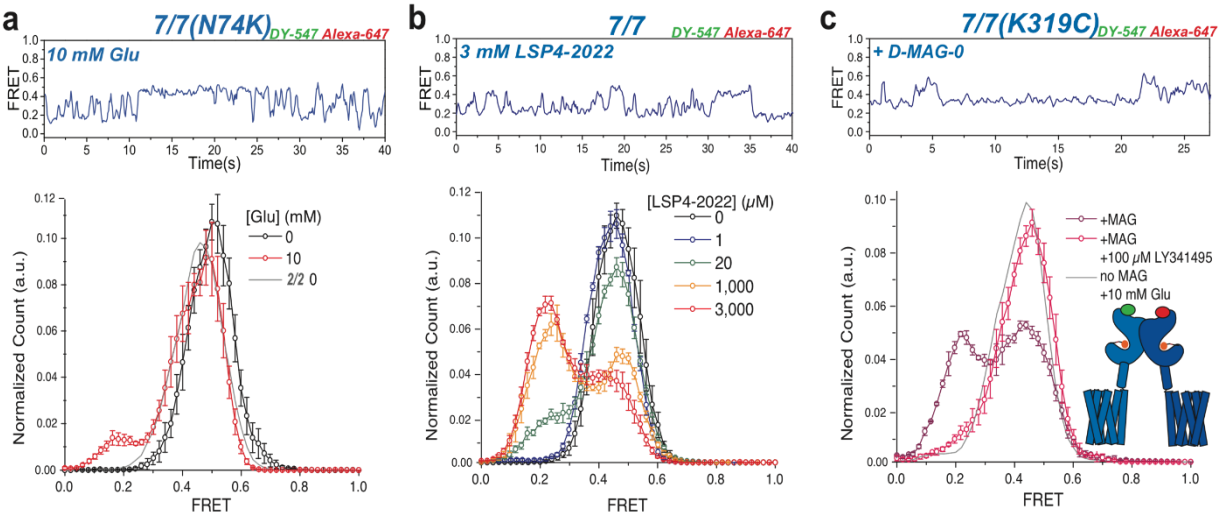

Figure 3.2, Increasing mGluR7 efficacy. a–c) Representative smFRET traces (top) and smFRET histograms (bottom) of homodimers of SNAP-mGluR7(N74K) (0 Glu: 4 movies, 124 moleucles, 10 mM Glu: 4 movies, 140 molecules, s.e.m. error bars) compared to SNAP-mGluR2 in glutamate (a); SNAP-mGluR7 in LSP4-2022 (0: 4 movies, 145 molecules, 1 μM: 5 movies, 197 molecules, 20 μM: 5 movies, 128 molecules, 1 mM: 5 movies, 122 molecules, 3 mM LSP4: 6 movies, 206 molecules, s.e.m. error bars) (b); and SNAP-mGluR7(K319C) conjugated to D-MAG-0 in the *trans* configuration (8 movies, 230 molecules, s.e.m error bars), in the presence of 100 μM LY341495, and unconjugated SNAP-mGluR7(K319C) (6 movies, 256 molecules, s.e.m. error bars) (c, and cartoon insert). Donor (BG-DY-547) and acceptor (BG-Alexa 647) dyes imaged at 10 Hz.

indicating an at least 6-fold greater efficacy than that of glutamate (compare Figs. 3.1e and 3.2b).

We next asked whether glutamate itself could be turned into a more potent agonist of mGluR7 if the glutamate were lodged stably into the LBD binding pocket. To achieve this, we used a photoswitchable tethered glutamate, maleimide-azobenzene-glutamate D-MAG-0 (Supplementary Fig. 3.2b), which attaches covalently to the LBD and docks its glutamate into the agonist binding pocket in mGluRs in one of the photo-isomeric configurations of azobenzene, achieving a high effective concentration[31,41,42]. When conjugated to an engineered cysteine on the lower lobe of the mGluR7 LBD (K319C), D-MAG-0 activated mGluR7 in the *trans* configuration of azobenzene (in the dark and under ~500 nm light), and deactivated in the *cis* configuration (~380 nm light), as measured by activation of the G protein activated inward rectifier potassium channel, GIRK1(F137S) (Supplementary Fig. 3.2c,d). The K319C mutation did not alter the apparent affinity of mGluR7 for glutamate (Supplementary Fig. 3.2e). Thus, D-MAG-0 is an agonist of mGluR7 in the *trans* configuration of azobenzene. This enabled us to perform FRET experiments to monitor the activation rearrangement of the LBD and photoswitch D-MAG-0. We used illumination at 532 nm to simultaneously excite the FRET donor and photo-isomerize D-MAG-0 into the agonistic *trans* state.

smFRET was performed on purified SNAP-mGluR7(K319C) homodimers that were labeled with donor and acceptor dyes on the SNAP and D-MAG-0 on K319C in the D-MAG-0 activated state. The smFRET trajectories showed frequent transitions into the low FRET activated state (Fig. 3.2c, top). Histograms that pooled the behavior of many dimers showed that the occupancy of the activated low FRET state was ~50% (Fig. 3.2c, bottom). Addition of the high affinity orthosteric antagonist LY341495 caused a nearly complete disappearance of the low FRET peak (Fig. 3.2c, bottom), consistent with displacement of the glutamate of D-MAG-0 from the orthosteric binding site. These observations show that the tethered glutamate of D-MAG-0 stabilizes the activated conformation of mGluR7 approximately 5-fold more effectively than does saturating free glutamate. This suggests that the low efficacy of glutamate in mGluR7 may result from a mismatch between the kinetics of glutamate binding and unbinding and the kinetics of LBD closure / activation rotation, which are overcome when *trans* D-MAG-0 jams its glutamate into the ligand binding pocket.

mGluR7 heterodimerization with mGluR2

Our observations, so far, suggest that mGluR7 has an active state conformation that is similar to that of other mGluRs, that this conformation is only weakly stabilized by glutamate, and that pointing glutamate into the binding pocket on a stiff tether boosts efficacy, indicating that mGluR7 is capable of strong activation by glutamate. We wondered whether some modification of mGluR7 could change its properties so that it would be more strongly activated by glutamate.

It is known that mGluR7 can heterodimerize with other mGluRs[30] and earlier work suggests that mGluR7 expression may overlap with that of other mGluRs in the mammalian brain[43]. We wondered, therefore, if mGluR7 heterodimerization occurs in neurons and, if so, whether a heterodimer containing mGluR7 would have stronger activation by physiological levels of glutamate. mGluR7 is expressed strongly in the hippocampus, olfactory bulb and tubercule, and cortex[44]. In the hippocampus, other mGluRs are also expressed, including group I members mGluR1 and 5 and group II members mGluR2 and 3, with the highest expression of mGluR5 and

2[45]. Earlier studies showed that mGluRs co-assemble within and between groups II and III members, but that these do not assemble with group I members, which only heterodimerize within group I[30,31]. This led us to consider possible assembly of mGluR2 with mGluR7. We found that mGluR2 expression overlaps with that of mGluR7 (Supplementary Fig. 3.3a-c). We used anti-mGluR7 antibody to immune-precipitate mGluR7 from adult rat hippocampi and found that mGluR2 co-precipitates with mGluR7 (Supplementary Fig. 3.3d). To further test the potential for mGluR7 heterodimerization in native tissue, we asked whether mGluR3 and mGluR7 interact in rat cortex. We find that we mGluR3 co-precipitates with mGluR7 (Supplementary Fig. 3.3d). These results suggest that mGluR7 either heterodimerizes with mGluR2 in the hippocampus and with mGluR3 in the cortex, or potentially associates with these proteins indirectly.

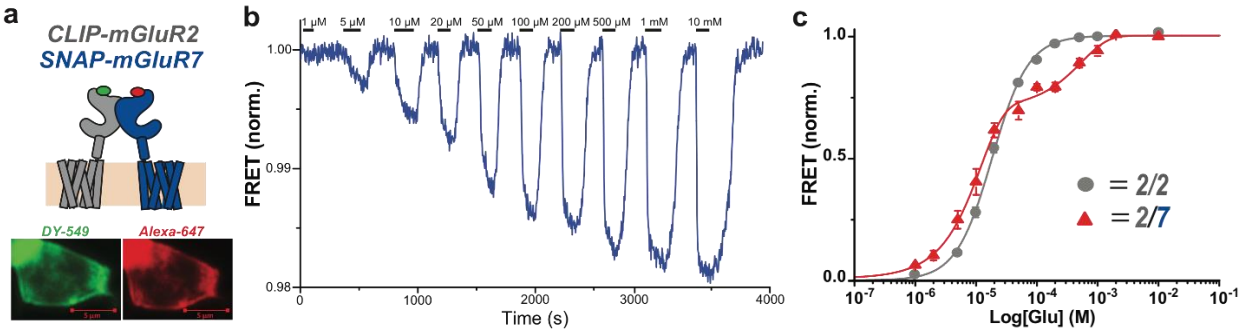

Figure 3.3, mGluR2/7 heterodimer has a biphasic glutamate concentration-response in HEK293 cells. a) mGluR2/7 heterodimer formed by CLIP-mGluR2 and SNAP-mGluR7 heterodimer. Schematic (top) and images of HEK293 cells (bottom, scale bars 5 µm) labeled with donor (BC-549) on CLIP-mGluR2 and acceptor (BG-Alexa-647) on SNAP-mGluR7. HEK293 cells expressing SNAP-mGluR7 and CLIP-mGluR2. b) Representative live-cell FRET trace of CLIP- mGluR2/SNAP-mGluR7 heterodimers in response to ascending concentrations of glutamate. c) Glutamate concentration-response relation of normalized FRET in CLIP-mGluR2/SNAP-mGluR7 heterodimer (red, *n* = 3, s.e.m. error bars) compared to SNAP-mGluR2/2 (gray, *n* = 3, s.e.m. error bars).

mGluR2/7 has high glutamate affinity

Having found that mGluR7 associates with mGluR2, we examined the functional properties of the mGluR2/7 heterodimer. We co-expressed SNAP-mGluR7 and CLIP-mGluR2 in HEK 293 cells and labeled SNAP-mGluR7 with the SNAP-selective acceptor dye BG-Alexa 647 and CLIP-mGluR2 with the CLIP-selective donor dye BC-DY-547 (Fig. 3.3a). Dye labeling was specific for SNAP or CLIP and labeling of SNAP-mGluR7 and CLIP-mGluR2 was comparable (Supplementary Fig 3.3f,g), indicating that they expressed at comparable levels. The co-expression of SNAP-mGluR7 and CLIP-mGluR2 is expected to yield three dimer stoichiometries: the homodimeric SNAP-mGluR7/SNAP-mGluR7; the homodimeric CLIP-mGluR2/CLIP-mGluR2, and the heterodimeric SNAP-mGluR7/CLIP-mGluR2. Of these, only the heterodimer combines the donor and acceptor and produces a FRET signal[34].

Live-cell ensemble FRET experiments on SNAP-mGluR7/CLIP-mGluR2 revealed large glutamate-induced concentration-dependent decreases in FRET for mGluR2/7 (Fig. 3.3b). The behavior of mGluR2/7 differed greatly from that of the mGluR7/7. mGluR2/7 had responses to low micromolar glutamate, whereas mGluR7/7 required 10 mM glutamate to give a measurable response (compare Figs. 3.3b to Fig. 3.1b). The reverse protein tagging--CLIP-mGluR7/SNAP-

mGluR2--showed a similar high apparent affinity for glutamate (Supplementary Fig. 3.3h). The glutamate concentration-response relation of mGluR2/7 was biphasic, consisting of a major component (~80% of total ΔFRET) with high affinity ($EC50_{high}$ = 2.7 μM SEM: 3.8 μM), which is 7 fold lower than mGluR2/2, and a minor component (~20% of total ΔFRET) with lower affinity ($EC50_{low}$ = 2.5 mM SEM: 0.58 mM) (Fig. 3c).

Live cell assays face challenges at both low and high glutamate concentrations. Unhealthy cells may release glutamate and interfere with detection of responses to low micromolar glutamate, and it is not possible to go above 10 mM glutamate. We therefore turned to single-molecule analysis on the purified protein, where glutamate concentration could be accurately defined throughout the concentration range and where we measure absolute FRET. Individual smFRET trajectories showed that in zero glutamate mGluR2/7 heterodimers spend most of the time at a FRET level of ~0.4, whereas at 10 mM glutamate they were mainly at a low FRET level of ~0.2,

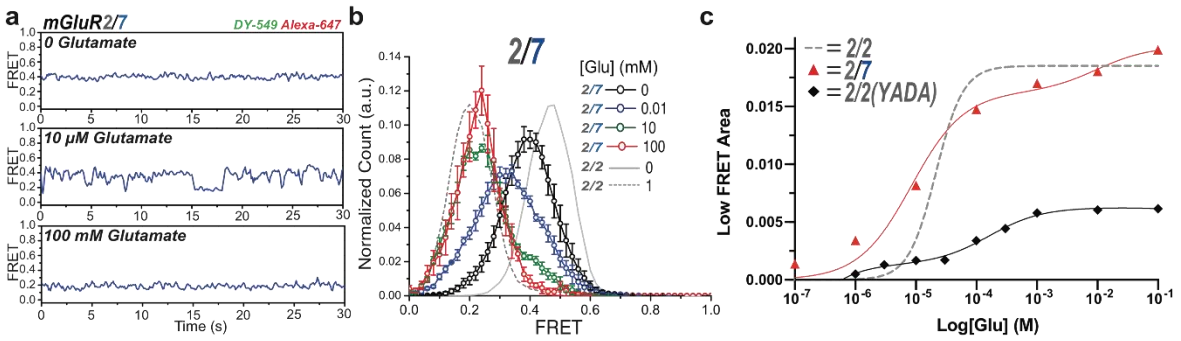

Figure 3.4, The mGluR2/7 heterodimer has high glutamate affinity and high efficacy. a) Representative smFRET traces of CLIP-mGluR2/SNAP-mGluR7 labeled with BC-549 (donor) and BG-Alexa-647 (acceptor), in different glutamate concentrations, imaged at 10 Hz. b) smFRET histograms of CLIP-mGluR2/SNAP-mGluR7 labeled with BC-549 and BG-Alexa-647 at 0 (5 movies, 191 molecules, s.e.m. error bars), 10 μM (7 movies, 267 molecules, s.e.m. error bars), 10 mM (6 movies, 167 molecules, s.e.m. error bars), and 100 mM (4 movies, 120 molecules, s.e.m. error bars) glutamate concentrations. Gray traces represent histograms of SNAP-mGluR2/SNAP-mGluR2 in 0 and 1 mM glutamate (solid and broken lines, respectively). c) Glutamate concentration-response relations of low FRET (activated state) peak of smFRET histograms of SNAP-mGluR2/SNAP-mGluR2 (gray dashed line single Boltzmann fit), CLIP-mGluR2/SNAP-mGluR7 (red triangles and red solid double Boltzmann fit) and CLIP-mGluR2/SNAP-mGluR2(YADA) (black diamonds and black solid double Boltzmann fit).

and at 10 μM glutamate they transitioned back and forth between these levels (Fig. 3.4a). Occupancy histograms that pooled many mGluR2/7 dimers showed ~50% occupancy of the low FRET active state at 10 μM glutamate (Fig. 3.4b,c). At 10 mM glutamate, mGluR2/7 mostly occupied the low FRET activated state, but there remained a small high FRET shoulder, which disappeared at 100mM glutamate (Fig. 3.4b). The low smFRET (activated state) concentration-response relation for mGluR2/7 was biphasic, consisting of a major (~80%) high affinity component ($EC50_{high}$ = 8.4 μM) and a minor (~20%) low affinity component ($EC50_{low}$ = 9.9 mM) (Fig. 4c).

We wondered if the glutamate response of mGluR3/7 heterodimers would also differ from that of the respective homodimers. Samples were prepared in the same manner as for mGluR2/7 heterodimers and imaged in smFRET. We found that, in absence of glutamate, mGluR3/7 occupies

the active state ~70% of the time (Supplementary Fig. 3.4a), significantly higher than what we previously observed in the mGluR3/3 homodimer[13]. In 10μM glutamate the active state occupancy was ~95% (Supplementary Fig. 3.4a).

We wondered whether the distinct components of the FRET concentration-response in mGluR2/7 reflect the closure at the different LBDs, i.e. if the high affinity mGluR2 LBD closes in sub-100 μM range and the low affinity mGluR7 LDB closes in the above-100 μM range. To examine this, we tested the behavior of a heterodimer that co-assembles a wildtype mGluR2 with a binding site mutant version of mGluR2, mGluR2 (Y216A and D295A; known as the YADA mutant). This YADA mutant was developed by J.P. Pin's group in mGluR5, where, as a homodimer, it was shown to not be activated by 10 mM glutamate and was shown to have a biphasic effector activation concentration-response as a heterodimer with a wildtype subunit of mGluR5 [mGluR5/mGluR5(YADA)][46]. The biphasic concentration-response was attributed to binding glutamate at low concentration by the wildtype LBD and at higher concentration by the YADA LBD, and closure of a single LBD was interpreted to be sufficient for only partial activation. We co-expressed CLIP-mGluR2 and SNAP-mGluR2(YADA) and labeled with the SNAP-selective acceptor dye BG-Alexa-647 and the CLIP-selective donor dye BC-DY-547. The mGluR2/mGluR2(YADA) dimer had a biphasic FRET concentration-response relation (Fig. 3.4c), confirming earlier observations[13], and supporting the notion that the biphasic concentration-response relation of mGluR2/7 does indeed represent the closure over different concentration ranges of the high affinity mGluR2 LBD and the low affinity mGluR7 LBD. The high affinity component of mGluR2/mGluR2(YADA) produced only a small fraction (~10%) of maximal activation, and this stood in stark contrast to what we observed in mGluR2/7 where the first component was 10-fold larger (Fig. 3.4c). These findings indicate that closure of a single wildtype mGluR2 subunit is much more efficient in activating the receptor when partnered in the dimer with an mGluR7 than with another mGluR2.

Enhanced efficacy of one-subunit liganding in mGluR2/7

The above results suggest that the heterodimeric interaction between mGluR2 and mGluR7 more strongly favors the activated state than do homodimeric interactions. We explored this further by examining trans-activation, whereby binding of ligand to one subunit activates G-protein interaction in the partner subunit[46,47]. To specifically activate only the mGluR2 subunit of the mGluR2/7 heterodimer, we selectively attached a photoswitched tethered ligand to mGluR2. We used the photoswitchable tethered glutamate, benzylguanine azobenzene glutamate ($BGAG_{12}$), which attaches covalently to the N-terminal SNAP tag of SNAP-mGluR2, where we conjugate fluorophore for our FRET analysis. As shown earlier[48], this $BGAG_{12}$-labeled SNAP-mGluR2 is photo-activated by illumination at 380 nm. The tether of $BGAG_{12}$ is short, so it only ligands and activates the subunit to which it is attached[31]. To cripple G protein signaling of the photoswitch-controlled SNAP-mGluR2 subunit, we introduced the mutation F756D, which prevents G-protein coupling[49]. SNAP-mGluR2(F756D) was co-expressed with wild-type mGluR7 along with the GIRK1 channel. The co-expression was expected to yield three mGluR dimer stoichiometries: the homodimeric SNAP-mGluR2(F756D)/SNAP-mGluR2(F756D), where both subunits would be conjugated to $BGAG_{12}$ but neither could couple to G protein; the homodimeric mGluR7/mGluR7,

which would be non-responsive to light because of lack of an attached $BGAG_{12}$; and the heterodimeric SNAP-mGluR2(F756D)/mGluR7, the only dimer potentially capable of signaling if $BGAG_{12}$ activation of the signaling-dead mGluR2 were able to trans-activate mGluR7 (Supplementary Fig. 3.4b).

Activation of $BGAG_{12}$ on the SNAP-mGluR2(F756D) subunit by illumination at 380 nm induced an inward GIRK1 current that was reversed by illumination at 500nm, the wavelength that causes unbinding (Supplementary Fig. 3.4c,d). As expected, cells expressing only the G-protein-coupling-dead SNAP-mGluR2(F756D) had no photocurrent (Supplementary Fig. 3.4d). These results demonstrate that the mGluR2/7 heterodimer possesses trans-activation. This result was confirmed by activation of GIRK1 channels with free glutamate over a concentration range corresponding to the high affinity activation rearrangement phase in mGluR2/7 (Supplementary Fig. 3.4e). As seen in the smFRET measure of the conformational change associated with activation, the foot of the curve was shifted to the left compared to that of the mGluR2/2 homodimer. The amplitude of the photocurrent was 19.7 $\pm$ 1.5 % (n = 42 cells) that of the current induced by 1 mM glutamate (Supplementary Fig. 3.4b).

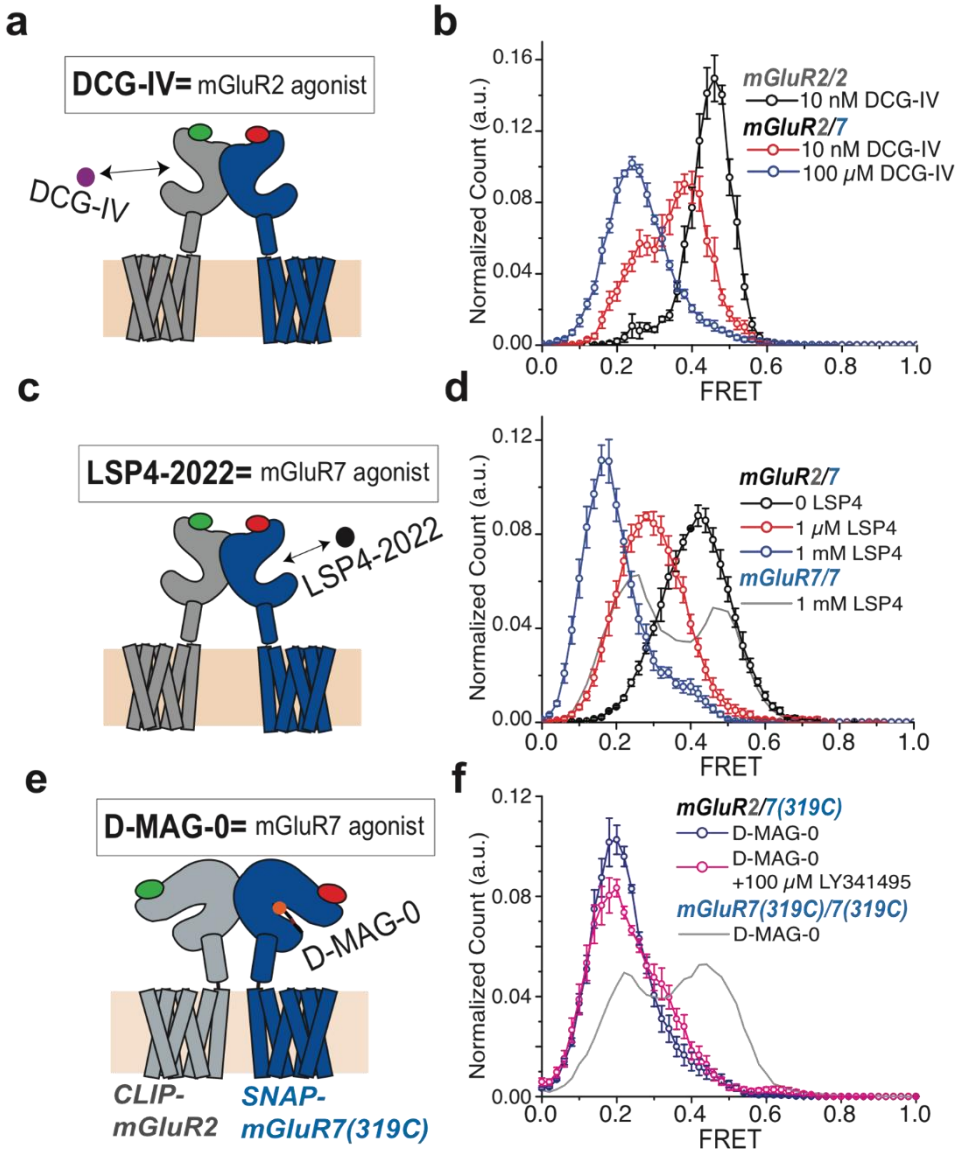

Figure 3.5, Enhanced agonism in the mGluR2/7 heterodimer. Single subunit agonism in mGluR2/7 drives greater activated state occupancy (lower FRET values) than agonism of both subunits in either mGluR2/2 or mGluR7/7. a) Schematic of CLIP-mGluR2/SNAP-mGluR7 binds DCG-IV only in mGluR2. b) smFRET histograms of CLIP-mGluR2/SNAP-mGluR7 and SNAP-mGluR2/SNAP-mGluR2 show greater activation at 10 nM DCG-IV in mGluR2/7 (red) (6 movies, 189 molecules, s.e.m. error bars) than in mGluR2/2 (black) (4 movies, 119 molecules, s.e.m. error bars). mGluR2/2 in the presence of 100 μM DCG-IV (blue) (4 movies, 234 molecules, s.e.m. error bars). c) Schematic of CLIP-mGluR2/SNAP-mGluR7 binds LSP4-2022 only in mGluR7. d) smFRET histograms of CLIP-mGluR2/SNAP-mGluR7 and SNAP-mGluR7/SNAP-mGluR7 show greater activation at 1 mM LSP4-2022 in mGluR2/7 (red) than mGluR7/7 (gray). CLIP-mGluR2/SNAP-mGluR7 in the presence of 0 (6 movies, 187 molecules, s.e.m. error bars), 1 μM (6 movies, 175 molecules, s.e.m error bars) and 1 mM (6 movies, 189 molecules, s.e.m. error bars) LSP4. e) Schematic of CLIP-mGluR2/SNAP-mGluR7(K319C) with D-MAG-0 attached to K319C docking glutamate into the mGluR7 LBD in the *trans* configuration. f) smFRET histograms of CLIP-mGluR2/SNAP-mGluR7(K319C) and SNAP-mGluR7(K319C)/ SNAP-mGluR7(K319C), with *trans* D-MAG-0 (6 movies, 158 molecules, s.e.m error bars), show greater activation in mGluR2/7 (blue) than mGluR7/7 (gray). 100 μM of the orthosteric antagonist LY341495 has little effect on activation by D-MAG-0 on mGluR2/7 (magenta) (6 movies, 174 molecules, s.e.m. error bars), in contrast to the complete block seen in mGluR7/7 (Fig.

We wondered if the enhanced efficacy in mGluR2/7 could be detected using a free agonist

that could only activate mGluR2 and antagonize mGluR7. The concentration-response relation for effector trans-activation by the group II agonist DCG-IV measured in patch clamp recordings in cells co-expressing the GIRK1 channel showed similar concentration-response relations for mGluR7/SNAP-mGluR2(F756D) and SNAP-mGluR2/SNAP-mGluR2, but, once again, at the foot of the concentration-response relation, the mGluR2/7 heterodimer was more sensitive than the mGluR2/2 homodimer (Supplementary Fig. 3.4f), even though mGluR2/2 possesses two subunits that bind DCG-IV and two subunits capable of G-protein activation, whereas the heterodimer has only one. The observation of higher apparent affinity of mGluR2/7 in effector activation by DCG-IV led us to ask whether we could detect a greater potency of DCG-IV in inducing transition to the activated conformation in mGluR2/7. In smFRET, 100 μM DCG-IV induced near-complete (~90%) occupancy of the activated conformation (Fig. 3.5b), confirming that mGluR2/7 can be strongly activated by liganding only the mGluR2 LBD and antagonizing mGluR7[50]. At 10 nM DCG-IV, mGluR2/2 had low (~5%) occupancy of the activated conformation, but mGluR2/7 had about 5-fold greater (~25%) activated conformation occupancy (Fig. 3.5b). Together, these observations of activation rearrangement in the receptor and activation of the effector show that liganding of an mGluR2 LBD activates the receptor more potently when mGluR7 is the partner subunit than when the partner is another mGluR2 subunit.

Having seen that liganding of just the mGluR2 subunit can strongly activate mGluR2/7, we examined the effect of agonist binding to only the mGluR7 subunit. We isolated receptor protein from cells co-expressing SNAP-mGluR7 and CLIP-mGluR2, where the group III selective agonist LSP4-2022 could be used to bind only to the mGluR7 subunit of mGluR2/7 (Fig. 3.5c). We observed two striking differences between LSP4-2022 activation of the mGluR7/7 homodimer and the mGluR2/7 heterodimer. A first difference was that, whereas 1 mM LSP4-2022 produced slightly more than 50% occupancy of the activated conformation in mGluR7/7, activation was almost complete in mGluR2/7 (Fig. 3.5d). Indeed, even 1 μM LSP4-2022 was sufficient to shift the smFRET distribution slightly more than half-way toward the activated low FRET state (Fig. 3.5d). This gives the mGluR7 subunit an approximately 1000-fold higher apparent affinity for LSP4-2022 when partnered with mGluR2 than when partnered with another mGluR7. A second difference was that in mGluR2/7 LSP4-2022 concentrations near the EC50 produced a single broad distribution with a peak, which was intermediate between the high FRET resting and low FRET activated states, as opposed to two resolved distributions of the high FRET resting and low FRET activated states, as seen in mGluR7/7 (Fig. 3.5d). This single broad smFRET distribution is similar to what we have seen with glutamate activation of the mGluR2/7 heterodimer and mGluR2/2 homodimer, above (Fig. 3.4b). We examine this further below.

Having seen that synthetic agonists that are selective for either the mGluR2 subunit or the mGluR7 subunit produce stronger activation in mGluR2/7 than in either mGluR2/2 or mGluR7/7, we wanted to determine if the native agonist glutamate is also a stronger activator in mGluR2/7. To confine the glutamate to one of the subunits, we once again tethered the photoswitchable tethered glutamate, D-MAG-0, to the mGluR7 LBD (Fig. 3.5e). smFRET analysis showed that mGluR2/7 with a tethered ligand only on the one mGluR7 subunit spends ~90% of the time in the activated low-FRET state of ~0.2, higher than the ~50% activation seen in the mGluR7/7 homodimer in which both subunits had the tethered agonist (Fig. 3.5f). In addition, we found that, whereas 100 μM of the competitive antagonist LY341495 almost completely blocked activation

of mGluR7/7 by *trans* D-MAG-0 (Fig. 3.2c), it had little effect on activation by *trans* D-MAG-0 of mGluR2/7 (Fig. 3.5f). The results suggest that D-MAG-0 binds with higher affinity to the mGluR7 LBD when it is partnered with mGluR2 than when it is partnered with another mGluR7.

Together these experiments show that mGluR7 enhances activation by mGluR2 and mGluR2 enhances activation by mGluR7, so that the heterodimer has greater sensitivity to glutamate and synthetic agonists and stronger activation by single subunit agonism than seen in either the mGluR2/2 homodimer, or the mGluR7/7 homodimer.

Spontaneous rearrangements and altered kinetics in mGluR2/7

One striking property of the mGluR2/7 heterodimer is the shape of the smFRET histogram at intermediate concentrations. mGluR7/7 had two well-resolved smFRET distributions—the resting high-FRET state and the activated low-FRET state (Fig. 3.1e and Fig. 3.2) and the occupancy of the former decreases as occupancy of the latter increases with a progressive rise in agonist concentration, as also observed earlier in the mGluR2/2 and mGluR3/3 homodimers and the mGluR2/3 heterodimer[13,31]. In contrast, the mGluR2/7 heterodimer smFRET histogram is a single, broadened distribution, which shifts progressively to lower FRET levels as agonist concentration increased, whether the agonist was glutamate, which could bind to both the mGluR2 and mBGluR7 LBDs (Fig. 3.4b), or the group III-selective ligand LSP4-2022, which binds to only the mGluR7 LBD (Fig. 3.5d).

We examined this further and found that at zero glutamate the smFRET distribution of mGluR2/7 was also broadened and left-shifted with respect to both mGluR2/2 and mGluR7/7 at zero glutamate (Fig. 3.6a). One possible explanation for such behavior is spontaneous closure of LBDs leading to basal activation. To test this, we applied 100 µM of the group II and group III competitive antagonist LY341495. LY341495 binds in the orthosteric site, holds the LBD in the open conformation (Doumazane et al., 2012) and blocks the activation rearrangement that is induced by glutamate bound in the orthosteric site of mGluR2/2 and mGluR3/3, as well as by calcium ion binding at an allosteric site in mGluR3/3[13]; PDB 3MQ4. However, LY341495 did not alter the smFRET distribution of the mGluR2/7 heterodimer (Fig. 3.6c), indicating that the broadening and shift to the left in mGluR2/7 is not due to spontaneous LBD closure in the Apo state.

mGluRs respond to agonist in a sequence of steps: agonist binding favors closure of the LBDs, the closed LBDs rotate, and this triggers a rotation of the transmembrane domain (TMD) that opens the intracellular-facing G protein docking site[29,51]. We tested negative allosteric modulators (NAMs) of mGluR7 (ADX-71743) and mGluR2 (Ro 64-5229 and MNI-137), which bind in the TMD and stabilize the resting state[52-55] and, so, would be expected to stabilize the open and non-rotated (resting) conformation of the LBD. A combination of either of the mGluR2 NAMs with the mGluR7 NAM narrowed the smFRET distribution and shifted it to the right (Fig. 3.6e), as would be expected for a negative allosteric effect that pushes a partially activated receptor into the resting state.

To understand the molecular motions underlying the shift in smFRET distribution, we analyzed single molecule trajectories in zero glutamate. We observed spontaneous transitions from a high FRET resting state of ~0.45 to an intermediate FRET state of ~0.3 (Figs. 3.6b and

Supplementary Fig. 3.5, top). These spontaneous transitions persisted in the presence of LY341495 (Figs. 3.6d and Supplementary Fig. 3.5, second from top), but were eliminated by the NAMs, which stabilized the receptors in the high FRET state (Fig. 3.6f, and Supplementary Fig. 3.5, bottom two). These findings suggest that, in the Apo state, mGluR2/7 spontaneously transitions into a conformational intermediate on the activation pathway in which the LBDs are open but rotated.

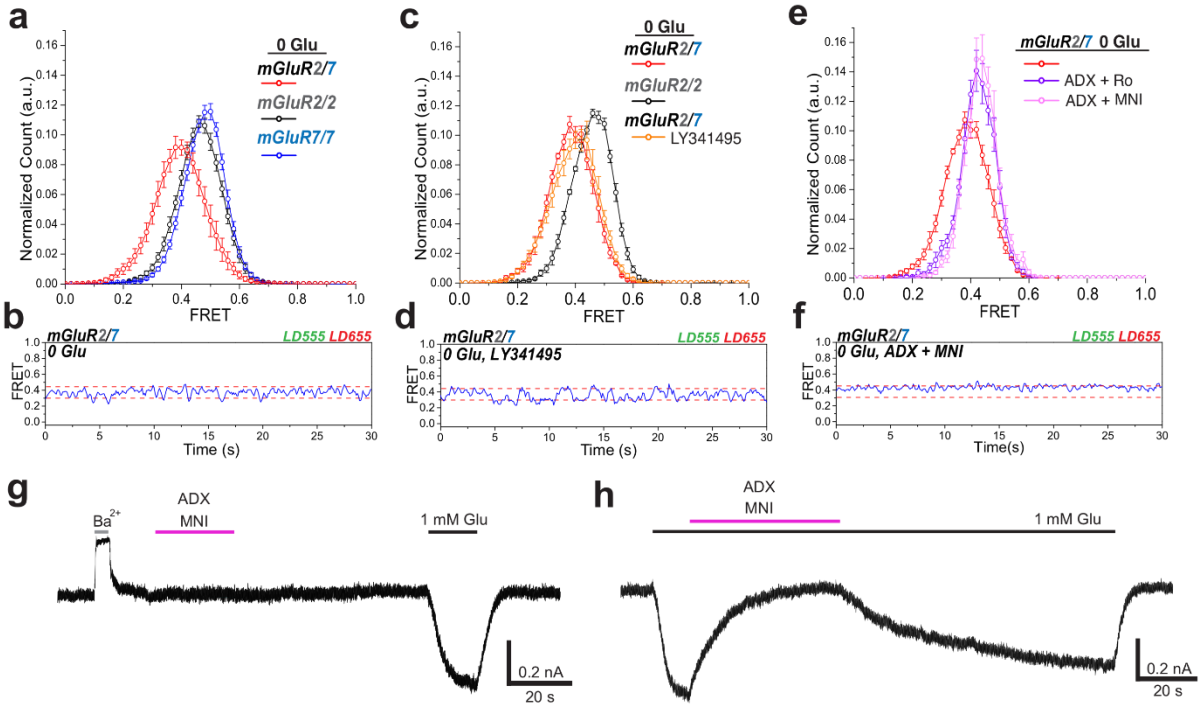

Figure 3.6, Spontaneous conformational rearrangements of mGluR2/7 in the Apo state. a, b) 0 glutamate smFRET histograms of SNAP-mGluR2/SNAP-mGluR2, SNAP-mGluR7/SNAP-mGluR7 and CLIP-mGluR2/SNAP-mGluR7 show a shift to lower FRET values in mGluR2/7 (a), associated with spontaneous transitions to an intermediate FRET state of ~0.3. c, d) The left shift of the 0 glutamate CLIP-mGluR2/SNAP-mGluR7 (5 movies, 191 molecules, s.e.m. error bars) smFRET histogram relative to that of SNAP-mGluR2/SNAP-mGluR2 (6 movies, 257 molecules, s.e.m. error bars) (c) and the spontaneous transitions to the intermediate FRET state (d) are not altered by 100 µM of the orthosteric antagonist LY341495 in 0 glutamate (5 movies, 230 molecules, s.e.m. error bars). e, f) The left shift of the 0 glutamate CLIP-mGluR2/SNAP-mGluR7 smFRET histogram (e) and the spontaneous transitions to the intermediate FRET state (f) are blocked by combined negative allosteric modulators for mGluR2 (either 11 µM Ro-5229 (6 movies, 160 molecules, s.e.m. error bars) or 1.2 µM MNI-137 (6 movies, 154 molecules, s.e.m. error bars)) and mGluR7 (125 µM ADX 71743) in 0 glutamate. a–f BC-DY-547 or BG-DY-547 (donor) and BG- Alexa-647 (acceptor) imaged at 10 Hz. g, h) Whole cell patch clamp recording (V_h = −60 mV; $[K+]_{in}$ = $[K+]_{out}$ = 150 mM) in HEK293T cells co- expressing mGluR2, mGluR7 and the GIRK1(F137S) channel have basal inward current, which is reversibly inhibited by the GIRK pore blocker Ba2+, but not affected by the combined negative allosteric modulators for mGluR2 (1 µM MNI-137) and mGluR7 (3 µM ADX 71743) (g), even though these are sufficient to completely block activation

We next asked whether the Apo state intermediate of mGluR2/7 represents the G protein signaling state of the receptor. To this test this we co-expressed mGluR2 and mGluR7 in HEK293T cells along with the GIRK channel and measured GIRK current. Application of 1 mM barium, to block the GIRK channels, elicited a reduction in standing inward current, which could be due to

either or both basal activity of the receptor and excess free Gβγ (Fig. 3.6g). 1 mM glutamate elicited a large inward current above this basal level and this was completely blocked (96.7 ± 2.1%, n = 4) by a combination of 3 μM ADX71743 (the mGluR7 NAM) and 1 μM MNI-137 (the mGluR2 NAM) (Fig. 3.6g, h). However, the combined NAMs on their own had no effect on basal current (2.1 ± 7.3%, n=6, t-test p = 0.542). These results suggest that the intermediate conformation visited in the Apo state is associated with a non-signaling state of the TMD.

An intermediate FRET state of ~0.3 has been observed previously in mGluR2/2, but it was very short-lived and could only be visualized as a low-incidence shoulder when large numbers of transitions, acquired at a glutamate concentration near the EC50, were aligned temporally[13]. We examined the single-molecule activation-deactivation dynamics at near the glutamate EC50 for mGluR2/7. We performed these experiments with a more photo-stable donor/acceptor dye pair (LD555/LD655, Förster radius 52Å) and 10-times faster acquisition (100 Hz). We found that, unlike mGluR2/2, which toggles back and forth between the resting 0.45 and activated 0.20 FRET states, with rarely resolved, brief occupancies at intermediate FRET levels (Figs. 3.7a and Supplementary Fig. 3.6a), mGluR2/7 divides its time between the ~0.45 FRET state, the ~0.20 FRET state and a ~0.30 intermediate FRET level, with short-lived occupancies of the resting and activated conformations and substantial time spent in the intermediate conformation (Figs. 3.7b and Supplementary Fig. 3.6b). The distinct activation/deactivation kinetics are reflected in a more extended donor/acceptor cross-correlation in mGluR2/7 (Fig. 3.7c**).**

Thus, along with enhanced affinity and boosted single subunit activation, the mGluR2/7 heterodimer displays a unique form of spontaneous partial activation, in absence of agonist and with the LBDs open, as well as altered conformational dynamics.

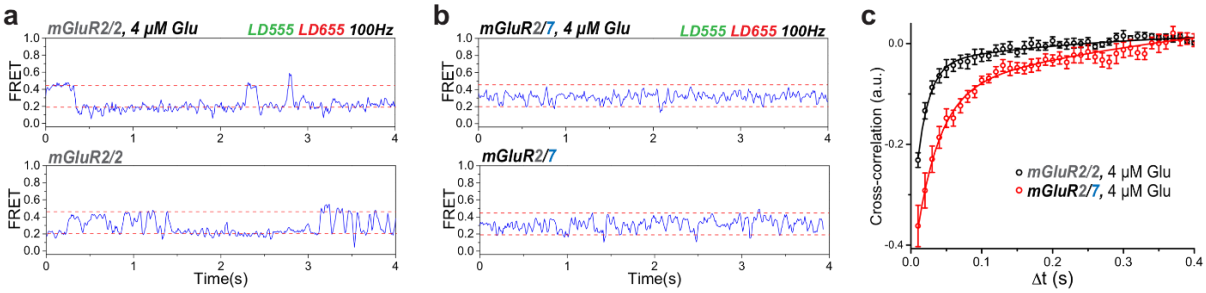

Figure 3.7, Fast glutamate-induced conformational dynamics in mGluR2/7. SNAP-mGluR2/SNAP-mGluR2 (mGluR2/2) and CLIP-mGluR2/SNAP- mGluR7 (m,GluR2/7) at a glutamate concentration near the EC50 (4 μM) imaged at 10× speed (100 Hz) with photobleaching resistant dyes (donor BC-LD555 or BG-LD555 and acceptor BG-LD655). a, b) mGluR2/2 and mGluR2/7 transition between resting (high FRET) and activated (low FRET), but CLIP-mGluR2/SNAP-mGluR7 spends much of the time at an intermediate FRET level. c) Donor/acceptor cross-correlation decays over longer time in mGluR2/7. Both samples fit with double exponential decay, mGluR2/2 R2 = 0.9120 (8 movies, 396 molecules, s.e.m. error bars) and mGluR2/7 R2 = 0.9740 (8 movies, 384 molecules, s.e.m. error bars).

Discussion:

The mGluR7/7 homodimer is known, based on effector activation, to have unusually low apparent affinity for glutamate[23]. Our measure of the glutamate-induced structural rearrangement of the LBDs reveals an EC50 of 38 mM, ~4,000-fold lower than that of the other mGluRs. Along with this, we find that maximal activation by glutamate only reaches ~10%, as determined from occupancy of the activated conformation, where the LBD clamshells are both closed and rotated, producing our measured low-FRET state. Despite this large difference in relative occupancy, the absolute smFRET levels of the resting and activated states in mGluR7/7 are similar to those of mGluR2/2, mGluR3/3 and mGluR2/3[13,31], suggesting that mGluR7/7 undergoes the same activation rearrangements. We show that occupancy of the activated conformation is elevated by a mutation that increases glutamate affinity, or by presentation of the glutamate on a stiff tethered linker that docks it into the binding pocket, or by a group III selective synthetic agonist, indicating that the problem with mGluR7/7 is not is ability to activate, but the ability of free glutamate to stabilize the activated conformation.

The very low affinity and low efficacy of activation by glutamate of mGluR7/7 poses a functional conundrum. Even within the low volume synaptic cleft, and immediately after glutamate release, glutamate is estimated to reach a peak of only 1-3 mM peak and for less than one millisecond[37,38]. Spillover from nearby synapses is thought to reach much lower concentrations [56]. Thus, the affinity and efficacy of mGluR7/7 appear to be too low for significant activation under physiological conditions. And yet, pharmacological and genetic knock-out studies suggest that mGluR7 does function at synapses[57-59]. Also, the pharmacological profile differs from what is measured from mGluR7 expressed alone in non-neuronal cell lines, and that which is measured in neuronal tissue[60] suggesting a biochemical difference between mGluR7 in neurons and in non-neuronal cells. We considered that heterodimerization, which is known to occur between mGluR7 and other group III mGluRs, as well as with group II mGluRs, may yield a receptor that operates in the range of physiological glutamate. We found that mGluR7 expression overlaps with that of mGluR2 in the hippocampus, that mGluR7 and mGluR2 co-immune precipitate. Strikingly, the mGluR2/7 heterodimer has high affinity and efficacy. But heterodimerization with mGluR2 does more than simply bring mGluR7 into the physiological range, it activates more efficiently and at lower agonist concentration than even mGluR2/2. This is associated with a form of cooperativity, in which an unliganded mGluR2 greatly enhances activation by agonist bound to mGluR7, and *vice versa*, and with a unique conformational pathway to activation, in which mGluR2/7 partially activates in the Apo state, even when its LBD is held open by antagonist.

mGluRs must dimerize to signa[32,61,62], and, in the dimer, activation of only one subunit produces low efficacy activation. This was originally shown in mGluR5/5, where a wildtype subunit was dimerized with one carrying the YADA binding site mutant subunit, which drastically lowers affinity[46]. The glutamate concentration-response curve of mGluR5/mGluR5(YADA) is biphasic: a first low glutamate concentration component, where only the wildtype subunit is expected to bind, yields ~20% of maximal activation achieved at much higher glutamate concentration, which is expected to also bind the YADA subunit. Similar behavior has been described for mGluR2/mGluR2(YADA)[13] and we confirm that here. We find that maximal

activation of mGluR2/mGluR2(YADA) at high glutamate (where both the high affinity wildtype and low affinity YADA subunits are both expected to be glutamate bound--only yields ~30% occupancy of the low FRET activated conformation, in contrast to the full occupancy seen in the wildtype mGluR2/2 dimer.

mGluR2/7 is expected to function similarly to mGluR2/mGluR2(YADA), with the naturally very low affinity wildtype mGluR7 subunit taking the place of the mutant mGluR2(YADA) subunit. However, mGluR2/7 breaks expectation in two ways. First, compared to mGluR2/2, the mGluR2/7 heterodimer activates at lower glutamate concentrations. Second, in contrast to mGluR2/mGluR2(YADA), mGluR2/7 has ~4-fold higher efficacy at 1mM glutamate, the top of the first component of the biphasic concentration-response relation, when only the wildtype mGluR2 subunit is expected to be liganded (~80% of maximal activation) and achieves full occupancy of the low FRET activated conformation at the top of the biphasic concentration-response relation, ~3-fold better than the maximal activation of mGluR2/mGluR2(YADA).

Compared to mGluR7/7, the mGluR2/7 heterodimer is activated with higher efficacy by both the group III selective agonist LSP4-2022 and by the tethered glutamate photoswitch D-MAG-0, even though in mGluR7/7 both subunits are bound by agonist, whereas in the mGluR2/7 heterodimer only the mGluR7 subunit has the agonist and the mGluR2 subunit is in the Apo state. This suggests that agonist-induced closure of the mGluR7 LBD drives the empty mGluR2 LBD to also close and rotate. This cooperative effect works in the opposite direction also: The presence of the mGluR2 subunit enhances agonist binding by the mGluR7 subunit. This is seen with the competitive antagonist 100 μM LY341495, which appears to completely displace D-MAG-0 from the binding site in the mGluR7/7 homodimer (shifting completely to the resting high FRET state), whereas in the mGluR2/7 heterodimer 100 μM LY341495 has almost no effect, suggesting that D-MAG-0 has a much higher affinity for mGluR7 when it is paired in the heterodimer with mGluR2.

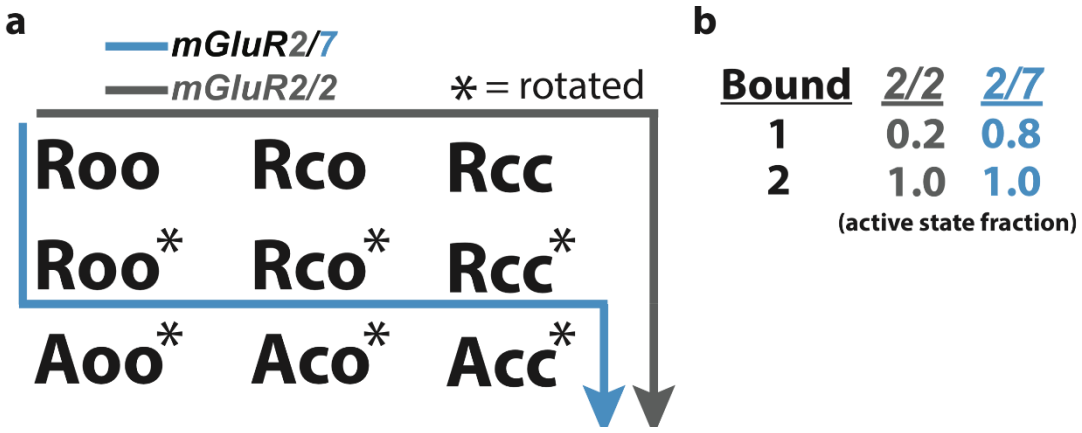

Figure 3.8, State diagram model of activation pathway. a) The transition of an mGluR from the resting state (Roo) to the active state (Acc) involves transition of the two LBDs from the open state (o) to the closed state (o), and rotation (*) of the LBDs relative to one another. In absence of agonist, mGluR2/2 is stable in Roo, and previous work has shown that the main route of activation is Roo → Roc → Rcc → Rcc*, although a small amount of activation is possible from Roc. In contrast, we find that mGluR2/7 spontaneously enters a partially activated (functionally inactive) conformation when both LBDs are held open by antagonist, which we propose as Roo → Roo*. b) The energetic difference results in much higher occupancy of the fully active state in mGluR2/7 in which only one subunit is liganded by agonist.

Thus, mGluR2/7 has a unique form of heteromeric cooperativity in which each subunit in its Apo state acts as a positive allosteric modulator of its partner subunit.

While some GPCRs, such as rhodopsin, have very low basal activation, others activate in absence of agonist[63]. Basal activation in absence of glutamate occurs in some mGluRs, including in mGluR3/3 and mGluR2/3, which are partially activated by calcium binding near the mGluR3 orthosteric site[13,64,65]. We see fundamental differences between basal activation of mGluR2/7 and examples described previously. mGluR3/3 and mGluR2/3 basal activation appears as FRET transitions from ~0.45 FRET to ~0.2 FRET and this transition is mediated by LBD closure and can be blocked by orthosteric antagonist LY341495 which stabilizes the open conformation of the LBD. However, the basal activity in mGluR2/7 is characterized by transitions between ~0.45 FRET and intermediate ~0.3 FRET and is not affected by LY341495, but is blocked by NAMs, which stabilize the inactive conformation of the TMD.

Activation is thought to proceed from the resting state (R) to the active state (A), starting with closure of the LBDs on the agonist (Roo→Rcc), followed by LBD rotation (Rcc→Rcc*), and by stabilization of a rearranged state of the TMD that includes a whole-TMD rotation and a tilt of TM6 to open the G-protein binding pocket: Rcc*→Acc* (Fig. 3.8a)[29,66]. Since spontaneous entry into the intermediate state occurs with the LBDs held open by LY341495 in zero glutamate (so that LBD closure does not contribute to the reduced FRET), and NAMs prevent entry into this state, we propose that the intermediate FRET state reflects a partially activated conformation in which the LBD is open but rotated. Our functional analysis indicates that this partially activated conformation is signaling inactive (Roo*) (Fig. 3.8a). This unusual activation pathway in mGluR2/7 is associated with a unique potency of single subunit liganding, which achieves ~80% of maximal activation as compared to only ~20% seen in mGluR2/mGluR2(YADA) **(**Fig. 3.8b**)**.

Near the EC50 glutamate concentration, where the receptor spends roughly equal time in the resting and activated states, mGluR2/7 is more dynamic than mGluR2/2 and spends substantial time in the partially activated state. Thus, the enhanced affinity and efficacy of mGluR2/7 are associated with a favored transition to a partially activated state where the LBD is rotated but the TMD is in the non-signaling state. Recent work has provided the first structure of a full length, dimeric mGluR complex in the resting and active conformations[29] that are compatible with earlier evidence for TMD rotation[67]. Our observations indicate that the conformational pathway between these states has several possible paths.

In conclusion, our study reveals a specialized heteromeric cooperativity in mGluRs in which an unliganded subunit confers on its dimer partner both enhanced glutamate affinity and the ability of the single subunit bound state to fully activate the receptor. This cooperativity is associated with a conformational pathway to activation that is not seen in other mGluRs. Instead of the canonical pathway of sequential LBD closure on agonist followed by LBD rotation, it appears that the LBD rotates even when it is open, leading to a partially activated state even when both members of the dimer are in the Apo state. Unusually too, while threshold sensitivity is enhanced, the concentration-response relation of the mGluR2/7 heteromer is shallower overall and saturates at higher concentration, adding to the ability to respond to low concentration spillover from a distance, a wider dynamic range to respond proportionately to particularly high glutamate from nearby sources.

Having observed the low glutamate affinity and efficacy of mGluR7 in this Chapter we further investigate the molecular underpinnings for this behavior in Chapter IV. This finding also acts a foundation to use mGluR7 homodimers as a gain-of function model which enables a much more detailed characterization of LBD interactions which have more subtle effects on activation properties. Results of mGluR2/7 heterodimers in this chapter also provides a framework for discovering the amino acids responsible for this modulation in Chapter IV. We find that just three amino acids are permit the heterodimeric modulation and confirm these findings using the data form Fig. 3.5 as a comparison.

Methods:

Drugs

LSP4-2022 was obtained according to the general procedure following scheme **1** [Selvam et al., JMedChem 2018], with improvements to minimize the formation and discard L-AP4, a side product with selective and potent group III mGluR agonist activity: (i) The use of degassed solvent during the formation of the second C-P bond dramatically reduces the presence of the corresponding phosphonate; (ii) The purification of the crude **LSP4-2022** by C-18 chromatography using a slow gradient (H_2O + 0.1% HCO_2H/MeCN + 0.1% HCO_2H: from 100/0 to 90/10), instead of successive cation- and anion- exchange resins, saves time and increases the overall yield of the final compound.

Scheme **1**: Improved synthesis of **LSP4-2022**[a]

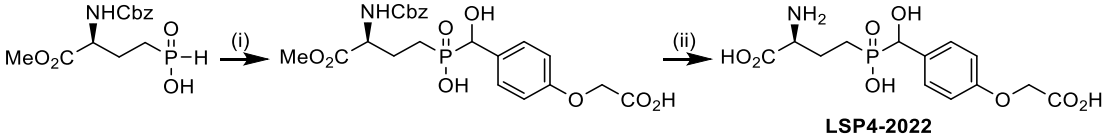

[a]Reagents and conditions: (i) 4-(Carboxymethoxy)benzaldehyde, BSA, degassed CH_2Cl_2, RT, 16 h; (ii) a) 6 M aqueous HCl, reflux, 5 h; b) C-18 flash chromatography.

Abbreviations: BSA: *N,O*-bis(trimethylsilyl)acetamide; Cbz: benzyloxycarbonyl; L-AP4: L-2-amino-4-phosphonobutyric acid; Me: methyl; RT: room temperature.

Cell culture and transfection

HEK293T cells were cultured in DMEM with 5% FBS on poly-L- lysine-coated glass coverslips. HEK293T cells were obtained from the UC Berkeley MCB tissue culture facility, authenticated by DDC Medical, and tested negative for mycoplasma contamination. Previously described HA–SNAP and Flag–CLIP-tagged rat mGluR cDNA were generously provided by J. P. Pin. DNA plasmids were transfected into cells using lipofectamine 2000 (Thermo Fisher). For electrophysiology experiments, cells were transfected with wild-type-mGluR2 or wild-type-mGluR7 or SNAP-mGluR2(F756D), GIRK1-F137S, and yellow fluorescent protein (YFP) (as a transfection marker) at a 7:7:1 ratio with 0.7 mg plasmid per well for receptor and channel. For FRET experiments, cells were transfected with SNAP and CLIP-tagged constructs at a ratio of 1:2 with 0.3 mg of SNAP–mGluR DNA per well.

Patch clamp electrophysiology

Whole-cell patch clamp recordings from single isolated cells were performed 24–48 h after transfection, in a high potassium extra-cellular solution containing (in mM): 120 KCl, 29 NaCl, 1 $MgCl_2$, 2 $CaCl_2$ and 10 HEPES, pH 7.4. Cells were voltage clamped to -60 mV using an Axopatch 200B amplifier (Axon Instruments) and membrane currents were recorded. Glass pipettes of resistance between 3 and 8 MΩ were filled with intracellular solution containing (in mM): 140 KCl, 10 HEPES, 3 Na_2ATP, 0.2 Na_2GTP, 5 EGTA and 3 $MgCl_2$, pH 7.4. Data were acquired with

a 2 kHz acquisition rate and low-pass filtered with a 4-pole Bessel filter at 1 kHz. Data acquisition and analysis were performed using pCLAMP 10 software (Axon Instruments).

Photoswitching

Illumination was applied to the entire field of view using either a Polychrome V monochromator (TILL Photonics) through a 20X objective, or a Lambda DG4 high-speed wavelength switcher (Sutter Instruments) with 380 nm and 500 nm filters through a 40X objective. pClamp software was used for both data acquisition and control of illumination. BGAG labeling was done by applying 1.5 μM BGAG for 45 min at 37°C. To conjugate D-MAG-0, cells were incubated in 50–100 μM D-MAG-0for 30–60 min in the dark at 23–27°C in standard extracellular cell buffer.

FRET pair fluorescent dye labeling of protein-tagged mGluRs

Approximately 24–48 h after transfection, cells were labeled while attached to poly-L-lysine-coated coverslips. Culture media was removed and coverslips were washed and transferred to extracellular solution containing (in mM): 135 NaCl, 5.4 KCl, 2 $CaCl_2$, 1 $MgCl_2$, 10 HEPES, pH 7.4. Cells were labeled at 37 °C with one or two SNAP-reactive (benzylguanine, BG) dyes at 1.5 μM for 45 minutes, and then, if a CLIP-tagged mGluR was used, they were washed and labeled with a CLIP-reactive (benzylcytosine, BC) dye at 3 μM for 45 minutes. For most of the experiments (Figs. 3.1-3.6 and Supplemental Fig. 3.1-3.5, except Supplemental Fig. 3.1c) DY-547 (NEB) was used as a donor and Alexa-647 (NEB) as an acceptor (in Supplemental Figure 1c Atto-488 was the donor and Atto-594 was the acceptor; Company). In Fig. 3.7 and Supplemental Fig. 3.6, LD-655 was the donor and LD-655 was the acceptor (Lumidyne). The fluorophores were diluted in extracellular solution and coverslips were washed in between labeling with donor and acceptor.

Ensemble FRET

After labeling, cells were mounted on an upright, scanning confocal microscope (Zeiss LSM 780) and imaged with a 20X objective. Donor excitation was performed using a 561-nm laser and images were taken in the donor and acceptor channels at 1 Hz. Clusters of cells were analyzed together and FRET was calculated as FRET=(I_A)/(I_D+I_A), in which I_D is the fluorescence donor intensity and I_A is the fluorescence acceptor intensity. For individual traces, FRET was normalized to the basal FRET value observed before application of drugs. FRET changes calculated for dose–response curves were normalized to the response to saturating glutamate (10 mM) and dose–response curves were obtained from multiple cell clusters and averaged from at least three experiments. Fitting of dose–response curves was performed using Prism (Graphpad). All drugs, except LSP4-2022, which we synthesized, were purchased from Tocris. Drugs were delivered with a gravity-driven perfusion system.

smPull receptor isolation and surface display

To inhibit nonspecific protein adsorption, flow cells for single-molecule experiments were prepared as previously described (Vafabhaksh et al,. 2015) using mPEG (Laysan Bio) passivated glass coverslips (VWR) and doped with biotin PEG16. Before each experiment, coverslips were incubated with NeutrAvidin (Thermo), followed by 10 nM biotinylated secondary antibody (donkey anti-rabbit, Jackson ImmunoResearch). For receptor immunopurification, 10 nM anti-mGluR2 primary antibody (abcam, ab150387) or 10 nM anti-mGluR7 antibody (abcam, ab53705), or 15 nM anti-HA antibody (abcam, ab26228) was incubated in the chamber (Fig. 3.1e). Between each conjugation step, the chambers were flushed to remove free reagents. The antibody dilutions and washes were done in T50 buffer (50 mM NaCl, 10 mM Tris, pH 7.5). For single-molecule experiments, fresh cells expressing tagged mGluR constructs were labeled, as described above, and recovered from coverslips by incubating with Ca^{2+} free PBS buffer for 5–10 min followed by gentle pipetting. Cells were then pelleted by spinning at 5,000g for 5 min and lysed in lysis buffer consisting of 150mM NaCl, 1 mM EDTA, protease inhibitor cocktail (Thermo Scientific) and 1.2% IGEPAL (Sigma).After 1 h incubation at 4 C°, lysate was centrifuged at 16,000g for 20 min. and the supernatant was collected and kept on ice. To achieve sparse immobilization of labeled receptors on the surface, the cell lysate was diluted (ranging from 5X to 50X dilution depending on the expression and labeling efficiency) and applied to coverslips. After achieving optimum surface immobilization (~400 molecules in a 2,000 μm^2 imaging area), unbound receptors were washed out of the flow chamber and the flow cells were then washed extensively (up to 50X the cell volume).

smFRET measurements

Receptors were imaged for smFRET in imaging buffer consisting of (in mM) 3 Trolox, 120 KCl, 29 NaCl, 2 CaCl2, 1 MgCl2, 50 HEPES, 0.04% IGEPAL and an oxygen scavenging system (0.8% dextrose, 0.8 mg ml^{-1} glucose oxidase, and 0.02 mg ml^{-1} catalase), pH 7.4. Reagents were purchased from Sigma and were all UltraPure grade (purity >99.99%). All buffers were made in UltraPure distilled water (Invitrogen). For the experiments done in the absence of Ca^{2+}, 10 mM EGTA and 1 mM EDTA were added to the imaging buffer. Catalase was diluted in T50 buffer and passed through a spin column 3X (BioRad).

Samples were imaged with a 1.65 na X60 objective (Olympus) on a total internal reflection fluorescence microscope with 100 ms time resolution unless stated otherwise. Lasers at 532 nm (Cobolt) and 632 nm (Melles Griot) were used for donor and acceptor excitation, respectively. FRET efficiency was calculated as $(I_A\text{-}0.1I_D)/(I_D+I_A)$, in which I_D and I_A are the donor and acceptor intensity, respectively, after back-ground subtraction. Imaging was with 100 ms acquisition time (10 Hz) with an Andor iXon 897 EMCCD camera (Figs. 3.1-3.6 and Supplemental Fig. 3.1-3.5) or with 10 ms acquisition time (100 Hz) with a Photometrics Prime 95B cMOS camera (Figs 3.7 and Supplemental Fig. 3.6) using Lumidyne LD555 as donor and Lumidyne LD655 as acceptor (Förster radius ~52Å). Dyes were conjugated to benzyguanine and benzylecytosine to allow for labeling of SNAP and CLIP proteins, respectively.

smFRET data analysis

Single-molecule intensity traces showing single-donor and single-acceptor photobleaching with a stable total intensity for longer than 5 s were collected (20–30% of total molecules per imaging area). Individual traces were smoothed using a nonlinear filter (Haran et al., 2004) with following filter parameters: window = 2, M = 2 and P = 15. Each experiment was performed ≥4 times to ensure reproducibility. smFRET histograms were compiled from ≥100 molecules per condition. (100 ms time resolution). Error bars in the histograms represent the standard error from ≥4 independent movies. To ensure that traces of different lengths contribute equally, histograms from individual traces were normalized to one before compiling. Gaussian fitting to histograms was done in Origin Pro. smFRET histograms were fit to two Gaussians, centered on high (~0.45) and low (~0.2) FRET levels for mGluR2/2 and mGluR2/7 and a single Gaussian for mGluR2/7 (center ranging from 0.2 to 0.45). For dose-response relations, the area underneath the low FRET Gaussian was used as a measure of active state occupancy.

Immunostaining for brain sections

Mice were anaesthetized and perfused transcardially with 4% paraformaldehyde (PFA) in 0.1 M phosphate buffer (pH 7.4). The brains were removed, postfixed overnight at 4 °C and sectioned at a thickness of 50 μm. Free-floating sections were incubated in blocking solution (PBS containing 10% normal sheep serum and 0.1% Triton X-100) overnight, followed by incubation with primary antibodies(diuluted 1 to 500) for 3 days and, after extensive washing, with Alexa 488- or Alexa 647-conjugated secondary antibodies (Molecular Probes) overnight at 4° C.

Western blot analysis

Cells were scraped into lysis buffer (50 mM Tris- HCl, pH 7.5, and 150 mM NaCl) containing 0.5% IGEPAL and protease inhibitor mixture (Roche) and incubated on ice for 20–30 min. The supernatant was separated from cell debris by centrifugation at 16,000X g for 10 min at 4°C. Aliquots of lysate were heated in SDS sample buffer (containing 10% SDS and 9.3% DTT) at 95°C for 5 min. Samples were loaded on SDS–PAGE and transferred to nitrocellulose membranes (Bio-Rad). After transfer, membranes were blocked in TBST (25 mM Tris, 150 mM NaCl, and 0.05% Tween 20) containing 5% nonfat milk at room temperature for 1 h. mGluR2 antibodies, mGluR7 and mGluR3 (Novus Biologicals, cat. # NBP2-61843) antibodies were diluted in blocking solution and incubated with the membranes at 4°C overnight. Membranes were then washed with TBST and incubated with HRP-conjugated goat anti-rabbit IgG secondary antibody (Santa Cruz Biotechnology, catalog #sc-2004, 1:7500 diluted in blocking buffer or Jackson ImmunoResearch Laboratories, catalog #111-035-144, 1:10,000 diluted in blocking buffer).

Co-immunoprecipitation from brain tissue

Brain samples were collected from Spraque Dawely rats, suspended in lysis buffer (50 mM Tris- HCl, pH 7.5, and 150 mM NaCl) containing protease inhibitor mixture (Roche). Tissue samples were homogenized and sonicated. Cell membrane fractions were separated by centrifugation at 100,000X g and cell pellet was resuspended in lysis buffer containing 1.5%

IGEPAL and protease inhibitor mixture (Roche). Cell were rocked at 4 °C for one hour then supernatant was cleared by centrifugation at 16,000X g for 20 min at 4 °C. Supernatant precleared with Pierce Protein A/G magnetic beads (Thermo-Fisher) followed by incubation with primary antibody conjugated protein A/G magnetic beads overnight at 4 °C. Beads were washed and protein was eluted in SDS sample buffer (containing 10% SDS and 9.3% DTT) at 95°C for 5 min. Samples were run on western blot as described above.

References:

1. Weis, W. I. & Kobilka, B. K. The molecular basis of G protein-coupled receptors activation. *Annu. Rev. Biochem.* 87, 897–919 (2018).
2. Erlandson, S. C., McMahon, C. & Kruse, A. C. Structural basis for G protein–coupled receptor signaling. *Annu. Rev. Biophys.* 47, 1–18 (2018).
3. Katritch, V., Cherezov, V. & Stevens, R. C. Structure-function of the G protein–coupled receptor superfamily. *Annu. Rev. Pharmacol. Toxicol.* 53,531–556 (2013).
4. Rasmussen, S. G. F. et al. Crystal structure of the β2 adrenergic receptor–Gs protein complex. *Nature* 477, 549–555 (2011).
5. Venkatakrishnan, A. J. et al. Molecular signatures of G-protein-coupled receptors. *Nature* 494, 185–194 (2013).
6. Dror, R. O. et al. Pathway and mechanism of drug binding to G-protein-coupled receptors. *Proc. Natl Acad. Sci. USA* 108, 13118–13123 (2011).
7. Isogai, S. et al. Backbone NMR reveals allosteric signal transduction networks in the β1-adrenergic receptor. *Nature* 530, 237–241 (2016).
8. Liu, W. et al. Structural basis for allosteric regulation of GPCRs by sodium ions. *Science* 337, 232–236 (2012).
9. Manglik, A. & Kobilka, B. The role of protein dynamics in GPCR function: insights from the β2AR and rhodopsin. *Curr. Opin. Cell Biol.* 27, 136–143 (2014).
10. Nygaard, R. et al. The dynamic process of β2-adrenergic receptor activation. *Cell* 152, 532–542 (2013).
11. Olofsson, L. et al. Fine tuning of sub-millisecond conformational dynamics controls metabotropic glutamate receptors agonist efficacy. *Nat. Commun.* 5,5206 (2014).
12. Sounier, R. et al. Propagation of conformational changes during μ-opioid receptor activation. *Nature* 524, 375–378 (2015).
13. Vafabakhsh, R., Levitz, J. & Isacoff, E. Y. Conformational dynamics of a class C G-protein-coupled receptor. *Nature* 524, 497–501 (2015).
14. Gregorio, G. G. et al. Single-molecule analysis of ligand efficacy in β2AR–G-protein activation. *Nature* 547, 68–73 (2017).
15. Lohse, M. J., Maiellaro, I. & Calebiro, D. Kinetics and mechanism of G protein-coupled receptor activation. *Curr. Opin. Cell Biol.* 27, 87–93 (2014).
16. Moussawi, K., Riegel, A., Nair, S., & Kalivas, P. W. Extracellular glutamate: functional compartments operate in different concentration ranges. *Front. Syst. Neurosci.* 5, 94 (2011).
17. Denis, C. et al. Probing heterotrimeric G protein activation: applications to biased ligands. *Curr. Pharm. Des.* 18, 128–144 (2012).
18. Eichel, K. & von Zastrow, M. Subcellular organization of GPCR signaling. *Trends Pharmacol. Sci.* 39, 200–208 (2018).
19. Missale, C. et al. Dopamine receptors: from structure to function. *Physiological Rev.* 78, 189–225 (1998).
20. Traynelis, S. F. et al. Glutamate receptor ion channels: structure, regulation, and function. *Pharmacol. Rev.* 62, 405–496 (2010).
21. Conn, P. J. & Pin, J.-P. Pharmacology and functions of metabotropic glutamate receptors. *Annu. Rev. Pharmacol. Toxicol.* 37, 205–237 (1997).
22. Niswender, C. M. & Conn, P. J. Metabotropic glutamate receptors: physiology, pharmacology, and disease. *Annu. Rev. Pharmacol. Toxicol.* 50, 295–322 (2010).
23. Okamoto, N. et al. Molecular characterization of a new metabotropic glutamate receptor mGluR7 coupled to inhibitory cyclic AMP signal transduction. *J. Biol. Chem.* 269, 1231–1236 (1994). 12.
24. Ohishi, H., Akazawa, C., Shigemoto, R., Nakanishi, S. & Mizuno, N. Distributions of the mRNAs for L-2-amino-4-phosphonobutyrate-sensitive metabotropic glutamate receptors, mGluR4 and mGluR7, in the rat brain. *J. Comp. Neurol.* 360, 555–570 (1995).
25. Brandstätter, J. H. et al. Compartmental localization of a metabotropic glutamate receptor (mGluR7): two different active sites at a retinal synapse. *J. Neurosci.* 16, 4749–4756 (1996).
26. Acher, F. & Goudet, C. Therapeutic potential of group III metabotropic glutamate receptor ligands in pain. *Curr. Opin. Pharmacol.* 20, 64–72 (2015).
27. Hovelso, N. et al. Therapeutic potential of metabotropic glutamate receptor modulators. *Curr. Neuropharmacol.* 10, 12–48 (2012).
28. Stansley, B. J. & Conn, P. J. The therapeutic potential of metabotropic glutamate receptor modulation for schizophrenia. *Curr. Opin. Pharmacol.* 38,31–36 (2018).
29. Koehl, A. et al. Structural insights into the activation of metabotropic glutamate receptors. *Nature* 566, 79–84 (2019).
30. Doumazane, E. et al. A new approach to analyze cell surface protein complexes reveals specific heterodimeric metabotropic glutamate receptors. *FASEB J.* 25, 66–77 (2011).
31. Levitz, J. et al. Mechanism of assembly and cooperativity of homomeric and heteromeric metabotropic glutamate receptors. *Neuron* 92, 143–159 (2016).
32. El Moustaine, D. et al. Distinct roles of metabotropic glutamate receptor dimerization in agonist activation and G-protein coupling. Proc. Natl Acad. Sci. USA 109, 16342–16347 (2012).
33. Yin, S. et al. Selective actions of novel allosteric modulators reveal functional heteromers of metabotropic glutamate receptors in the CNS. *J. Neurosci.* 34, 79–94 (2013).

34. Moreno Delgado, D. et al. Pharmacological evidence for a metabotropic glutamate receptor heterodimer in neuronal cells. *eLife* 6, e25233 (2017).
35. Pin, J.-P. & Bettler, B. Organization and functions of mGlu and GABAB receptor complexes. *Nature* 540, 60–68 (2016).
36. Rosemond, E. et al. Molecular determinants of high affinity binding to group III metabotropic glutamate receptors. *J. Biol. Chem.* 277, 7333–7340 (2001).
37. Dzubay, J. A. & Jahr, C. E. The concentration of synaptically released glutamate outside of the climbing fiber–Purkinje cell synaptic cleft. *J. Neurosci.* 19, 5265–5274 (1999).
38. Clements, J. et al. The time course of glutamate in the synaptic cleft. *Science* 258, 1498–1501 (1992).
39. Goudet, C. et al. A novel selective metabotropic glutamate receptor 4 agonist reveals new possibilities for developing subtype selective ligands with therapeutic potential. *FASEB J.* 26, 1682–1693 (2012).
40. Podkowa, K. et al. A novel mGlu4 selective agonist LSP4-2022 increases behavioral despair in mouse models of antidepressant action. *Neuropharmacology* 97, 338–345 (2015).
41. Gorostiza, P. et al. Mechanisms of photoswitch conjugation and light activation of an ionotropic glutamate receptor. *Proc. Natl Acad. Sci. USA* 104, 10865–10870 (2007).
42. Levitz, J. et al. Optical control of metabotropic glutamate receptors. *Nat. Neurosci.* 16, 507–516 (2013).
43. Shigemoto, R. et al. Differential presynaptic localization of metabotropic glutamate receptor subtypes in the rat hippocampus. *J. Neurosci.* 17, 7503–7522 (1997).
44. Kinzie, J. M., Saugstad, J. A., Westbrook, G. L. & Segerson, T. P. Distribution of metabotropic glutamate receptor 7 messenger RNA in the developing and adult rat brain. *Neuroscience* 69, 167–176 (1995).
45. Simonyi, A., Schachtman, T. R. & Christoffersen, G. R. J. The role of metabotropic glutamate receptor 5 in learning and memory processes. *Drug News Perspect.* 18, 353 (2005).
46. Kniazeff, J. et al. Closed state of both binding domains of homodimeric mGlu receptors is required for full activity. *Nat. Struct. Mol. Biol.* 11, 706–713 (2004).
47. Brock, C. et al. Activation of a dimeric metabotropic glutamate receptor by intersubunit rearrangement. *J. Biol. Chem.* 282, 33000–33008 (2007).
48. Broichhagen, J. et al. Orthogonal optical control of a G protein-coupled receptor with a SNAP-tethered photochromic ligand. *ACS Cent. Sci.* 1, 383–393 (2015).
49. Francesconi, A. & Duvoisin, R. M. Role of the second and third intracellular loops of metabotropic glutamate receptors in mediating dual signal transduction activation. *J. Biol. Chem.* 273, 5615–5624 (1998).
50. Brabet, I. et al. Comparative effect of l-CCG-I, DCG-IV and γ-carboxy-l-glutamate on all cloned metabotropic glutamate receptor subtypes. *Neuropharmacology* 37, 1043–1051 (1998).
51. Rondard, P. & Pin, J.-P. Dynamics and modulation of metabotropic glutamate receptors. *Curr. Opin. Pharmacol.* 20, 95–101 (2015).
52. Hemstapat, K. et al. A novel family of potent negative allosteric modulators of group II metabotropic glutamate receptors. *J. Pharmacol. Exp. Therapeutics* 322, 254–264 (2007).
53. Kalinichev, M. et al. ADX71743, a potent and selective negative allosteric modulator of metabotropic glutamate receptor 7: in vitro and in vivo characterization. *J. Pharmacol. Exp. Therapeutics* 344, 624–636 (2012).
54. Kolczewski, S. et al. Synthesis of heterocyclic enol ethers and their use as group 2 metabotropic glutamate receptor antagonists. *Bioorg. Medicinal Chem. Lett.* 9, 2173–2176 (1999)
55. Brauner-Osborne, H., Wellendorph, P. & Jensen, A. Structure, pharmacology and therapeutic prospects of family C G-protein coupled receptors. *Curr. Drug Targets* 8, 169–184 (2007).
56. Hires, S. A., Zhu, Y. & Tsien, R. Y. Optical measurement of synaptic glutamate spillover and reuptake by linker optimized glutamate-sensitive fluorescent reporters. Proc. Natl Acad. Sci. USA 105, 4411–4416 (2008).
57. Goddyn, H. et al. Deficits in acquisition and extinction of conditioned responses in mGluR7 knockout mice. Neurobiol. Learn. Mem. 90, 103–111 (2008).
58. Hölscher, C. et al. Lack of the metabotropic glutamate receptor subtype 7 selectively impairs short-term working memory but not long-term memory. Behavioural Brain Res. 154, 473–481 (2004).
59. Masugi, M. et al. Metabotropic glutamate receptor subtype 7 ablation causes deficit in fear response and conditioned taste aversion. J. Neurosci. 19, 955–963 (1999).
60. Pelkey, K. A. et al. mGluR7 is a metaplastic switch controlling bidirectional plasticity of feedforward inhibition. Neuron 46, 89–102 (2005)
61. Kammermeier, P. J. Activation of metabotropic glutamate receptor 1 dimers requires glutamate binding in both subunits. *J. Pharmacol. Exp. Therapeutics* 312, 502–508 (2004).
62. Tateyama, M. & Kubo, Y. The intra-molecular activation mechanisms of the dimeric metabotropic glutamate receptor 1 differ depending on the type of G proteins. *Neuropharmacology* 61, 832–841 (2011).
63. Cohen, G. B., Yang, T., Robinson, P. R. & Oprian, D. D. Constitutive activation of opsin: influence of charge at position 134 and size at position 296. *Biochemistry* 32, 6111–6115 (1993).
64. Kubo, Y. Structural basis for a Ca2+-Sensing Function of the Metabotropic Glutamate Receptors. *Science* 279, 1722–1725 (1998).
65. Levitz, J. et al. Dual optical control and mechanistic insights into photoswitchable group II and III metabotropic glutamate receptors. *Proc. Natl Acad. Sci. USA* 114, E3546–E3554 (2017).

66. Xue, L. et al. Major ligand-induced rearrangement of the heptahelical domain interface in a GPCR dimer. *Nat. Chem. Biol.* 11, 134–140 (2014).
67. Selvam, C. et al. Increased potency and selectivity for group III metabotropic glutamate receptor agonists binding at dual sites. *J. Medicinal Chem.* 61, 1969–1989 (2018).

Supplementary Figures:

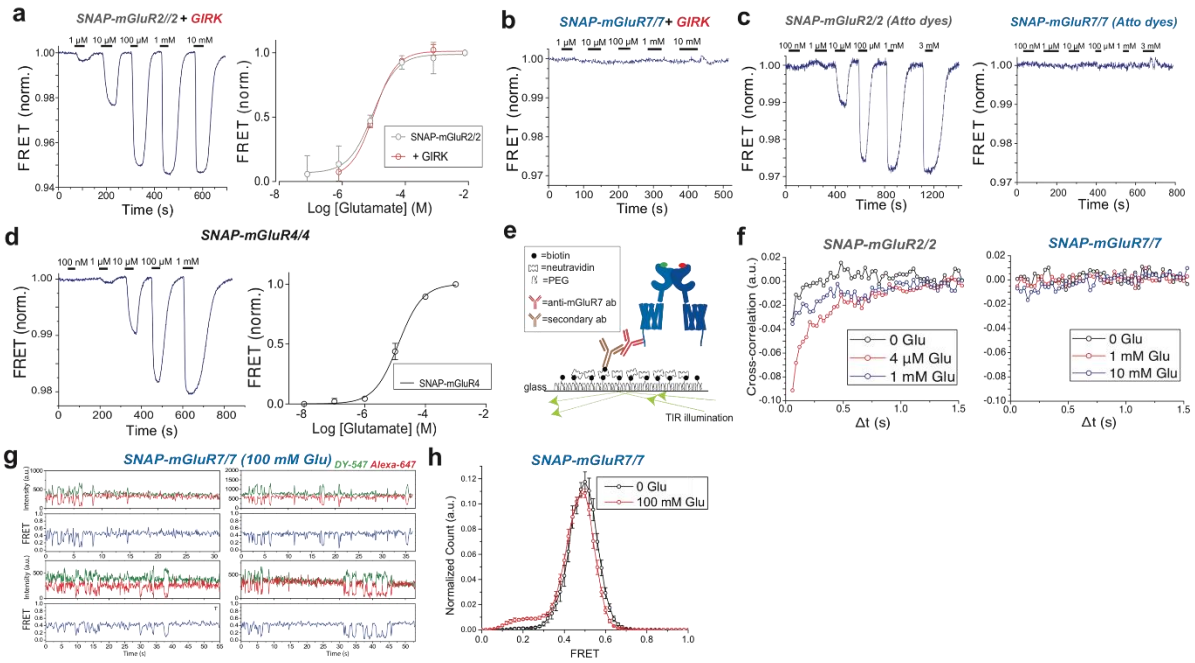

Figure S3.1: Glutamate-induced FRET response of mGluR2/2, mGluR7/7 and

mGluR4/4 homodimers. a-d) Live HEK293 cell ensemble FRET glutamate representative dose-response traces (a and d, left; b and c) and dose-response relations (a and d, right) for SNAP-mGluR2/2 coexpressed with GIRK, s.e.m error bars. (a); SNAP-mGluR7/7 co-expressed with GIRK **(**b); SNAP-mGluR2/2 (left) and SNAP-mGluR7/7 (right) (c); and SNAP-mGluR4/4, s.e.m. error bars (d). Receptors labeled with SNAP-selective, BG dyes: DY-547 (donor) and Alexa 647 (acceptor) (a,b,d) or Atto-488 (donor) and Atto-594 (acceptor) (c), imaged at 10 Hz. e) Schematic of individual dimer antibody pulldown and TIRF imaging of solubilized receptor. f) Donor/acceptor fluorescence cross-correlation for SNAP-mGluR2/2 (left) and SNAPmGluR7/7 (right) at different glutamate concentrations shows greater dynamics in mGluR2/2 at 4 μM glutamate (4 movies, 311 molecules), near the EC50 where receptors transition most frequently between resting (high FRET) and activated (low FRET) states, than seen in 10 mM glutamate, the foot of the mGluR7/7 dose-response relation. g) Single molecule donor (green), acceptor (red) and FRET (blue) traces of SNAPmGluR7/7 in 100 mM glutamate. h) Histograms from distinct data set from Fig. 1f of SNAP-mGluR7/7 in 0 (6 movies, 254 molecules, s.e.m. error bars) and 100 mM (6 movies, 308 molecules, s.e.m. error bars) glutamate. f-h) smFRET donor (BG-DY-547) and acceptor (BG-Alexa 647) dyes imaged at 10 Hz.

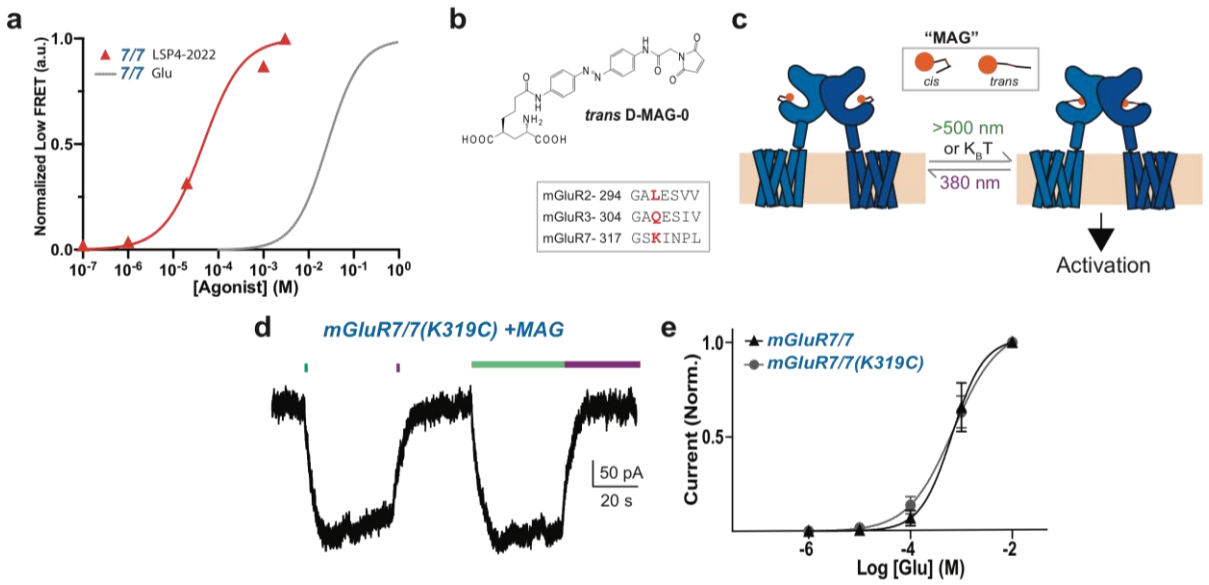

Figure S3.2: LSP4-2022 and D-MAG activation of mGluR7/7. a) LSP4-2022 dose-response relation (red symbols and single Boltzmann fit) compared to that for glutamate (grey single Boltzmann fit from Fig. 1f) of low FRET (activated state) peak from smFRET histograms of SNAP-mGluR7. Donor (BG-DY-547) and acceptor (BG-Alexa 647) dyes imaged at 10 Hz. b) *Trans* D-MAG-0 structure (top) and amino acid sequence in lower lobe of three mGluRs around site of cysteine substitution for D-MAG-0 attachment (bottom, red single letter amino acid code). c) Schematic of mGluR7(K319C) homodimer photoactivation in *trans* configuration of DMAG-0. d) Whole cell patch clamp recording in HEK293 cell of GIRK current activated by photoisomerization of D-MAG-0 on mGluR7(K319C) to *trans* with 532 nm light (green bars) and deactivated with 380nm light (violet vertical bars). e) Glutamate dose-response of GIRK current activation by wildtype mGluR7 (wt) same as by mGluR7(K319C), s.e.m. error bars.

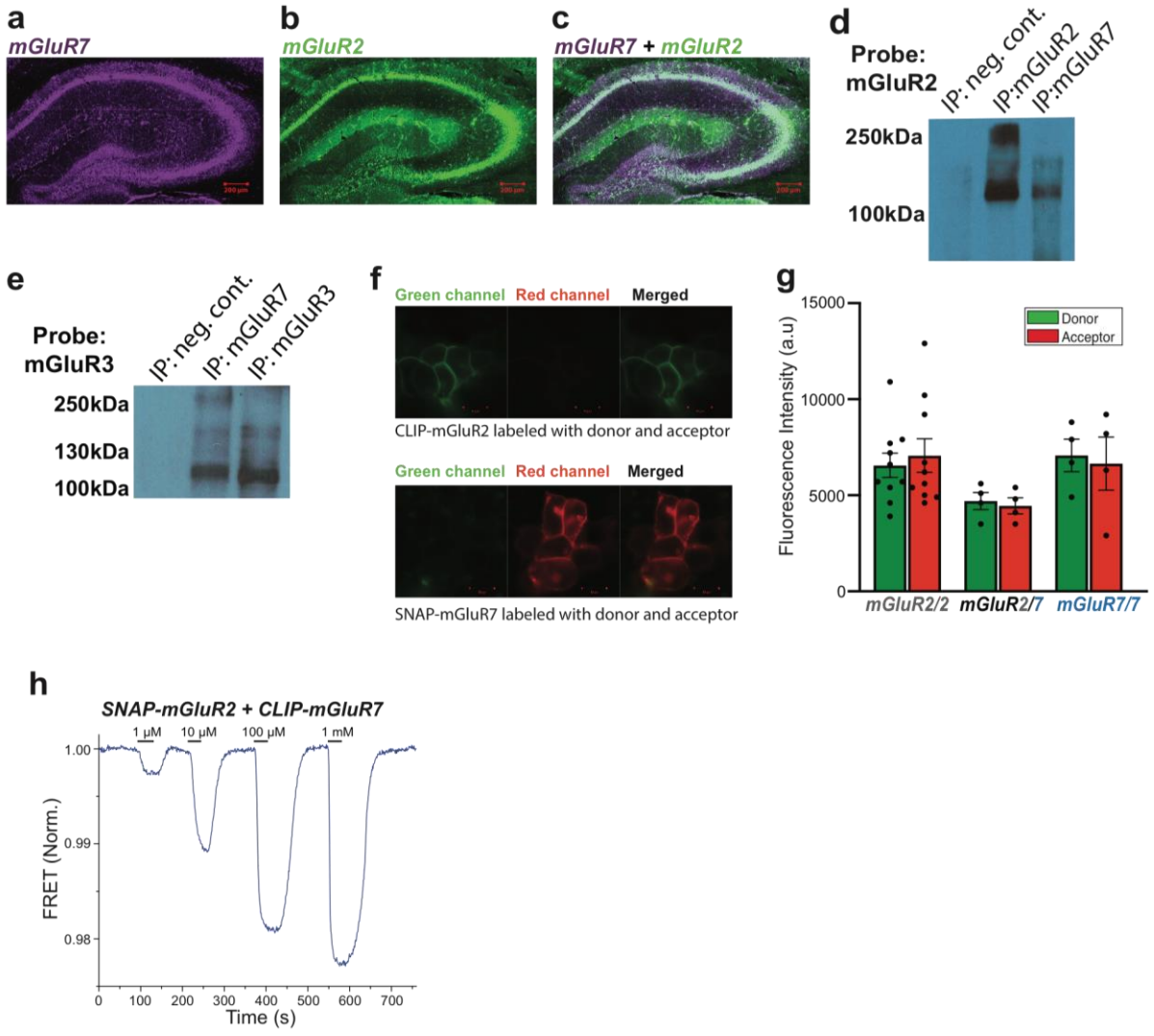

Figure S3.3: mGluR2 and mGluR7 associate in hippocampus and assemble into a functional heterodimer in HEK293 cells. a-c) Adult mouse hippocampus section labeled with antibodies against mGluR7 (a and c, violet) and mGluR2 (b and c, green) with overlap indicated (c), white. Scale bar 200 µm. d) Immune precipitation from adult rat hippocampus with either anti-mGluR2 antibody (middle lane) or anti-mGluR7 antibody (right lane) probed with anti-mGluR2 antibody shows that mGluR2 is associated with mGluR7. The negative control (left lane) is immune precipitation without primary antibody. e) Immune precipitation from adult rat cortex with either anti-mGluR7 antibody (ab53705, middle lane) or anti-mGluR3 antibody (NBP2-61843, right lane) probed with antimGluR3 antibody shows that mGluR3 is associated with mGluR7. The negative control (left lane) is immune precipitation without primary antibody. f) HEK293 cells expressing CLIP-mGluR2 are selectively labeled by donor BC-549 (green), whereas cells expressing SNAP-mGluR7 are selectively labeled by acceptor BG-Alexa-647 (red). Scale bars 10 µm. g) Donor and acceptor fluorescence intensities are similar in: SNAP-mGluR2/SNAPmGluR2 and SNAP-mGluR7/SNAP-mGluR7 labeled with donor BG-549 (green) and acceptor BG-Alexa-647 (red), and CLIP-mGluR2/SNAP-mGluR7 labeled with donor BC-549 (green) and acceptor BG-Alexa-647 (red). Individual data points (black dots) and s.e.m. (error bars). h) Representative live-cell FRET trace of SNAP-mGluR2/CLIP-mGluR7 heterodimer in response to ascending concentrations of glutamate.

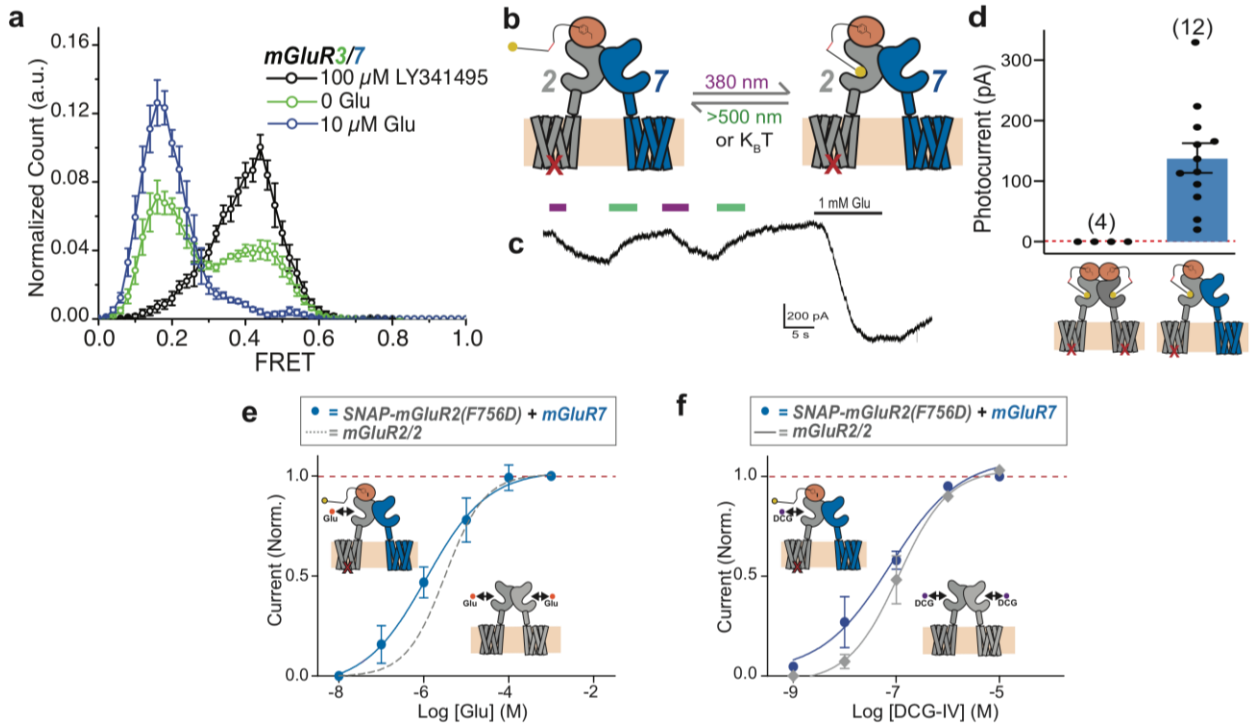

Figure S3.4: mGluR2/7 enhanced affinity in effector activation. a) smFRET histograms of CLIP-mGluR3/SNAP-mGluR7 labeled with BC-549 and BGAlexa-647 at 0 glutamate (green symbols, 7 movies, 298 molecules, s.e.m. error bars), 10 μM glutamate (blue symbols, 7 movies, 217 molecules, s.e.m. error bars) and 100 μM LY341495 (black symbols, 4 movies, 120 molecules, s.e.m. error bars). b) Schematic of mGluR2/7 heterodimer containing a signaling-dead SNAPmGluR2(F756D) (containing a mutation at the G protein binding site, red X) and a wildtype mGluR7. The Photoswitched Orthogonal Remotely Tethered Ligand (PORTL) BGAG attaches to the SNAP tag on mGluR2(F756D) and signals to effector via transactivation of the signaling-competent mGluR7. c) Whole cell patch clamp trace of SNAP-mGluR2(F756D)/mGluR7 co-expressed with GIRK1(F137S), which forms homotetrameric channels, in HEK293. The SNAP tag of SNAP-mGluR2(F756D) is labeled with BGAG and photo-activated by 380 nm light (violet bars) and photo-deactivated by 532 nm light (green bars), yielding reversible activation of inward GIRK current. d) No photocurrent detected in GIRK1(F137S) expressing HEK293 cells co-expressing just SNAP-mGluR2(F756D), but substantial photocurrent in cells co-expressing SNAPmGluR2(F756D) and mGluR7. Numbers above bars indicate number of cells tested Individual data points (black dots) and s.e.m. (error bars). e) Glutamate dose-response relation of SNAP-mGluR2(F756D)/mGluR7 (blue symbols and solid blue single Boltzmann fit) is left-shifted compared to that of mGluR2/2 (grey dashed single Boltzmann fit), s.e.m. error bars. f) DCG-IV dose-response relation of SNAP-mGluR2(F756D)/mGluR7 (blue symbols and solid blue single Boltzmann fit) is left-shifted compared to that of mGluR2/2 (grey symbols and solid grey single Boltzmann fit), s.e.m. error bars.

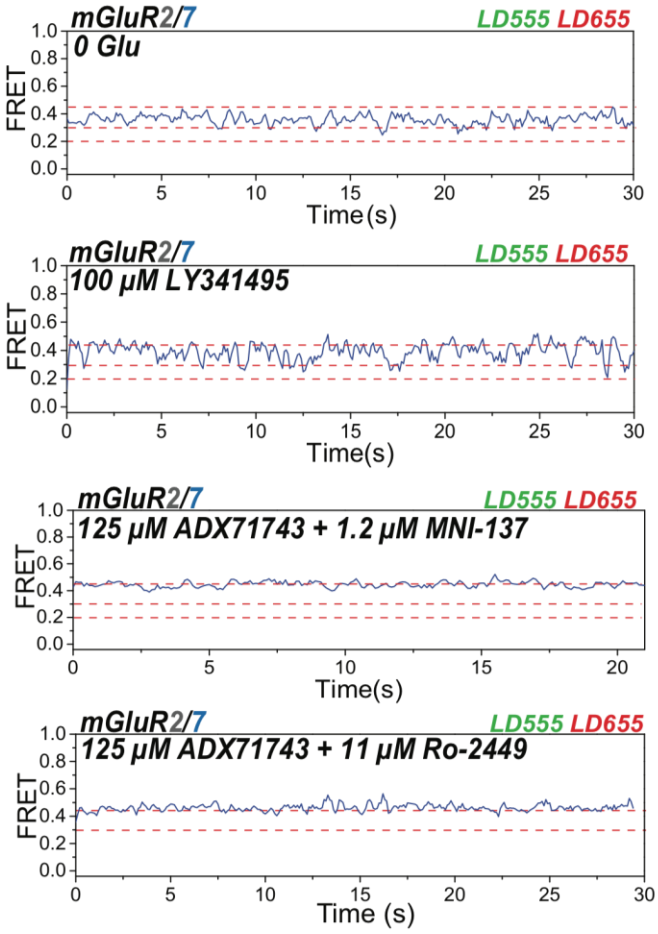

Figure S3.5: Spontaneous rearrangements in mGluR2/7. Representative smFRET trace of CLIP-mGluR2/SNAP-mGluR7 in 0 glutamate (top), 0 glutamate + 100 μM of the orthosteric antagonist LY341495 (middle), 0 glutamate + 1.2 μM MNI-137 + 125 μM ADX 71743, the mGluR2 and mGluR7 negative allosteric modulators, respectively (bottom). BC-DY-547 (donor) and BG-Alexa-647 (acceptor) imaged at 10 Hz.

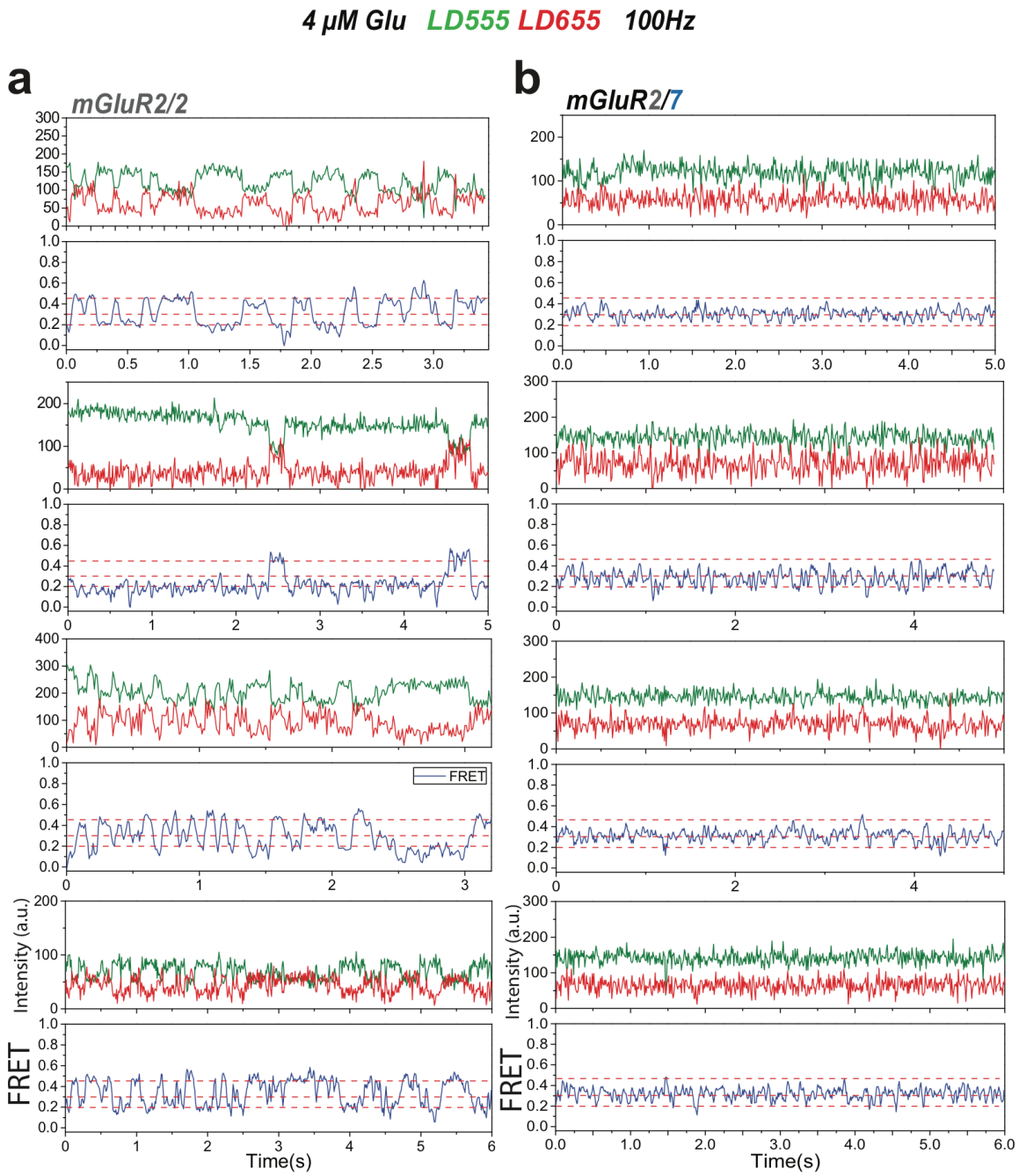

Figure S3.6: Distinct LBD conformational dynamics in mGluR2/2 and mGluR2/7. SNAP-mGluR2/SNAP-mGluR2 (mGluR2/2) (a) and CLIP-mGluR2/SNAP-mGluR7 (mGluR2/7) (b) in 4μM glutamate show that mGluR2/2 toggles between long occupancy high and low FRET states and mGluR2/7 spends most of the time in the intermediate FRET state, with brief excursions to the high or low FRET states. Donor BC-LD555 or BG-LD555 (green traces), acceptor BG-LD655 (red traces) and FRET (blue traces) imaged at 100 Hz.

Chapter IV: Allosteric mechanisms controlling affinity and efficacy of mGluR homodimers and heterodimers

Introduction:

G-protein-coupled receptors (GPCRs) are the largest class of membrane signaling proteins and respond to a wide array of extracellular stimuli to initiate intracellular signaling through G-proteins and arrestins[1]. There is a large and rapidly growing catalog of GPCRs structures in stable distinct conformations[2-5] which have revealed they are extremely dynamic[6-13]. Conformational dynamics appear to be central to ligand recognition, activation and signaling by GPCRs[9,14,15]. Unfortunately the amount of information on the conformational dynamics of GPCRs has lagged behind the amount of structural information.

The region of the mammalian system with the highest diversity of GPCRs is the central nervous system (CNS)[16]. The structures within the CNS that see the highest concentration of receptors are synapses with concentrations reaching up to 3 mM[17] . In the mammalian CNS glutamate acts as the main excitatory neurotransmitter and synapses experience a wide spectrum glutamate concentrations in very precise spatio-temporal profiles[18,19]. Appropriate responses to these glutamate transients is critical to maintaining normal brain function and encoding changes that underlie learning and memory. As a result receptors must be tuned to the different synaptic environments that can be found in the central nervous system. mGluRs contain a very large N-terminal extracellular that houses multiple inter-molecular interaction surfaces[20].

mGluRs allow the central nervous system to sense and respond to the glutamate environment subsequently enacting long-term cell signaling input[21]. To deal with these varied transients the mammalian CNS has 8 mGluR subtypes responsible for proper spatio-temporal responses[22]. Two of the subtypes are expressed post-synaptically and signal through G_q. The other six subtypes are expressed pre- or peri-synaptically and signal through Gi[21]. Characterization of the entire family has revealed that seven subtypes have glutamate sensitivities that are very similar between 1-10 uM[23,24]. This raises the question as to how this family of receptors which seem very functionally similar in glutamate sensitivity has the capacity for glutamate regulation in the CNS? One potential route to diversify the potential responses of mGluR receptors is to modulate their activation by glutamate. It has been shown that heterodimerization is one route to modulate mGluR ligand sensitivity as well as kinetics of activation[25]. Interaction with other proteins has also been shown to modulate receptor activation[26]. As the evidence grows that mGluRs can be modulated in multiple ways or specific properties can emerge depending on protomeric composition the need to understand how different molecular interactions effect or can give rise to these properties increases.

To better understand the molecular determinants that control mGluR activation and heterodimer modulation we designed chimeric receptors using mGluR2, mGluR4 and mGluR7. mGluR2 represents a Group II high affinity mGluR while mGluR4 represents a Group III high affinity mGluR and mGluR7 represents a Group III low affinity mGluR[21]. Domain swaps between mGluR2 and mGluR7 reveals that the low sensitivity observed in mGluR7 is critically dependent on the ligand binding domain (LBD) while the mGluR7 transmembrane domain (TMD) does not affect mGluR7 activation and the cysteine rich domain (CRD) of mGluR7 has a negative effect on glutamate activation. We next investigated what about the mGluR7 LBD results in the low glutamate sensitivity. Surprisingly we find that the ligand binding domain has

almost no effect on glutamate sensitivity while the lower LBD dimer interface is responsible for the very low glutamate affinity and sensitivity. We next investigated the source of heterodimer modulation seen in mGluR2/7. We find that the cysteine loop flexibility is key to heterodimer modulation and mutation of three glycine residues within the mGluR4 cysteine loop allows mGluR4 to mimic the emergent properties seen in mGluR2/7. Finally we examine the contribution of the CRD in mGluR activation. Swapping CRDs between mGluR2 and mGluR4 we find that the Group III CRDs are responsible for the lower maximal efficacy seen in Group III activation.

Results:

LBD and CRD contributions to mGluR7 glutamate activation

In order to understand how the three domains of mGluR7 contribute to its glutamate response we designed mGluR7 mGluR2 chimera where entire domains were swapped between the two receptors. N-terminally SNAP-tagged mGluR7 expressed in HEK293T cells and labeled with Alexa-647 (acceptor) and DY-547 (donor) fluorophores (Förster radius 52 Å). Cells were labeled with and lysed in detergent to solubilize receptors. Receptors were then immune-purified and tethered by biotinylated secondary antibodies at low density to coverslips that were passivated with polyethylene glycol. We used single molecule FRET (smFRET) to measure the

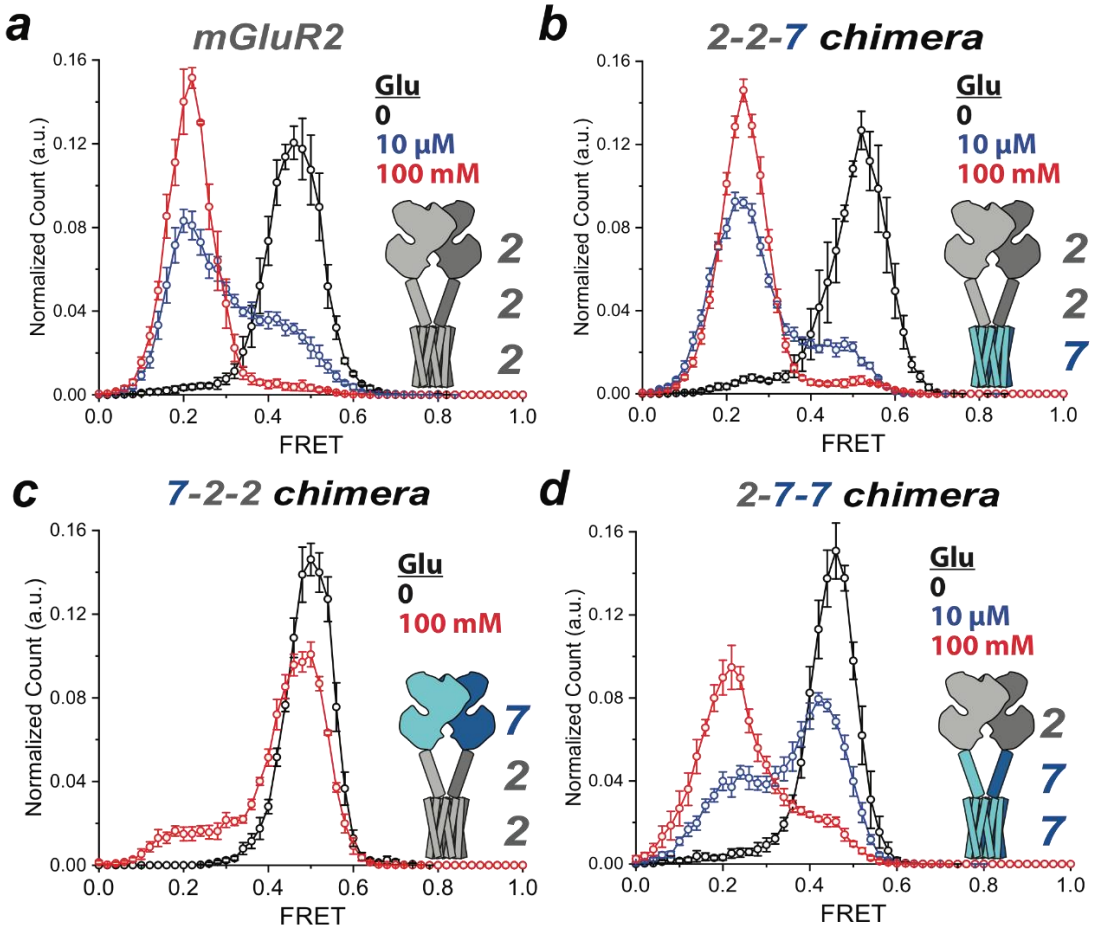

Figure 4.1, LBD and CRD are responsible for mGluR7 low glutamate sensitivity. a) Histograms of smFRET distribution of SNAP-mGluR2 in 0, 10 µM and 100 mM glutamate concentrations. b) Histograms of smFRET distribution of SNAP-mGluR2(mGluR7 TMD) in 0, 10 µM and 100 mM glutamate concentrations. c) Histograms of smFRET distribution of SNAP-mGluR2(mGluR7 LBD) in 0, 10 µM and 100 mM glutamate concentrations. d) Histograms of smFRET distribution of SNAP-mGluR7(mGluR2 LBD) in 0, 10 µM and 100 mM glutamate concentrations.

absolute FRET levels and dynamic changes associated with ligand induced conformational changes in the LBDs using total internal reflection fluorescence (TIRF) microscopy. Imaging of

smFRET of SNAP-mGluR2 in zero glutamate produces a single peak at FRET value ~0.5 (Fig. 4.1a, black). At an intermediate glutamate concentration of 10 uM glutamate we see a bimodal distribution with about 75% of the time spent at FRET value ~0.45 and 25% of time spent at FRET value ~0.2 (Fig. 4.1a, blue). At a saturating concentration of 100 mM glutamate we see complete occupation of the low FRET state ~0.2 (Fig. 4.1a, red). Swapping both the LBD and CRD of mGluR2 on the TMD of mGluR7 produces 2-2-7 chimera. In zero glutamate 2-2-7 chimers produces a single peak at FRET value ~0.45 (Fig 4.1b, black). At 10 uM glutamate 2-2-7 chimera produces a bimodal distribution with about 80% of the time spent at FRET value ~0.25 and about 20% occupancy of the high FRET state ~0.5 (Fig, 4.1b, blue). At 100 mM glutamate 2-2-7 chimera gives a stable low FRET value of ~0.25 (Fig. 4.1b, red). These data suggest that mGluR7 TMD does not contribute negatively to activation by glutamate.

In order to test the contribution of the mGluR7 LBD to glutamate activation we designed a construct containing an mGluR7 LBD followed by a mGluR2 CRD and TMD named 7-2-2 chimera. In zero glutamate 7-2-2 chimera produces a single histogram peak at FRET value ~0.5 (Fig. 4.1c, black). At 100 mM glutamate 7-2-2 chimera spends about 90% of the time at the high FRET value ~0.5 (Fig. 4.1c, red). This data suggests that the mGluR7 LBD is critical to the low glutamate sensitivity observed for mGluR7.

We next swapped the mGluR2 LBD onto mGluR7 CRD and TMD to examine how a high sensitivity of glutamate alters subsequent steps of mGluR7 activation. 2-7-7 chimera in zero glutamate produces a stable FRET value of ~0.5 (Fig. 4.1d, black). At 10 uM glutamate 2-7-7 chimera produces a bimodal distribution with about 60% of time spent at FRET value ~0.45 and 40% of time spent at FRET value ~0.2 (Fig. 4.1d, blue). At 100 mM glutamate 2-7-7 chimera spends about 80% of time at the low FRET value ~0.2 and about 20% of the time at the high FRET value ~0.45 (Fig. 4.1d, red). These data combined with the observations of 2-2-7 chimera suggest that the mGluR7 CRD is decreasing both glutamate sensitivity and maximal efficacy.

Lower LBD interface controls affinity and efficacy of mGluR7

To understand what region of mGluR7 is responsible for it's incredibly low glutamate affinity and efficacy we designed a chimeric approach utilizing mGluR4. mGluR4 has 70% homology and 42% identical to mGluR7, yet mGluR7 has a glutamate affinity of 4uM and maximum efficacy of 60%. In zero glutamate had a stable FRET value ~0.50 (figure 4.2a, black) representing the open-open/inactive conformation. SNAP-mGluR7 in 100 mM glutamate produces a small shift to lower FRET value ~0.2 (figure 4.2a, red) representing the closed/closed active conformation demonstrating the low efficacy of glutamate on mGluR7. N-terminally SNAP-tagged mGluR4 expressed in HEK293T cells and labeled with Alexa-647 and DY-547 fluorophores in zero glutamate had a stable FRET level ~0.45 (Fig. 4.2b, black), similar to mGluR7. mGluR4 in an intermediate glutamate concentration of 10 uM produces a bimodal distribution between ~0.2 and ~0.45 (Fig. 4.2b, blue) with about half the time spent in the active state and half spent in the inactive state. In a saturating concentration of 100 mM glutamate mGluR4 again produced a bimodal distribution between ~0.2 and ~0.45 with about 60% of the time spent in the ~0.2 FRET value (Fig. 4.2b, red). This data shows that mGluR4 is much more sensitive and has a higher max efficacy in response to glutamate compared to mGluR7. To understand the molecular determinants that cause the very low glutamate sensitivity in mGluR7 we designed gain-of-function chimeras of mGluR7 containing amino acid changes to match that found in mGluR4.

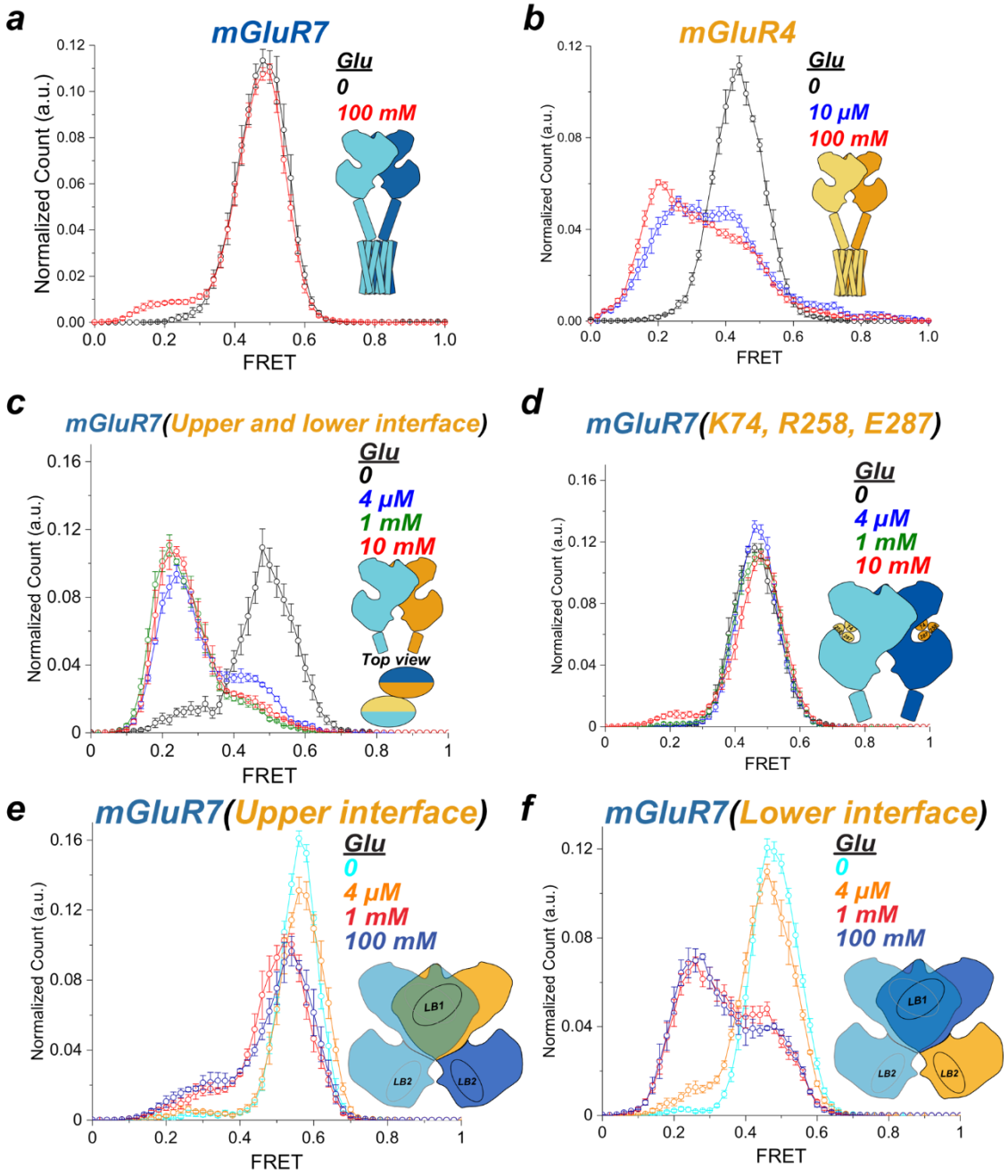

Figure 4.2, Low glutamate affinity and efficacy of mGluR7/7 is dependent on lower LBD dimer interface. a Histograms of smFRET distributions of SNAP-mGluR7/SNAP-mGluR7 in 0 and 100 mM glutamate concentrations. b) Histograms of smFRET distributions of SNAP-mGluR4/SNAP-mGluR4 in 0, 10 μM and 100 mM glutamate concentrations. c) smFRET histograms of chimeric SNAP-mGluR7 with first 301 amino acids replaced with sequence from mGluR4 encompassing upper and lower dimer interfaces and thirteen amino acids within the ligand binding pocket in 0, 4 μM, 1mM and 10 mM glutamate. d) smFRET histograms of SNAP-mGluR7 chimera with three binding sites residues changed to match that found in mGluR4 binding site in 0, 4 μM, 1 mM and 10 mM glutamate. e) smFRET histograms of SNAP-mGluR7 chimera with first 163 amino acids replaced with the sequence from mGluR4 encompassing upper dimer interface in 0, 4 μM, 1mM and 100 mM glutamate. f) smFRET histograms of SNAP-mGluR7 chimera with amino acids 164 through 301 replaced with the sequence from mGluR4 encompassing lower dimer interface in 0, 4 μM, 1mM and 100 mM glutamate.

The first 300 amino acids encompass the upper and lower regions of the ligand binding

domain which make up the dimer interfaces and thirteen residues that make up the ligand binding pocket named mGluR7 (Upper and lower interface). mGluR (Upper and lower interface) in zero glutamate produces one large peak at FRET value ~0.5 and a small peak at FRET value ~0.3 (Fig. 4.2c, black). At an intermediate concentration of 4 uM glutamate mGluR7 (Upper and lower interface) shifts the distribution to roughly 80% of the time spent in the active state of ~0.2 FRET and 20% of the time spent in the inactive ~0.45 FRET value (Fig. 4.2c, blue). At saturating glutamate concentrations of 1 mM and 10 mM glutamate mGluR7 (Upper and lower interface) spends about 90% of time in the ~0.2 FRET value and 10% in the ~0.45 FRET value (Fig. 4.2c, green and red). These data provide evidence that the difference between mGluR7 and mGluR4 glutamate sensitivity is determined by molecular interactions within the first 300 amino acids. Since this region contains both dimer interface residues and ligand binding residues we sought to test the contribution of only the ligand binding site. Three of these thirteen residues within the ligand binding pocket differ between mGluR4 and mGluR7. To test the contribution of these residues in mGluR7 we mutated residue 74, 258 and 287 to residues found in mGluR4[27]. mGluR7 (K74, R258, E287) had a stable FRET value ~0.5 at 0, 4 uM and 1 mM glutamate (Fig. 4.2d, black, blue and green) and produces a very small shift to ~0.2 FRET in 10 mM glutamate (Fig. 4.2d, red). This suggests that the ligand binding pocket of mGluR7 contributes very little to mGluR7's low sensitivity to glutamate.

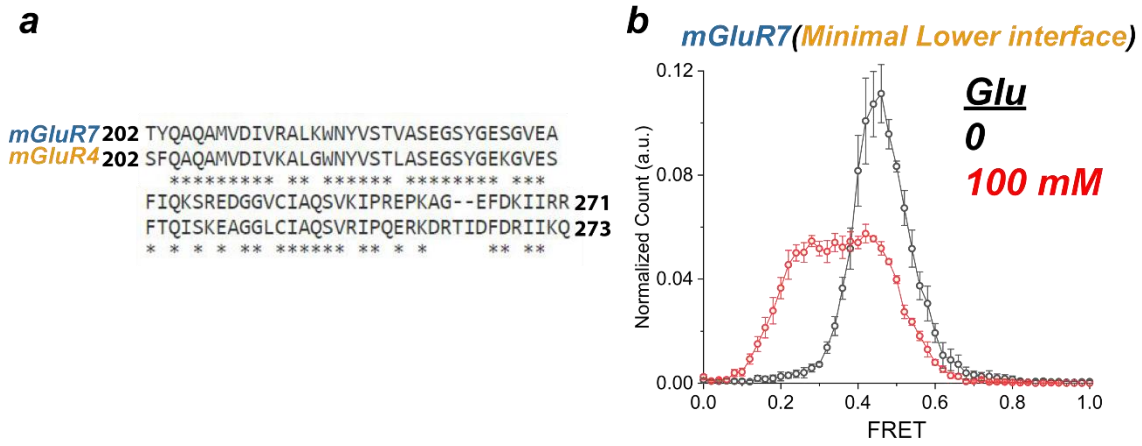

Figure 4.3, Multiple surfaces in lower LBD responsible for low affinity and efficacy of mGluR7/7. a) Amino acid sequence alignment of mGluR4 and mGluR7 minimal lower dimer interface region. b) smFRET histograms of SNAP-mGluR7 chimera containing 22 amino acid changes to residues found in mGluR4 lower dimer interface in 0 and 100 mM glutamate.

To further examine the effects of the upper and lower dimer interfaces we created chimeras of mGluR7 with each interface swapped for residues found in mGluR4. mGluR7 (Upper interface) produces a stable FRET value ~0.55 in zero and 4 uM glutamate (Fig. 4.2e cyan and orange). In 1 mM and 100 mM glutamate mGluR7 (Upper interface) spends roughly 90% of the time at FRET value ~0.55 and 10% in the lower FRET value of ~0.3 (Fig. 4.2e, red and blue) suggesting the upper dimer interface of mGluR7 is not critically responsible for mGluR7's low glutamate sensitivity. Next we tested the lower interface of mGluR7 by swapping the residues with that of mGluR4. mGluR7 (Lower interface) in zero glutamate produces a stable FRET value of ~0.50 (Fig. 4.2f, cyan). In 4 uM glutamate mGluR7 (Lower interface) spends about 90% of the time in the high FRET value of ~0.50 and 10% of time in the lower FRET value of ~0.25 (Fig. 4.2f, orange). In both 1 mM and 100 mM glutamate mGluR7 (Lower interface) spends about 60% of time in the FRET value of ~0.25 and 40% of time in the FRET

value ~0.50. Together these data show that the lower dimer interface of mGluR7 is responsible for the low glutamate sensitivity.

To gain a more precise understanding of the residues in the lower LBD interface responsible for mGluR7's low glutamate sensitivity we creates mGluR7 (Minimal Lower interface) chimera with swaps residues 202-273 in mGluR7 for residues 202-271 in mGluR4 (Fig. 4.3a). This 71 amino acid section contains 48 identical residues, 21 residues that are not identical and 2 residues inserted in mGluR7. mGluR7 (Minimal Lower interface) in zero glutamate produces a single histogram peak at FRET value ~0.5 (Fig 4.3b, black). In 100 mM glutamate we see a bimodal distribution with equal time spent at ~0.25 FRET and ~0.45 FRET. This suggests that multiple residues within these 71 amino acids are the cause of the low glutamate sensitivity we observe in mGluR7. These residues most likely interact between dimeric partners destabilizing the active state preventing occupation of the closed/closed LBD confirmation.

Source of mGluR heterodimer modulation

One other mutation we have seen that alters occupation of the active state is the C121A in mGluR2[28]. This mutant reduces active state occupancy. We sought to use this observation to begin to examine mGluR2/7 heterodimers. Previously we reported that mGluR2/7 displays unique properties relative to mGluR2/2 and mGluR7/7 homodimers including a higher glutamate sensitivity than mGluR2/2, a much higher ability to occupy the fully active conformation while only singly liganded and faster conformational dynamics than mGluR2/2[25]. We also provided evidence that the source of these properties was due to mGluR2/7's unique ability to undergo an apo state rotation. To examine the molecular determinants of these properties we use mGluR2/4 as a comparative example. We co-expressed CLIP-mGluR2 and either SNAP-mGluR7 or SNAP-mGluR4 in HEK 293T cells and labeled SNAP-mGluR7 or SNAP-mGluR4 with SNAP-selective BG-LD655 and CLIP-mGluR2 with CLIP-selective BC-LD555. Using this strategy only dimeric combinations containing a single SNAP-acceptor and single CLIP-donor will produce a FRET signal allowing us to only image heterodimer combinations. mGluR2/7 in zero glutamate produces a single peak with a FRET value ~0.4 (Fig. 4.4a, black). In 10 uM and 100 mM glutamate most of the time is spent at FRET value ~0.25 (Fig 4.4a, blue and red). We next imaged mGluR2/4 heterodimers. In zero glutamate we see a stable FRET value of ~0.50 (Fig. 4.4b, black). At an intermediate glutamate concentration of 10 uM we see widening of the histogram centering at around ~0.3 FRET (Fig. 4.4b, blue). At a saturating glutamate concentration of 100 mM we see a bimodal distribution with about 75% of the time spent at ~0.2 FRET value and 25% of time spent at ~0.50 FRET value (Fig. 4.4b, red). These data show show that while mGluR2/7 is very sensitive to 10 uM glutamate and has almost 100% efficacy at saturating glutamate, mGluR2/4 is less sensitive to 10 uM glutamate and is only about 75% max efficacy at saturating glutamate. This suggests that the mechanism responsible for making mGluR2/7 more sensitive to glutamate than mGluR2/2 is absent in mGluR2/4. We sought a gain-of-function in mGluR2/4 similar to that which we observe in mGluR2/7. Comparing the cysteine loops of mGluR4 and mGluR7 there are four glycine residues in mGluR4 and only one glycine in mGluR7. To test whether these glycines alter the behavior of the heterodimer we mutated the three glycines within mGluR4's cysteine loop to residues seen at matching positions within mGluR7. mGluR2/4 (G131T, G137T, G140E) in zero glutamate produces a stable FRET value ~0.35 (Fig. 4.4c, black). At an intermediate glutamate concentration of 10 uM we see a wide

histogram with a peak at FRET value ~0.25 (Fig. 4.4c, blue). At a saturating glutamate concentration of 100 mM we see a single narrow gaussian at ~0.2 FRET value (Fig. 4.4c, red). The glutamate response of mGluR2/4 (G131T, G137T, G140E) closely resembles that mGluR2/7 suggesting that the flexibility in the cysteine loop is critical in determining heterodimeric mGluR properties.

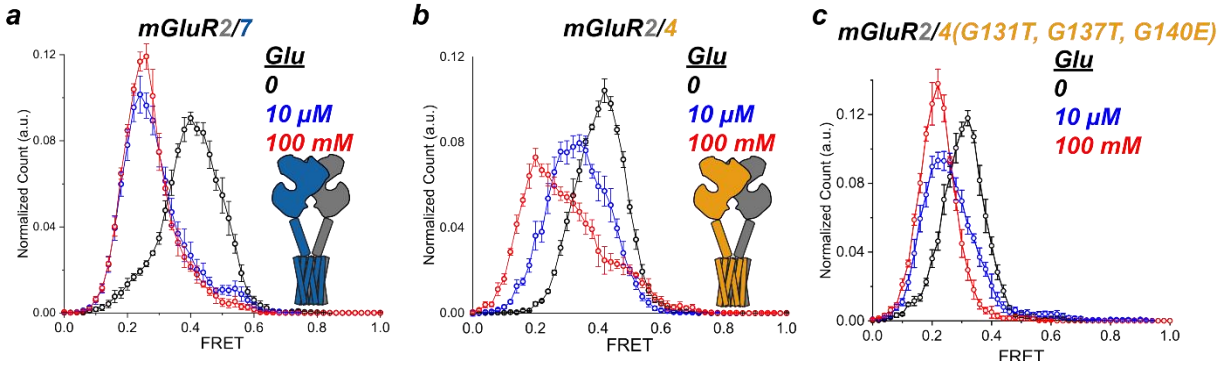

Figure 4.4, Cysteine loop flexibility controls heterodimer affinity and efficacy. a) smFRET histograms of CLIP-mGluR2/SNAP-mGluR7 labeled with BC-LD55 and BG-LD655 in 0, 10 µM 100 mM glutamate. b) smFRET histograms of CLIP-mGluR2/SNAP-mGluR4 labeled with BC-LD55 and BG-LD655 in 0, 10 µM 100 mM glutamate. c) smFRET histograms of CLIP-mGluR2/SNAP-mGluR4(G131T, G137T, G140E) labeled with BC-LD55 and BG-LD655 in 0, 10 µM 100 mM glutamate.

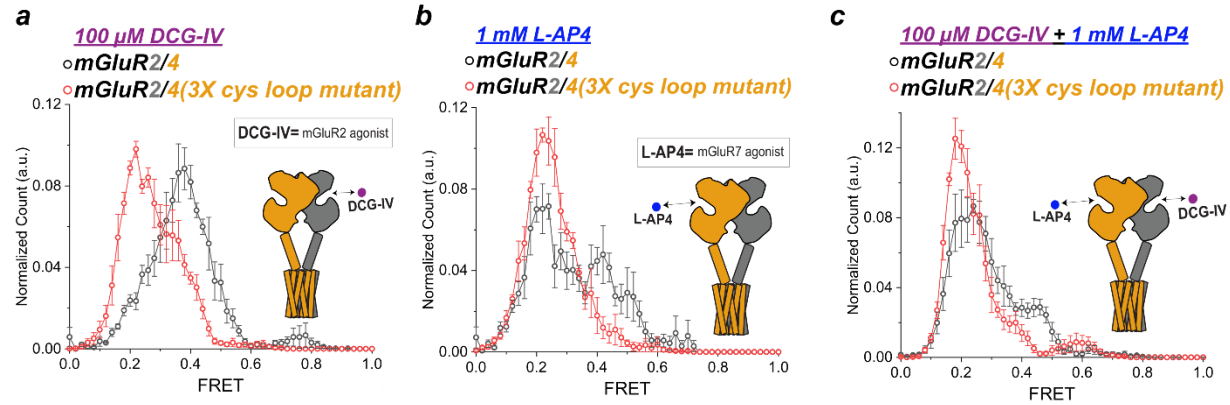

Figure 4.5, Removal of cysteine loop glycines allows for increased single subunit activation. a) smFRET histograms of CLIP-mGluR2/SNAP-mGluR4 and CLIP-mGluR2/SNAP-mGluR4(G131T, G137T, G140E) labeled with BC-LD55 and BG-LD655 in 100 µM DCG-IV. b) smFRET histograms of CLIP-mGluR2/SNAP-mGluR4 and CLIP-mGluR2/SNAP-mGluR4(G131T, G137T, G140E) labeled with BC-LD55 and BG-LD655 in 1 mM L-AP4. c) smFRET histograms of CLIP-mGluR2/SNAP-mGluR4 and CLIP-mGluR2/SNAP-mGluR4(G131T, G137T, G140E) labeled with BC-LD55 and BG-LD655 in 100 µM DCG-IV and 1 mM L-AP4.

After finding the increased sensitivity glutamate of mGluR2/4 (G131T, G137T, G140E) we next asked if this construct exhibits higher single ligand efficacy. DCG-IV is an Group II partial agonist. 100 uM DCG-IV on mGluR2/4 produces a large peak at FRET value ~0.4 and a smaller peak, roughly 20%, at ~0.2 FRET value (Fig. 4.5a, black). mGluR2/4 (G131T, G137T, G140E) in 100 uM DCG-IV spends about 75% of the time in the low FRET value ~0.2 and about 25% of the time in the higher FRET value ~0.4 (Fig. 4.5a, red). L-AP4 is a Group III specific agonist. mGluR2/4 in 1 mM L-AP4 produces a histogram with about 40% of the time

spent at FRET value ~0.4 and about 60% of the time spent at FRET value ~0.2 (Fig. 4.5b, black). mGluR2/4 (G131T, G137T, G140E) on the other hand in 1 mM L-AP4 produces a single peak at ~0.2 FRET value (Fig. 4.5b, red). The higher efficacy seen in mGluR2/4 (G131T, G137T, G140E) when singly liganded suggests that the cysteine loop can allosterically dictate whether a liganded LBD can cause closure of an empty LBD partner. To examine the maximal efficacy we imaged smFRET samples in the presence of both DCG-IV and L-AP4. mGluR2/4 in 100 uM DCG-IV and 1 mM L-AP4 has shorter occupancy (~20%) at FRET value ~0.45 and spends about 80% of the time at FRET value ~0.25 (Fig. 4.5c, black). mGluR2/4 (G131T, G137T, G140E) in 100 uM DCG-IV and 1 mM L-AP4 creates a single peak at FRET value ~0.2 (Fig. 5c, red) display a higher maximal efficacy.

CRD effect maximal efficacy of Group II and Group III mGluRs

Comparison of Group II and Group III mGluR glutamate activation using smFRET reveal that Group II mGluRs display a higher maximal efficacy. Compared to mGluR4 under saturating glutamate (Fig. 2b, red) which spends about 60% of time in the active state, mGluR2 displays complete maximal efficacy (Fig. 1a, red). Based on results seen with chimeric domain swaps between mGluR2 and mGluR7 (Fig. 1), we suspected that the CRD may be playing a role in the difference between these two groups. We designed CRD swaps between mGluR2 and

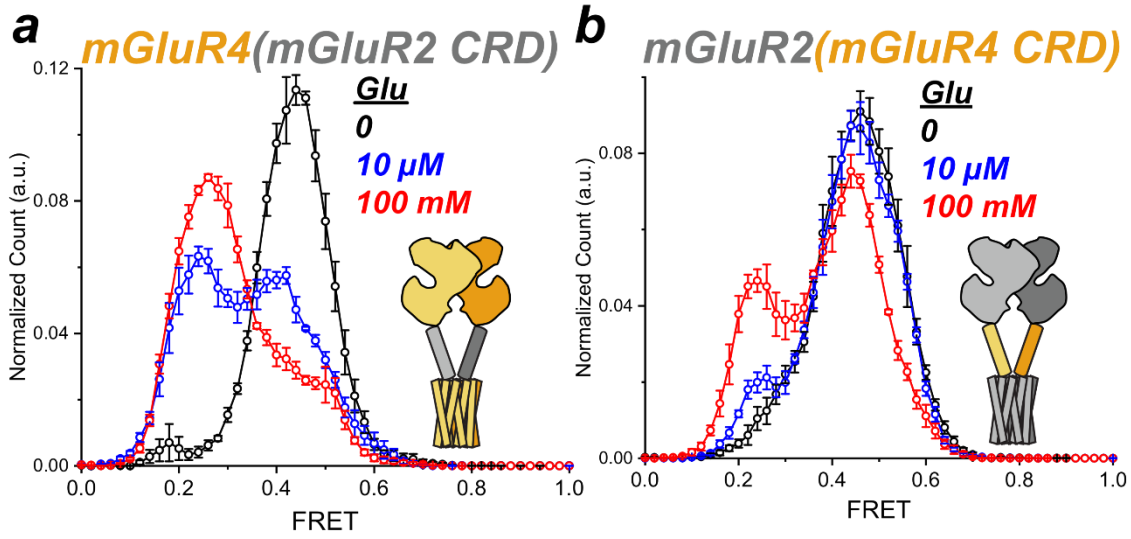

Figure 4.6, CRD contributes to maximal efficacy. a) Histograms of smFRET distribution of SNAP-mGluR4(mGluR2 CRD) in 0, 10 μM and 100 mM glutamate concentrations. **b)** Histograms of smFRET distribution of SNAP-mGluR2(mGluR4 CRD) in 0, 10 μM and 100 mM glutamate concentrations.

mGluR4 and imaged them using smFRET. mGluR4 (mGluR2 CRD) in zero glutamate produces a single peak at FRET value ~0.45 and a second very small peak (less than 5%) at FRET value ~0.2 (Fig 6a, black). Similar to mGluR2, mGluR4 (mGluR2 CRD) in 10 uM glutamate spends about 50% of time at FRET value ~0.45 and 50% of time at FRET value ~0.2 (Fig. 6a, blue). At saturating glutamate concentration of 100 mM mGluR4 (mGluR2 CRD) spends about 80% of the time in the low FRET value ~0.25 and 20% of time at high FRET value ~0.45 (Fig. 6a, red). This level of active state occupancy is higher than that seen in mGluR4 (Fig. 2b, red). mGluR2 (mGluR4 CRD) in zero glutamate produces a wide single peak at ~0.5 FRET value (Fig. 6b,

black). At 10 uM glutamate mGluR2 (mGluR4 CRD) produces one large peak (~95%) at FRET value ~0.45 and a small peak (~5%) at FRET value ~0.25 (Fig. 6b, blue). At 100 mM glutamate mGluR2 (mGluR4 CRD) a bimodal distribution is seen with about 70% of the time spent in the high FRET value of ~0.45 and about 30% of time spent in the low FRET value ~0.25 (Fig. 6b, red). This is a lower maximal efficacy seen in mGluR2 (Fig. 1a, red). The decrease in efficacy measured with the mGluR4 CRD and increase in efficacy seen with the mGluR2 CRD suggests that relative to the Group III CRD, the Group II CRD confers a higher level of maximal efficacy.

Discussion:

A defining feature of mGluRs is the large N-terminal extracellular domain (ECD), but our understanding of how this domain shapes the glutamate activation profile or communicates with its dimeric partner is lacking. In this work we address several aspects how the ECD can shape a glutamate response first by finding that the low ligand sensitivity of mGluR7 is caused by the lower LBD dimer interface, then by showing that cysteine loop flexibility controls heterodimeric modulation and finally demonstrating that Group III mGluR CRDs contribute to the incomplete maximal efficacy observed in Group III mGluRs. These insights into how inter-dimeric interactions alter glutamate sensitivity and efficacy provides new avenues to understand the tuning of mGluRs.

Observing that the lower LBD dimer-interface is critical to maximal activation suggests a mechanism whereby stabilization of the active state by this interface is required for extended occupation of the active state. This results in allosteric control of glutamate activation. This combined with that observation that an mGluR dimer can only signal through one TMD at a time means that two mGluR ECD act as allosteric sensors for glutamate.

mGluR7 homodimer lower LBD interface controls glutamate sensitivity

mGluR7 has a very low glutamate affinity and efficacy[23,29]. This has led to the proposal that mGluR7 acts as a low-pass filter for glutamate levels in the CNS[30] but, glutamate concentrations in the CNS only reach 1-3 mM[31]. While there are potential avenues of modulation of mGluR7, understanding the molecular determinants for the low sensitivity of mGluR7 homodimers provides an opportunity to deconstruct allosteric mechanisms within mGluR activation. We find that both the LBD and CRD of mGluR7 contribute negatively to mGluR7's low glutamate affinity and efficacy while the TMD apparently provides a positive contribution(Fig 4.6). mGluR7 and mGluR4 are both Group III mGluRs and share 70% homology and 42% identity yet, mGluR4 EC50 for glutamate is 10,000 fold lower and mGluR4 maximal efficacy is ~10 fold higher than mGluR7[25]. Surprisingly, these vastly different sensitivities are not caused by the ligand binding pocket residues(Fig. 3.2b), but instead is allosterically caused by the lower dimmer interface. This suggests that ligand activation is not a single conformational change of clamshell closure and instead relies on a network of interactions in the LBD.

mGluR modulation through heterodimerization is dependent on cysteine loop flexibility

We show previously that heterodimerization between mGluR2/7 enhances ligand sensitivity for both subunits[25]. In this work we also we demonstrate that mGluR2/4 does exhibit ligand enhancement, but this property can be induced through mutation of three glycine residues within the mGluR4 cysteine loop to two threonines and one glutamic acid as is found in the cysteine loop of mGluR7. This suggests that the higher level of flexibility in the mGluR4 prevents mGluR2/4 modulation and that decreasing the flexibility of the loop allows for allosteric enhancement of both subunits. Due to the lack of structural information regarding the cysteine loop it is difficult to know what specific interactions are made by these three residues in both mGluR4 and mGluR7 which controls this enhancement. We can however hypothesize that the cysteine loops act to limit the conformational freedom of the N-termi of dimeric LBDs. This

can apparently act as a conduit in a manner that allows closure of one subunit to force the partner subunit closed while empty.

Group II and Group III CRDs differentially stabilize the active conformation

Group II and III mGluRs both signal through G_i proteins, but tend to be found at different synaptic sites[23,29]. Group II tend to be found peri-synaptically while Group III are found within the pre-synaptic active zone. We show here that the most apparent difference between Group II and Group III mGluR activation profiles is that Group III mGluRs display much lower maximal efficacy. We see this in Figs. 4.1 and 4.2 in mGluR2 and mGluR4. While the affinity to glutamate is very similar between the mGluR2 and mGluR4, at saturating glutamate mGluR4 spends almost half the time in the active state. This suggests that while glutamate binding is similar between the two subtypes, some force is destabilizing the mGluR4 active state. We see in Fig. 4.6 that the CRD of mGluR2 can improve the maximal efficacy of mGluR4 and that the CRD of mGluR4 decreases the maximal efficacy of mGluR2. We see a similar pattern when the CRD of mGluR7 is swapped into mGluR2, Fig. 4.1. This leads us to conclude that while Group II mGluR's CRD allow indefinite occupation of the active state, Group III mGluR's CRD cause destabilization of the active state preventing indefinite occupation. One potential biological explanation for this biophysical measurement is that the pre-synaptic active zone experiences very large and fast glutamate transients and destabilization of the active state allows faster reset of Group III mGluRs to the inactive state leading to faster potential readout rates of glutamate transients. Together these observations of between group differences, allosteric pathways of glutamate activation and allosteric modulation through heterodimerization improves our understanding of exact biophysical differences between mGluRs allowing improved models of interactions and specific roles within the CNS.

Summary

Key questions about mGluR signaling in the CNS are driven by the desire to construct a spatial and temporal map of activation properties of each receptor subtype and downstream signaling pathways. While technologies committed to *in-vivo* brain imaging have advanced greatly in recent years, it is far from the resolution and imaging speed required to observe these events directly and this technological accomplishment may never be reached due to physical limitations of light and the optical properties of the brain. Due to the reality of this situation and the immense value a glutaminergic spatio-temporal map would provide for advancing our understanding of brain function and therapeutic design we must approach this question from the perspective of the receptors and work upwards. smFRET provides the ideal capabilities to study these receptors in a highly controlled environment and enables highly detailed characterization spatially and temporally of each receptor subtype and combination of receptors. Armed with the very precise characterizations we can develop highly specific hypotheses of glutamatergic signaling within the brain and design much more targeted experimental tests paired with more informed interpretations allowing the potential to deconstruct the signaling map without direct observation.

The findings of this chapter contribute to this ultimate goal of a detailed characterization of different receptor subtypes, combinations and molecular interactions that can modulate ligand response and activation. Understanding the molecular forces that differentiate Group II and Group III mGluR activity is one of the most fundamental questions to address if we plan to

assign specific roles for each receptor. We see that differences in the CRD between groups can dictate active state occupancy which provides a molecular explanation to the expression pattern that has been observed for many years. Several studies have shown mGluRs heterodimerize with native brain tissue and mGluR2/7 heterodimers were the first to display emergent properties through modulation giving us clues to a potential biological role of heterodimerization. We show in this chapter that these properties are caused by the specific combinations of cysteine loops suggesting that cysteine loops act as avenues for interprotomer communication dictating how LBDs can affect one another. The observation of mGluR7 having very low glutamate affinity and efficacy led to the proposal of mGluR7 acting as a low-pass filter for glutamatergic transients. Our finding that the insensitivity of glutamate is caused by allosteric interactions which destabilize the active state suggest that mGluR7 is not simply a mGluR with a diminished capacity for glutamate binding, but a mGluR with a unique activation energy landscape which can be greatly modulated through heterodimerization.

Methods:

Cell culture and transfection

HEK293T cells were cultured in DMEM with 5% FBS on poly-L- lysine-coated glass coverslips. HEK293T cells were obtained from the UC Berkeley MCB tissue culture facility, authenticated by DDC Medical, and tested negative for mycoplasma contamination. Previously described HA–SNAP and Flag–CLIP-tagged rat mGluR cDNA were generously provided by J. P. Pin. DNA plasmids were transfected into cells using lipofectamine 2000 (Thermo Fisher). For FRET experiments, cells were transfected with SNAP and CLIP-tagged constructs at a ratio of 1:2 with 0.3 mg of SNAP–mGluR DNA per well.

FRET dye labeling of SNAP- and CLIP- tagged mGluRs

Approximately 24–48 h after transfection, cells were labeled while attached to poly-L-lysine-coated coverslips. Culture media was removed and coverslips were washed and transferred to extracellular solution containing (in mM): 135 NaCl, 5.4 KCl, 2 $CaCl_2$, 1 $MgCl_2$, 10 HEPES, pH 7.4. Cells were labeled at 37 °C with one or two SNAP-reactive (benzylguanine, BG) dyes at 1.5 μM for 45 minutes, and then, if a CLIP-tagged mGluR was used, they were washed and labeled with a CLIP-reactive (benzylcytosine, BC) dye at 3 μM for 45 minutes. For most of the experiments DY-547 (NEB) was used as a donor and Alexa-647 (NEB) as an acceptor. Heterodimer experiments were labeled using LD-655 as the donor and LD-655 as the acceptor (Lumidyne). The fluorophores were diluted in extracellular solution and coverslips were washed in between labeling with donor and acceptor.

smPull receptor isolation and surface display

To inhibit nonspecific protein adsorption, flow cells for single-molecule experiments were prepared as previously described (Vafabhaksh et al,. 2015) using mPEG (Laysan Bio) passivated glass coverslips (VWR) and doped with biotin PEG16. Before each experiment, coverslips were incubated with NeutrAvidin (Thermo), followed by 10 nM biotinylated secondary antibody (donkey anti-rabbit, Jackson ImmunoResearch). For receptor immunopurification, 10 nM anti-mGluR2 primary antibody (abcam, ab150387) or 10 nM anti-mGluR7 antibody (abcam, ab53705), or 15 nM anti-HA antibody (abcam, ab26228) was incubated in the chamber (Fig. 1e). Between each conjugation step, the chambers were flushed to remove free reagents. The antibody dilutions and washes were done in T50 buffer (50 mM NaCl, 10 mM Tris, pH 7.5). For single-molecule experiments, fresh cells expressing tagged mGluR constructs were labeled, as described above, and recovered from coverslips by incubating with Ca^{2+} free PBS buffer for 5–10 min followed by gentle pipetting. Cells were then pelleted by spinning at 5,000g for 5 min and lysed in lysis buffer consisting of 150mM NaCl, 1 mM EDTA, protease inhibitor cocktail (Thermo Scientific) and 1.2% IGEPAL (Sigma).After 1 h incubation at 4 C°, lysate was centrifuged at 16,000g for 20 min. and the supernatant was collected and kept on ice. To achieve sparse immobilization of labeled receptors on the surface, the cell lysate was diluted (ranging from 5X to 50X dilution depending on the expression and labeling efficiency) and applied to coverslips. After achieving optimum surface immobilization (~400 molecules in a 2,000 μm^2 imaging area), unbound receptors were washed out of the flow chamber and the flow cells were then washed extensively (up to 50X the cell volume).

smFRET measurements

Receptors were imaged for smFRET in imaging buffer consisting of (in mM) 3 Trolox, 120 KCl, 29 NaCl, 2 CaCl2, 1 MgCl2, 50 HEPES, 0.04% IGEPAL and an oxygen scavenging system (0.8% dextrose, 0.8 mg ml^{-1} glucose oxidase, and 0.02 mg ml^{-1} catalase), pH 7.4. Reagents were purchased from Sigma and were all UltraPure grade (purity >99.99%). All buffers were made in UltraPure distilled water (Invitrogen). For the experiments done in the absence of Ca^{2+}, 10 mM EGTA and 1 mM EDTA were added to the imaging buffer. Catalase was diluted in T50 buffer and passed through a spin column 3X (BioRad). Samples were imaged with a 1.65 na X60 objective (Olympus) on a total internal reflection fluorescence microscope with 100 ms time resolution unless stated otherwise. Lasers at 532 nm (Cobolt) and 632 nm (Melles Griot) were used for donor and acceptor excitation, respectively. FRET efficiency was calculated as $(I_A - 0.1I_D)/(I_D+I_A)$, in which I_D and I_A are the donor and acceptor intensity, respectively, after background subtraction. Imaging was with 100 ms acquisition time (10 Hz) with a Photometrics Prime 95B cMOS camera using Lumidyne LD555 as donor and Lumidyne LD655 as acceptor (Förster radius ~52Å). Dyes were conjugated to benzyguanine and benzylecytosine to allow for labeling of SNAP and CLIP proteins, respectively.

smFRET data analysis

Single-molecule intensity traces showing single-donor and single-acceptor photobleaching with a stable total intensity for longer than 5 s were collected (20–30% of total molecules per imaging area). Individual traces were smoothed using a nonlinear filter (Haran et al., 2004) with following filter parameters: window = 2, M = 2 and P = 15. Each experiment was performed $\geq$4 times to ensure reproducibility. smFRET histograms were compiled from $\geq$100 molecules per condition. (100 ms time resolution). Error bars in the histograms represent the standard error from $\geq$4 independent movies. To ensure that traces of different lengths contribute equally, histograms from individual traces were normalized to one before compiling. Gaussian fitting to histograms was done in Origin Pro. smFRET histograms were fit to two Gaussians, centered on high (~0.45) and low (~0.2) FRET levels for mGluR2/2 and mGluR2/7 and a single Gaussian for mGluR2/7 (center ranging from 0.2 to 0.45). For dose-response relations, the area underneath the low FRET Gaussian was used as a measure of active state occupancy.

References:

1. Weis, W. I. & Kobilka, B. K. The molecular basis of G protein-coupledreceptors activation. *Annu. Rev. Biochem.* 87, 897–919 (2018).
2. Erlandson, S. C., McMahon, C. & Kruse, A. C. Structural basis for G protein–coupled receptor signaling. *Annu. Rev. Biophys.* 47, 1–18 (2018).
3. Katritch, V., Cherezov, V. & Stevens, R. C. Structure-function of the G protein–coupled receptor superfamily. *Annu. Rev. Pharmacol. Toxicol.* 53,531–556 (2013).
4. Rasmussen, S. G. F. et al. Crystal structure of the β2 adrenergic receptor–Gsprotein complex. *Nature* 477, 549–555 (2011).
5. Venkatakrishnan, A. J. et al. Molecular signatures of G-protein-coupledreceptors. *Nature* 494, 185–194 (2013).
6. Dror, R. O. et al. Pathway and mechanism of drug binding to G-protein-coupled receptors. *Proc. Natl Acad. Sci. USA* 108, 13118–13123 (2011).
7. Isogai, S. et al. Backbone NMR reveals allosteric signal transduction networksin the β1-adrenergic receptor. *Nature* 530, 237–241 (2016).
8. Liu, W. et al. Structural basis for allosteric regulation of GPCRs by sodiumions. *Science* 337, 232–236 (2012).
9. Manglik, A. & Kobilka, B. The role of protein dynamics in GPCR function:insights from the β2AR and rhodopsin. *Curr. Opin. Cell Biol.* 27, 136–143 (2014).
10. Nygaard, R. et al. The dynamic process of β2-adrenergic receptor activation. *Cell* 152, 532–542 (2013).
11. Olofsson, L. et al. Fine tuning of sub-millisecond conformational dynamics controls metabotropic glutamate receptors agonist efficacy. *Nat. Commun.* 5,5206 (2014).
12. Sounier, R. et al. Propagation of conformational changes during μ-opioidreceptor activation. *Nature* 524, 375–378 (2015).
13. Vafabakhsh, R., Levitz, J. & Isacoff, E. Y. Conformational dynamics of a classC G-protein-coupled receptor. *Nature* 524, 497–501 (2015).
14. Gregorio, G. G. et al. Single-molecule analysis of ligand efficacy in β2AR–G-protein activation. *Nature* 547, 68–73 (2017).
15. Lohse, M. J., Maiellaro, I. & Calebiro, D. Kinetics and mechanism of G protein-coupled receptor activation. *Curr. Opin. Cell Biol.* 27, 87–93 (2014).
16. Huang, Y., & Thathiah, A. (2015). Regulation of neuronal communication by G protein-coupled receptors. FEBS Letters, 589(14), 1607–1619. doi:10.1016/j.febslet.2015.05.007
17. Clements, J. et al. The time course of glutamate in the synaptic cleft. *Science* 258, 1498-1501 (1992).
18. Zhou, Y., & Danbolt, N. C. (2014). Glutamate as a neurotransmitter in the healthy brain. Journal of Neural Transmission, 121(8), 799–817. doi:10.1007/s00702-014-1180-8
19. Moussawi, K., Riegel, A., Nair, S., & Kalivas, P. W. Extracellular glutamate:functional compartments operate in different concentration ranges. *Front. Syst. Neurosci.* 5, 94 (2011).
20. Koehl, A. et al. Structural insights into the activation of metabotropicglutamate receptors. *Nature* 566, 79–84 (2019).
21. Niswender, C. M. & Conn, P. J. Metabotropic glutamate receptors: physiology,pharmacology, and disease. *Annu. Rev. Pharmacol. Toxicol.* 50, 295–322 (2010).
22. Stansley, B. J. & Conn, P. J. The therapeutic potential of metabotropic glutamate receptor modulation for schizophrenia. *Curr. Opin. Pharmacol.* 38,31–36 (2018).
23. Traynelis, S. F. et al. Glutamate receptor ion channels: structure, regulation,and function. *Pharmacol. Rev.* 62, 405–496 (2010).
24. Conn, P. J. & Pin, J.-P. Pharmacology and functions of metabotropic glutamate receptors. *Annu. Rev. Pharmacol. Toxicol.* 37, 205–237 (1997).
25. Habrian, C. H., Levitz, J., Vyklicky, V., Fu, Z., Hoagland, A., McCort-Tranchepain, I., … Isacoff, E. Y. (2019). Conformational pathway provides unique sensitivity to a synaptic mGluR. Nature Communications, 10(1). doi:10.1038/s41467-019-13407-8
26. Dunn, H. A., Patil, D. N., Cao, Y., Orlandi, C., & Martemyanov, K. A. (2018). Synaptic adhesion protein ELFN1 is a selective allosteric modulator of group III metabotropic glutamate receptors in trans. Proceedings of the National Academy of Sciences, 115(19), 5022–5027. doi:10.1073/pnas.1722498115
27. Rosemond, E. et al. Molecular determinants of high affinity binding to groupIII metabotropic glutamate receptors. *J. Biol. Chem.* 277, 7333–7340 (2001).
28. Levitz, J. et al. Mechanism of assembly and cooperativity of homomeric andheteromeric metabotropic glutamate receptors. *Neuron* 92, 143–159 (2016).
29. Okamoto, N. et al. Molecular characterization of a new metabotropic glutamate receptor mGluR7 coupled to inhibitory cyclic AMP signal transduction. *J. Biol. Chem.* 269, 1231–1236 (1994). 12.
30. Ohishi, H., Akazawa, C., Shigemoto, R., Nakanishi, S. & Mizuno, N. Distributions of the mRNAs for L-2-amino-4-phosphonobutyrate-sensitive metabotropic glutamate receptors, mGluR4 and mGluR7, in the rat brain. *J.Comp. Neurol.* 360, 555–570 (1995).
31. Clements, J. et al. The time course of glutamate in the synaptic cleft. *Science* 258, 1498–1501 (1992).